
Submitted to the Proceedings of the US Community Study
on the Future of Particle Physics (Snowmass 2021)

[October 14, 2022]

Global SMEFT Fits at Future Colliders

JORGE DE BLAS^{a,b}, YONG DU^c, CHRISTOPHE GROJEAN^d, JIAYIN GU^e,
VÍCTOR MIRALLES^f, MICHAEL E. PESKIN^g, JUNPING TIAN^h, MARCEL VOSⁱ,
AND ELENI VRYONIDOU^j

^a *CAFPE and Departamento de Física Teórica y del Cosmos, Universidad de Granada, Campus de Fuentenueva, E-18071 Granada, Spain*

^b *CERN, Theoretical Physics Department, Geneva, Switzerland*

^c *CAS Key Laboratory of Theoretical Physics, Institute of Theoretical Physics, Chinese Academy of Sciences, Beijing 100190, China*

^d *DESY, Notkestrasse 85, 22607 Hamburg, GERMANY*

^e *Department of Physics, Center for Field Theory and Particle Physics, Key Laboratory of Nuclear Physics and Ion-beam Application (MOE), Fudan University, Shanghai 200438, China*

^f *INFN, Sezione di Roma, Piazzale A. Moro 2, I-00185 Roma, Italy*

^g *SLAC, Stanford University, Menlo Park, CA 94025, USA*

^h *ICEPP, The University of Tokyo, Hongo 7-3-1, Tokyo 113-0033, JAPAN*

ⁱ *IFIC, Universitat de València and CSIC, c./ Catedrático José Beltrán 2, E-46980 Paterna, Spain*

^j *University of Manchester, Oxford Road, Manchester M13 9PL, United Kingdom*

ABSTRACT

Based on the framework of Standard Model Effective Field Theory, we performed a few global fits, each containing a subset of dimension-6 operators, for the measurements that are expected at future colliders. The fit for the Higgs and electroweak sector improves what has been done for the European Strategy Update in 2020 on both EFT treatments and experimental inputs. A new comprehensive fit is performed focusing on 4-fermion interactions at future colliders. Top-quark sector is studied in a dedicated fit which restricts the operators and measurements to be directly related to top-quark. A small subset of CP-violating operators involving bosonic fields alone are also investigated. Various running scenarios for future e^+e^- and Muon Colliders that are suggested in the Snowmass 2021 discussion are considered in the global fits. The outcomes from each fit are expressed in terms of either direct constraint on Wilson Coefficients or precision on Higgs and electroweak effective couplings.

Contents

1	Introduction	1
2	The Standard Model Effective Field Theory Lagrangian	4
2.1	Effective Lagrangian in the mass eigenstate basis	7
2.2	Effective couplings	9
3	Recap on SMEFT fits for ESG	10
4	Input measurements	12
4.1	Electroweak Precision Measurements	12
4.2	Higgs Measurements	16
4.3	Light fermion pair measurements	17
4.4	Top-quark measurements	21
4.5	Diboson measurements	29
5	Higgs + EW fit	31
5.1	Impact of the Standard Model uncertainties on the results	35
5.2	Relaxing $U(2)$ assumption	40
6	Four-fermion operators	42
6.1	Observables	42
6.1.1	Z - and W -pole observables	42
6.1.2	High-energy observables for 4-fermion operators	43
6.1.3	Low-energy precision observables	45
6.2	Flat directions	48
6.3	SMEFT global fit results	51
6.4	Implication on some benchmark UV models	55
6.4.1	The Y-Universal Z' model	55
6.4.2	The scalar leptoquark model	55

7	CP-odd operators	57
8	The top-quark sector in the global EFT fit	62
9	Conclusion and Outlook	69

1 Introduction

In particle physics today, we have a Standard Model that, arguably, accounts for all experimental measurements. At the same time, we are convinced that this model is not a complete description of nature. First, we know from astrophysical observations that the universe contains elements such as dark matter and dark energy that this model does not include. But also, this Standard Model contains a large number of free parameters that control many of its most important properties, such as the mass scale of W and Z bosons, the mass spectrum of fermions, and the appearance of CP violation. It is not straightforward to complete the Standard Model (SM) to repair these difficulties. Essentially, in all of these directions, the SM is powerless, so that a new model with additional fields and interactions is needed to make progress.

There are many possibilities for what this new model should be. But, none of these seem to be particularly favored, either from experiment anomalies or on theoretical grounds. All approaches, including extensions of the SM particle content and composite models of the SM particles, are highly constrained by the data from electroweak interactions and accelerator searches. In particular, the idea of TeV-scale supersymmetry, which held pride of place among SM extensions in the 2000's, has been brought down in stature by the absence of supersymmetric particles in the energy range of the LHC.

In this situation, we would like to have a language for exploring physics beyond the SM in a “model agnostic” way. We would like to have a theoretical framework that allows us to evaluate evidence for the widest possible variety of new physics models, bringing together data from the broadest set of experimental measurements.

Such a framework is actually at hand, under a particular hypothesis—that the mass scale of the new particles in the SM extension is much larger than the energies used in our experimental probes. This hypothesis is suggested by the absence of new particle discoveries at the LHC. If beyond-SM physics is manifested in very weakly coupled light particles or in states that, because of details of their production and decay, are difficult to observe at the LHC, this hypothesis will not strictly apply and a more general analysis would be needed. Still, the hypothesis leads to a tight conceptual structure that can organize our exploration for physics beyond the SM.

Under the hypothesis that new physics has a high mass scale above the reach of our current experiments, the new fields of any particular model can be integrated out, producing an effective Lagrangian containing only SM fields that can equally well describe the physics that we observe. If the number of parameters in this Lagrangian is restricted by gauge invariance and other observed symmetries, it might be possible to determine the parameters of the effective Lagrangian from experiment without any further model assumptions. Then we can use these determinations as a guide to formulate models of the new, underlying, theory.

The general effective field theory built from SM fields is called Standard Model Effective Field Theory (SMEFT). The Lagrangian of SMEFT is organized by the dimension of the possible operators that can appear. The most general Lagrangian built from SM fields with operators of dimension up to dimension 4 — that is, with renormalizable interactions — is the SM itself. The Lagrangian of SMEFT then takes the form

$$\mathcal{L}_{\text{SMEFT}} = \mathcal{L}_{\text{SM}} + \sum_{d=5}^{\infty} \sum_j \frac{C_j^{(d)}}{\Lambda^{d-4}} \mathcal{O}_j^{(d)} , \quad (1)$$

where $\mathcal{O}_j^{(d)}$ is an operator of dimension d invariant under the $SU(3)_c \times SU(2)_L \times U(1)_Y$ gauge group of the SM, Λ is the mass scale of new particles, with the power of Λ in each term determined by dimensional analysis, and $C_j^{(d)}$ is a dimensionless number, the “Wilson coefficient” of the operator. For any new physics model satisfying the hypothesis above, integrating out the new fields produces a Lagrangian with this structure. If the model is weakly coupled at the scale Λ , the Wilson coefficients can be determined systematically by Feynman diagram calculations.

At each value d of the operator dimensions, there is only a finite number of non-redundant operators. Thus, in principle, it is possible to make a closed determination of the Wilson coefficients for all operators up to some dimension D from experiment, and these can be compared to the predictions of specific models.

The goal of this paper is to present the current status of our understanding of this experimental determination, to illustrate some of its subtleties, and to prepare for the determination of the Wilson coefficients in experiments at future accelerators.

The program described in the previous two paragraphs is a very general one, but we will need to make some simplifications to make progress. The number of operators appearing in each term in the sum over d in (1) increases very rapidly with d . For this reason, we will restrict our study to the first relevant corrections to the SM. The Lagrangian (1) contains 2 operators of dimension $d = 5$, but these contribute only to the neutrino masses and are not relevant to collider physics. More generally, operators of odd dimension require lepton- or baryon-number violation and will be omitted from our study. The first relevant corrections to the SM then occur at dimension 6. In this paper, we will restrict ourselves to dimension 6 effects, and we will consider their effects only in linear order. These contributions are of the order of $1/\Lambda^2$. Effects proportional to the squares of the dimension 6 amplitudes are proportional to $1/\Lambda^4$ and therefore are on the same footing as the (much more numerous and complex) dimension 8 contributions.

Even in this simplified contexts, further restrictions are needed. At dimension 6, the SMEFT Lagrangian still contains a large number of unknown coefficients. The total number of dimension 6 gauge-invariant operators is 84 for 1 generation of fermions (76 if one restricts to baryon- and lepton-number conserving operators, 59

if one further restricts to CP-conserving operators) and 3045 (2499 without baryon- and lepton-number violation) for 3 generations [1]. Thus, it is necessary to make physically motivated restrictions on the class of operators being considered. We will discuss fits to subsets of data in which the total number of relevant operators is manageable. Also, although many published SMEFT analyses consider the effects of one operator at a time, a model-independent analysis requires that the coefficients of all relevant operators be varied simultaneously. Otherwise, we cannot match the effects generated by an arbitrary underlying new physics theory. In fits with a large number of free coefficients, one often finds “flat directions” that are not constrained by the fit, each corresponding to a linear combinations of operators for which the collective effect is not measured by the experimental inputs. To address these cases, we need to add inputs or find good reasons to further restrict the class of relevant operators. This issue of balancing the number of operators considered in the fit with the available experimental inputs comes front and center in formulating meaningful global fits using SMEFT. Our main goal in this paper is to understand how to make this balance in practical examples.

The outline of this paper is as follows: In Section 2, we will present the SMEFT Lagrangian at dimension 6, presenting a preferred operator basis for our analysis and defining the various SMEFT Wilson coefficients that will appear. In Section 3, we will discuss the relation between this operator basis and the one used in the recent ECFA study of the capabilities of future facilities. In Section 4, we will review the input measurements for our global fit.

In Section 5, we will present the results of an analysis of a subset of the global fit using Higgs and electroweak operators only, together with relevant experimental inputs. We will discuss the current constraints, and the constraints expected from future data from HL-LHC, from e^+e^- Higgs factories and muon colliders. We will also address the impact of theory errors in this global fit. In Section 6, we will present the results of a subset of the global fit focusing on 4-fermion operators, together with relevant experimental inputs, both current and future. These two analyses will be done with CP-conserving operators only. In Section 7, we will extend the fit of Section 5 to CP-violating operators.

All of the analyses up to this point will be done for fermions that can be considered massless in collider physics. Inclusion of the massive top quark brings in an additional set of operators. In Section 8, we will present an analysis that constrains this operator set using current LHC data and data from future facilities.

In Section 9, we will address the findings from above global fits and implications for future colliders. We will also put out some outlook about potential studies that can future bring improvement to this work.

In this report, we will not address the question of distinguishing the SMEFT from more general effective field theories of electroweak symmetry breaking such as Higgs

Effective Field Theory (HEFT). Distinguishing these models and demonstrating that SMEFT is not sufficient requires measurements beyond the scope of this report, such as measurements of multiple Higgs boson production. Please see [2–4] for a detailed discussion.

2 The Standard Model Effective Field Theory Lagrangian

As we have introduced above, we will study experimental constraints on the SMEFT Lagrangian, truncating the EFT expansion to dimension 6,

$$\mathcal{L}_{\text{SMEFT}} = \mathcal{L}_{\text{SM}} + \sum_j \frac{C_j^{(6)}}{\Lambda^2} \mathcal{O}_j^{(6)}, \quad (2)$$

and including only the leading-order new physics effects in observables, i.e. the linear $\mathcal{O}(1/\Lambda^2)$ contributions. In what follows, as we will only consider dimension-6 operators, we drop the superscript “(6)” from the Wilson coefficients and operators. In this section, we will write out this Lagrangian explicitly in our preferred basis, the so-called *Warsaw basis* [5], for the cases of baryon- and lepton-number-conserving operators, giving a total of 59 dimension-6 operator coefficients for 1 generation (not counting hermitian conjugates separately).

We start first with those operators which, after electroweak symmetry breaking, modify the vertices already present in \mathcal{L}_{SM} (possibly introducing new tensor structures):

$$\begin{aligned} \mathcal{L}_{\text{SMEFT}}^{d=6} \supset & \frac{C_\phi}{\Lambda^2} (\phi^\dagger \phi)^3 + \frac{C_{\phi\Box}}{\Lambda^2} (\phi^\dagger \phi) \Box (\phi^\dagger \phi) + \frac{C_{\phi D}}{\Lambda^2} (\phi^\dagger D_\mu \phi) ((D^\mu \phi)^\dagger \phi) \\ & + \frac{C_W}{\Lambda^2} \varepsilon_{abc} W_\mu^{a\nu} W_\nu^{b\rho} W_\rho^{c\mu} + \frac{C_G}{\Lambda^2} f_{ABC} G_\mu^{A\nu} G_\nu^{B\rho} G_\rho^{C\mu} \\ & + \frac{C_{\phi B}}{\Lambda^2} \phi^\dagger \phi B_{\mu\nu} B^{\mu\nu} + \frac{C_{\phi W}}{\Lambda^2} \phi^\dagger \phi W_{\mu\nu}^a W^{a\mu\nu} + \frac{C_{\phi WB}}{\Lambda^2} \phi^\dagger \sigma_a \phi W_{\mu\nu}^a B^{\mu\nu} + \frac{C_{\phi G}}{\Lambda^2} \phi^\dagger \phi G_{\mu\nu}^A G^{A\mu\nu} \\ & + \left(\frac{(C_{e\phi})_{ij}}{\Lambda^2} (\phi^\dagger \phi) (\bar{l}_L^i \phi e_R^j) + \frac{(C_{d\phi})_{ij}}{\Lambda^2} (\phi^\dagger \phi) (\bar{q}_L^i \phi d_R^j) + \frac{(C_{u\phi})_{ij}}{\Lambda^2} (\phi^\dagger \phi) (\bar{q}_L^i \tilde{\phi} u_R^j) + \text{h.c.} \right) \\ & + \left(\frac{(C_{eB})_{ij}}{\Lambda^2} B^{\mu\nu} (\bar{l}_L^i \phi \sigma_{\mu\nu} e_R^j) + \frac{(C_{dB})_{ij}}{\Lambda^2} B^{\mu\nu} (\bar{q}_L^i \phi \sigma_{\mu\nu} d_R^j) + \frac{(C_{uB})_{ij}}{\Lambda^2} B^{\mu\nu} (\bar{q}_L^i \tilde{\phi} \sigma_{\mu\nu} u_R^j) + \text{h.c.} \right) \\ & + \left(\frac{(C_{eW})_{ij}}{\Lambda^2} W^{a\mu\nu} (\bar{l}_L^i \phi \sigma_{\mu\nu} \sigma_a e_R^j) + \frac{(C_{dW})_{ij}}{\Lambda^2} W^{a\mu\nu} (\bar{q}_L^i \phi \sigma_{\mu\nu} \sigma_a d_R^j) \right. \\ & \left. + \frac{(C_{uW})_{ij}}{\Lambda^2} W^{a\mu\nu} (\bar{q}_L^i \tilde{\phi} \sigma_{\mu\nu} \sigma_a u_R^j) + \text{h.c.} \right) \end{aligned}$$

$$\begin{aligned}
& + \left(\frac{(C_{dG})_{ij}}{\Lambda^2} G^{A\mu\nu} (\bar{q}_L^i \phi \sigma_{\mu\nu} T_A d_R^j) + \frac{(C_{uG})_{ij}}{\Lambda^2} G^{A\mu\nu} (\bar{q}_L^i \tilde{\phi} \sigma_{\mu\nu} T_A u_R^j) + \text{h.c.} \right) \\
& + \frac{(C_{\phi l}^{(1)})_{ij}}{\Lambda^2} (\phi^\dagger i \overleftrightarrow{D}_\mu \phi) (\bar{l}_L^i \gamma^\mu l_L^j) + \frac{(C_{\phi l}^{(3)})_{ij}}{\Lambda^2} (\phi^\dagger i \overleftrightarrow{D}_\mu^a \phi) (\bar{l}_L^i \gamma^\mu \sigma_a l_L^j) \\
& + \frac{(C_{\phi e})_{ij}}{\Lambda^2} (\phi^\dagger i \overleftrightarrow{D}_\mu \phi) (\bar{e}_R^i \gamma^\mu e_R^j) \\
& + \frac{(C_{\phi q}^{(1)})_{ij}}{\Lambda^2} (\phi^\dagger i \overleftrightarrow{D}_\mu \phi) (\bar{q}_L^i \gamma^\mu q_L^j) + \frac{(C_{\phi q}^{(3)})_{ij}}{\Lambda^2} (\phi^\dagger i \overleftrightarrow{D}_\mu^a \phi) (\bar{q}_L^i \gamma^\mu \sigma_a q_L^j) \\
& + \frac{(C_{\phi u})_{ij}}{\Lambda^2} (\phi^\dagger i \overleftrightarrow{D}_\mu \phi) (\bar{u}_R^i \gamma^\mu u_R^j) + \frac{(C_{\phi d})_{ij}}{\Lambda^2} (\phi^\dagger i \overleftrightarrow{D}_\mu \phi) (\bar{d}_R^i \gamma^\mu d_R^j) \\
& + \frac{(C_{\phi ud})_{ij}}{\Lambda^2} (\tilde{\phi}^\dagger i \overleftrightarrow{D}_\mu \phi) (\bar{u}_R^i \gamma^\mu d_R^j).
\end{aligned} \tag{3}$$

The hermitian derivatives \overleftrightarrow{D} and \overleftrightarrow{D}^a are defined as:

$$\overleftrightarrow{D}_\mu \equiv \overrightarrow{D}_\mu - \overleftarrow{D}_\mu$$

and

$$\overleftrightarrow{D}_\mu^a \equiv \sigma_a \overrightarrow{D}_\mu - \overleftarrow{D}_\mu \sigma_a,$$

with $D_\mu = \partial_\mu - ig' B_\mu Y - ig W_\mu^a T_a - ig_s G_\mu^A T_A$, and Y , T_a , T_A the hypercharge and $SU(2)_L$ and $SU(3)_c$ generators, respectively, and σ_a the Pauli matrices. The symbols $B_{\mu\nu}$, $W_{\mu\nu}^a$ and $G_{\mu\nu}^A$ denote the corresponding SM gauge-boson field strengths. Finally, for the scalar doublet, $\tilde{\phi} = i\sigma_2 \phi^*$. In the fermionic operators, summation over the flavour indices is implicit. In practice, only diagonal entries will contribute to most of the observables we will consider.

The previous set of interactions do not include any purely bosonic CP-odd operator. These will be relevant for the discussion in Section 7 and are also listed here for completeness:

$$\begin{aligned}
\mathcal{L}_{\text{SMEFT}}^{d=6, \text{CP-odd, bos}} &= \frac{C_{\tilde{W}}}{\Lambda^2} \varepsilon_{abc} \tilde{W}_\mu^{a\nu} W_\nu^{b\rho} W_\rho^{c\mu} + \frac{C_{\tilde{G}}}{\Lambda^2} f_{ABC} \tilde{G}_\mu^{A\nu} G_\nu^{B\rho} G_\rho^{C\mu} \\
&+ \frac{C_{\phi \tilde{B}}}{\Lambda^2} \phi^\dagger \phi \tilde{B}_{\mu\nu} B^{\mu\nu} + \frac{C_{\phi \tilde{W}}}{\Lambda^2} \phi^\dagger \phi \tilde{W}_{\mu\nu}^a W^{a\mu\nu} + \frac{C_{\phi \tilde{W} B}}{\Lambda^2} \phi^\dagger \sigma_a \phi \tilde{W}_{\mu\nu}^a B^{\mu\nu} \\
&+ \frac{C_{\phi \tilde{G}}}{\Lambda^2} \phi^\dagger \phi \tilde{G}_{\mu\nu}^A G^{A\mu\nu},
\end{aligned} \tag{4}$$

with $\tilde{X}_{\mu\nu} = \frac{1}{2} \varepsilon_{\mu\nu\sigma\rho} X^{\sigma\rho}$ the Hodge dual of the corresponding field-strength tensors.

For the electroweak Z -pole and diboson observables, and most of the Higgs processes considered here, four-fermion operators do not contribute or are expected to have negligible effects under the resonances. The exceptions are $t\bar{t}H$ and, if one chooses G_F as part of the SM electroweak input parameters, as we will do here, the four-lepton operator $(\bar{l}_L\gamma^\mu l_L)(\bar{l}_L\gamma_\mu l_L)$. In the studies presented in this report, however, we will also consider the constraints induced by 2 to 2 fermion processes, in which case contact interactions between four fermions need to be considered. Those relevant at future lepton colliders are:

$$\begin{aligned}
\mathcal{L}_{\text{SMEFT}}^{d=6,\ell^2\psi^2} \supset & \frac{(C_{ll})_{ijkl}}{\Lambda^2} (\bar{l}_L^i\gamma^\mu l_L^j) (\bar{l}_L^k\gamma_\mu l_L^l) \\
& + \frac{(C_{lq}^{(1)})_{ijkl}}{\Lambda^2} (\bar{l}_L^i\gamma^\mu l_L^j) (\bar{q}_L^k\gamma_\mu q_L^l) + \frac{(C_{lq}^{(3)})_{ijkl}}{\Lambda^2} (\bar{l}_L^i\gamma^\mu\sigma_a l_L^j) (\bar{q}_L^k\gamma_\mu\sigma_a q_L^l) \\
& + \frac{(C_{ee})_{ijkl}}{\Lambda^2} (\bar{e}_R^i\gamma^\mu e_R^j) (\bar{e}_R^k\gamma_\mu e_R^l) \\
& + \frac{(C_{eu})_{ijkl}}{\Lambda^2} (\bar{e}_R^i\gamma^\mu e_R^j) (\bar{u}_R^k\gamma_\mu u_R^l) + \frac{(C_{ed})_{ijkl}}{\Lambda^2} (\bar{e}_R^i\gamma^\mu e_R^j) (\bar{d}_R^k\gamma_\mu d_R^l) \\
& + \frac{(C_{le})_{ijkl}}{\Lambda^2} (\bar{l}_L^i\gamma^\mu l_L^j) (\bar{e}_R^k\gamma_\mu e_R^l) + \frac{(C_{qe})_{ijkl}}{\Lambda^2} (\bar{q}_L^i\gamma^\mu q_L^j) (\bar{e}_R^k\gamma_\mu e_R^l) \\
& + \frac{(C_{lu})_{ijkl}}{\Lambda^2} (\bar{l}_L^i\gamma^\mu l_L^j) (\bar{u}_R^k\gamma_\mu u_R^l) + \frac{(C_{ld})_{ijkl}}{\Lambda^2} (\bar{l}_L^i\gamma^\mu l_L^j) (\bar{d}_R^k\gamma_\mu d_R^l) \\
& + \frac{(C_{lequ})_{ijkl}}{\Lambda^2} (\bar{l}_L^i e_R^j) i\sigma_2 (\bar{q}_L^k T u_R^l) + \frac{(C_{ledu})_{ijkl}}{\Lambda^2} (\bar{l}_L^i\sigma^{\mu\nu} e_R^j) i\sigma_2 (\bar{q}_L^k T \sigma_{\mu\nu} u_R^l) \\
& + \frac{(C_{ledq})_{ijkl}}{\Lambda^2} (\bar{l}_L^i e_R^j) (\bar{d}_R^k q_L^l), \tag{5}
\end{aligned}$$

where T denotes the transpose in the $SU(2)_L$ indices and, again, summation over flavour indices is understood. We will also include results pertaining the limits that can be obtained from Top processes at the HL-LHC, so we also need to consider the following relevant four-quark operators

$$\begin{aligned}
\mathcal{L}_{\text{SMEFT}}^{d=6,q^4} \supset & \frac{(C_{qq}^{(1)})_{ijkl}}{\Lambda^2} (\bar{q}_L^i\gamma^\mu q_L^j) (\bar{q}_L^k\gamma_\mu q_L^l) + \frac{(C_{qq}^{(3)})_{ijkl}}{\Lambda^2} (\bar{q}_L^i\gamma^\mu\sigma_a q_L^j) (\bar{q}_L^k\gamma_\mu\sigma_a q_L^l) \\
& + \frac{(C_{uu})_{ijkl}}{\Lambda^2} (\bar{u}_R^i\gamma^\mu u_R^j) (\bar{u}_R^k\gamma_\mu u_R^l) + \frac{(C_{ud}^{(8)})_{ijkl}}{\Lambda^2} (\bar{u}_R^i\gamma^\mu T_A u_R^j) (\bar{d}_R^k\gamma_\mu T_A d_R^l) \\
& + \frac{(C_{qu}^{(8)})_{ijkl}}{\Lambda^2} (\bar{q}_L^i\gamma^\mu T_A q_L^j) (\bar{u}_R^k\gamma_\mu T_A u_R^l) + \frac{(C_{qd}^{(8)})_{ijkl}}{\Lambda^2} (\bar{q}_L^i\gamma^\mu T_A q_L^j) (\bar{d}_R^k\gamma_\mu T_A d_R^l), \tag{6}
\end{aligned}$$

where we only considered those that can interfere with the SM QCD contributions. For the Top constraints we will follow the recommendations of [6] and then express the results in terms of the combinations of Wilson coefficients reported in Table 1.

Coefficients fitted in the top-quark processes			
2-quark	$C_{tG} = (C_{uG})_{33}$ $C_{\phi t} = (C_{\phi u})_{33}$ -	$C_{\phi Q}^3 = \left(C_{\phi q}^{(3)}\right)_{33}$ $C_{\phi b} = (C_{\phi d})_{33}$ $C_{t\phi} = (C_{u\phi})_{33}$	$C_{\phi Q}^- = \left(C_{\phi q}^{(1)}\right)_{33} - \left(C_{\phi q}^{(3)}\right)_{33}$ $C_{tZ} = \cos\theta_w(C_{uW})_{33} - \sin\theta_w(C_{uB})_{33}$ $C_{tW} = (C_{uW})_{33}$
4-quark	$C_{tu}^8 = \sum_{i=1,2} 2(C_{uu})_{i33i}$ $C_{Qu}^8 = \sum_{i=1,2} \left(C_{qu}^{(8)}\right)_{33ii}$ -	$C_{td}^8 = \sum_{i=1,2,3} \left(C_{ud}^{(8)}\right)_{33ii}$ $C_{Qd}^8 = \sum_{i=1,2,3} \left(C_{qd}^{(8)}\right)_{33ii}$ -	$C_{Qq}^{1,8} = \sum_{i=1,2} \left(\left(C_{qq}^{(1)}\right)_{i33i} + 3 \left(C_{qq}^{(3)}\right)_{i33i} \right)$ $C_{Qq}^{3,8} = \sum_{i=1,2} \left(\left(C_{qq}^{(1)}\right)_{i33i} - \left(C_{qq}^{(3)}\right)_{i33i} \right)$ $C_{tq}^8 = \sum_{i=1,2} \left(C_{qu}^{(8)}\right)_{ii33}$
2-quark 2-lepton	$C_{eb} = (C_{ed})_{1133}$ $C_{lb} = (C_{ld})_{1133}$ -	$C_{et} = (C_{eu})_{1133}$ $C_{lt} = (C_{lu})_{1133}$ -	$C_{lQ}^+ = \left(C_{lq}^{(1)}\right)_{1133} + \left(C_{lq}^{(3)}\right)_{1133}$ $C_{lQ}^- = \left(C_{lq}^{(1)}\right)_{1133} - \left(C_{lq}^{(3)}\right)_{1133}$ $C_{eQ} = (C_{qe})_{3311}$

Table 1: Here we present the Wilson coefficients that have been fitted in our top-quark analysis in terms of those of Eqs. (3),(5) and (6). The first block are related with the 2-quark operators, the second block are related with the 4-quark operators and the last block is related with the 2-quark 2-lepton operators.

2.1 Effective Lagrangian in the mass eigenstate basis

After electroweak symmetry breaking and upon writing the Lagrangian in the physical basis, the dimension-six operator introduced above give rise to both modifications of the SM interactions as well as to new terms not present in the SM Lagrangian. Following [7], using the $\{\alpha, M_Z, G_F\}$ input scheme, putting our focus on the electroweak and Higgs interactions, and restricting to CP-even interactions for the moment, the effective Lagrangian including dimension-6 terms contain the following pieces:

- **Higgs couplings to vector bosons:**

$$\begin{aligned}
\Delta\mathcal{L}_6^{\text{hVV}} = & \frac{h}{v} \left[2\delta c_W m_W^2 W_\mu^+ W^{-\mu} + \delta c_Z m_Z^2 Z_\mu Z^\mu \right. \\
& + c_{WW} \frac{g^2}{2} W_{\mu\nu}^+ W^{-\mu\nu} + c_{W\Box} g^2 (W^{-\mu} \partial^\nu W_{\mu\nu}^+ + \text{h.c.}) \\
& + c_{gg} \frac{g_s^2}{4} G_{\mu\nu}^A G^{A\mu\nu} + c_{\gamma\gamma} \frac{e^2}{4} A_{\mu\nu} A^{\mu\nu} + c_{Z\gamma} \frac{e\sqrt{g^2 + g'^2}}{2} Z_{\mu\nu} A^{\mu\nu} + c_{ZZ} \frac{g^2 + g'^2}{4} Z_{\mu\nu} Z^{\mu\nu} \\
& \left. + c_{Z\Box} g^2 Z^\mu \partial^\nu Z_{\mu\nu} + c_{\gamma\Box} g g' Z^\mu \partial^\nu A_{\mu\nu} \right], \tag{7}
\end{aligned}$$

where only c_{gg} , δc_Z , $c_{\gamma\gamma}$, $c_{Z\gamma}$, c_{ZZ} , $c_{Z\Box}$ are independent parameters:

$$\begin{aligned}
\delta c_W &= \delta c_Z + 4\delta m, \\
c_{WW} &= c_{ZZ} + 2\sin^2\theta_w c_{Z\gamma} + \sin^4\theta_w c_{\gamma\gamma}, \\
c_{W\Box} &= \frac{1}{g^2 - g'^2} [g^2 c_{Z\Box} + g'^2 c_{ZZ} - e^2 \sin^2\theta_w c_{\gamma\gamma} - (g^2 - g'^2) \sin^2\theta_w c_{Z\gamma}], \\
c_{\gamma\Box} &= \frac{1}{g^2 - g'^2} [2g^2 c_{Z\Box} + (g^2 + g'^2) c_{ZZ} - e^2 c_{\gamma\gamma} - (g^2 - g'^2) c_{Z\gamma}], \tag{8}
\end{aligned}$$

with θ_w the weak mixing angle and the parameter δm contains the dimension-6 contributions to M_W with respect to the SM value,

$$\Delta\mathcal{L}_{W,Z}^{\text{mass}} = \frac{(g^2 + g'^2)v^2}{8} Z_\mu Z^\mu + \frac{g^2 v^2}{4} (1 + \delta m)^2 W_\mu^+ W^{-\mu}. \tag{9}$$

- **Trilinear Gauge Couplings:**

$$\begin{aligned}
\Delta\mathcal{L}^{\text{aTGC}} = & ie\delta\kappa_\gamma A^{\mu\nu} W_\mu^+ W_\nu^- + ig \cos\theta_w [\delta g_{1,Z} (W_{\mu\nu}^+ W^{-\mu} - W_{\mu\nu}^- W^{+\mu}) Z^\nu \\
& + (\delta g_{1,Z} - \frac{g'^2}{g^2} \delta\kappa_\gamma) Z^{\mu\nu} W_\mu^+ W_\nu^-] \\
& + \frac{ig\lambda_Z}{m_W^2} (\sin\theta_w W_\mu^{+\nu} W_\nu^{-\rho} A_\rho^\mu + \cos\theta_w W_\mu^{+\nu} W_\nu^{-\rho} Z_\rho^\mu), \tag{10}
\end{aligned}$$

where two of the three coefficients, $\delta g_{1,Z}$ and $\delta\kappa_\gamma$ depend on c_{gg} , δc_Z , $c_{\gamma\gamma}$, $c_{Z\gamma}$, c_{ZZ} , $c_{Z\Box}$:

$$\begin{aligned}
\delta g_{1,Z} &= \frac{1}{2}(g^2 - g'^2) [c_{\gamma\gamma} e^2 g'^2 + c_{Z\gamma} (g^2 - g'^2) g'^2 - c_{ZZ} (g^2 + g'^2) g'^2 - c_{Z\Box} (g^2 + g'^2) g^2], \\
\delta\kappa_\gamma &= -\frac{g^2}{2} \left(c_{\gamma\gamma} \frac{e^2}{g^2 + g'^2} + c_{Z\gamma} \frac{g^2 - g'^2}{g^2 + g'^2} - c_{ZZ} \right), \tag{11}
\end{aligned}$$

while λ_Z is an independent parameter. Quartic gauge couplings also receive contributions in the effective Lagrangian but, to dimension 6, they are always connected to the trilinear ones.

- **Yukawa couplings:**

$$\Delta\mathcal{L}_6^{\text{hff}} = -\frac{h}{v} \sum_{f \in u,d,e} \hat{\delta}y_f m_f \bar{f}f + \text{h.c.}, \quad (12)$$

where $\hat{\delta}y_f m_f$ should be thought as 3×3 matrices in flavour space. FCNC are avoided when $\hat{\delta}y_f$ is diagonal in the same basis as m_f . Note that once we include dimension-6 contributions, the SM relation between the fermion masses and Yukawa interactions no longer holds and these are two sets of independent parameters.

- **Vector couplings to fermions:** while corrections to the QED and QCD vertices are protected by gauge invariance, the electroweak interactions of fermions Vff ($V = Z, W$) are modified at dimension 6. These modifications are directly related to contact interactions of the form $hVff$:

$$\begin{aligned} \Delta\mathcal{L}_6^{\text{Vff,hVff}} &= \frac{g}{\sqrt{2}} \left(1 + 2\frac{h}{v}\right) W_\mu^+ \left(\hat{\Delta}g_{W,L}^\ell \bar{\nu}_L \gamma^\mu e_L + \hat{\Delta}g_{W,L}^q \bar{u}_L \gamma^\mu d_L + \hat{\Delta}g_{W,R}^q \bar{u}_R \gamma^\mu d_R + \text{h.c.} \right) \\ &+ \sqrt{g^2 + g'^2} \left(1 + 2\frac{h}{v}\right) Z_\mu \left[\sum_{f=u,d,e,\nu} \hat{\Delta}g_{Z,L}^f \bar{f}_L \gamma^\mu f_L + \sum_{f=u,d,e} \hat{\Delta}g_{Z,R}^f \bar{f}_R \gamma^\mu f_R \right]. \end{aligned} \quad (13)$$

The $\hat{\Delta}g_{X,L/R}^Y$ are, again, 3×3 matrices in flavor space and parameterize, in particular, *absolute* modifications of the EW couplings. Also, not all terms in the previous equation are independent and the following relations hold to dimension 6:

$$\hat{\Delta}g_W^\ell = \hat{\Delta}g_{Z,L}^\nu - \hat{\Delta}g_{Z,L}^e, \quad \hat{\Delta}g_{W,L}^q = \hat{\Delta}g_{Z,L}^u V_{\text{CKM}} - V_{\text{CKM}} \hat{\Delta}g_{Z,L}^d, \quad (14)$$

with V_{CKM} the *Cabibbo-Kobayashi-Maskawa* (CKM) matrix which, unless otherwise is stated, we approximate to the identity matrix.

2.2 Effective couplings

As done in [8, 9], some of the results will be presented, not in terms of the Wilson coefficients of the manifestly gauge-invariant operators, but in terms of pseudo-observable quantities, referred to as *effective Higgs and electroweak couplings*, computed from physical observables and thus, independent of the basis one could have chosen for the dimension-6 Lagrangian. This is done by performing the fit *internally* in terms of the Wilson coefficients and then, from the posterior of the fit, compute the posterior prediction for the quantities

$$g_{HX}^{\text{eff}^2} \equiv \frac{\Gamma_{H \rightarrow X}}{\Gamma_{H \rightarrow X}^{\text{SM}}}. \quad (15)$$

for the *Higgs effective couplings*, or the quantities $g_{Zff,L/R}^{\text{eff}}$ for the *electroweak effective couplings*, defined from:

$$\Gamma_{Z \rightarrow e^+ e^-} = \frac{\alpha M_Z}{6 \sin^2 \theta_w \cos^2 \theta_w} (|g_{Zee,L}^{\text{eff}}|^2 + |g_{Zee,R}^{\text{eff}}|^2), \quad A_e = \frac{|g_{Zee,L}^{\text{eff}}|^2 - |g_{Zee,R}^{\text{eff}}|^2}{|g_{Zee,L}^{\text{eff}}|^2 + |g_{Zee,R}^{\text{eff}}|^2}. \quad (16)$$

Note that the definition in Eq. (15) is not phenomenologically possible for the top-Higgs coupling and the Higgs self-interaction. Being aware of this, for presentational purpose we will nevertheless still apply similar definition for g_{Htt}^{eff} . To further connect with diboson processes, and even though they are technically not pseudo-observables, we will also use the aTGC $\delta g_{1,Z}$, $\delta \kappa_\gamma$ and λ_Z . Finally, we use $g_{HHH} \equiv \lambda_3/\lambda_3^{\text{SM}}$, to describe modifications of the Higgs self coupling.

In the results presented below, we will report the expected sensitivities to relative modifications of these effective couplings with respect to the SM values, whenever these are non-zero. Such relative shifts are always indicated by the symbol δ , whereas absolute shifts will be indicated with Δ , i.e., given a quantity X :

$$\Delta X \equiv X - X_{\text{SM}}, \quad \delta X \equiv \frac{\Delta X}{X_{\text{SM}}}. \quad (17)$$

For instance, in this notation, the new physics contributions to the effective couplings between fermions and electroweak bosons are given by:

$$\delta g_{V,L/R}^{ff} \equiv \frac{(\hat{\Delta} g_{V,L/R}^f)_{ff}}{g_{V,L/R}^{f,\text{SM}}}. \quad (18)$$

Whenever a given quantity is zero in the SM, e.g. λ_Z or any of the Wilson coefficients C_i , the sensitivity will be reported directly on the parameter.

3 Recap on SMEFT fits for ESG

Global fits of the data expected at HL-LHC and future colliders have been carried out in the context of the 2020 European Strategy Update for Particle Physics [9] with a special emphasis on the Higgs sector. One key question addressed was the sensitivity of the various colliders to the deformations of the Higgs couplings to the different SM particles compared to their values predicted robustly in SM itself. These fits relied on the measurements of the Higgs production cross section times its decay branching ratios in the different channels. Two different approaches, as model-independent as possible, were adopted. On the one hand, in the κ -framework, it is assumed that the structure of the Higgs interactions remain identical to the SM one. While

rather simple and adequate to capture dominant effects in well-motivated New Physics scenarios like composite Higgs models, this approach lacks some generality and makes it difficult to fully exploit information collected away from the Higgs pole and is not easily amenable to a full inclusion of quantum higher-order corrections. The more general Effective Field Theory approach aims to remedy these limitations and to fully capture all possible effects generated by new heavy degrees of freedom.

The ESU fits made use of only inclusive cross section times branching ratio measurements (or even ratios thereof), omitting precious kinematic information, like Higgs transverse momentum distribution, which could reveal higher sensitivity to New Physics but requires more detailed estimates of the theoretical uncertainties.

The resulting fits have been produced using the fitting framework of the HEPfit package [10], a general tool to combine information from direct and indirect searches and test the Standard Model. It used the Markov-Chain Monte-Carlo implementation provided by the Bayesian Analysis Toolkit [11–13], to perform a Bayesian statistical analysis of the sensitivity to deformations from the SM at the different future collider projects. The experimental projections for the different observables included in the fits have been implemented in the likelihood assuming Gaussian distributions, with SM central values and standard deviations given by the corresponding projected uncertainties estimated by the different future collider projects. Finally, theory uncertainties, when included, were introduced via nuisance parameters with Gaussian priors. Intrinsic theory uncertainties, arising from missing higher-order corrections, were not included, while parametric theory uncertainties arising from the propagation of experimental errors on SM parameters have been properly taken into account. Experimental uncertainties accounted for statistical uncertainties and the estimated experimental systematic uncertainties, as well as background theory uncertainties and signal-acceptance related theory uncertainties.

Four benchmark scenarios for the κ analyses: the kappa-0 benchmark assumed that there exist no light BSM particles to which the Higgs boson can decay; the kappa-1,2 benchmarks considered possible new BSM Higgs decays and explored their impact on the determination of the Higgs width, i.e. the absolute normalisation of all the Higgs couplings. Finally, in the kappa-3 benchmark, the combination of the HL-LHC data with each of the future accelerators were studied. The results are summarised in Figure 1.

For the EFT analyses, a set of assumptions were made to reduce the set of operators considered to 18 and 30 independent parameters for two specific flavour scenarios: (1) flavour universality, or linear minimal flavour violation, where the only sources of violation of the maximal flavour symmetry group originate from the Yukawa matrices; (2) neutral diagonality where all the new physics flavour interactions remain diagonal in the same basis as the Yukawa matrices. Additionally, it was considered that the vast subset of 4-fermion operators, with the only exception of the one that

contributes to the muon decay and thus directly affects the Fermi constant, could be more strongly constrained by other processes and were thus omitted. It was further argued that all the dipole operators should exhibit the same chiral suppression of the Yukawa couplings and could be safely ignored, at least for the light quarks. For the sake of simplicity, the top quark dipole operators were not considered, even though their effects could be relevant.

To assess the New Physics deformations with respect to the SM in a operator-basis independent way, the results of the SMEFT fit were projected onto a set of Higgs effective couplings capturing the on-shell properties of the Higgs boson, defined exactly as those presented in Section 2.2. Detailed results are reported in the report [9]. The results for the more general neutral diagonality flavour scenario are also shown in Figure 2 where the results are compared across colliders, emphasising the relative improvement compared to the HL-LHC results.

4 Input measurements

The inputs observables and their measurement uncertainties that will be needed in following global fits are summarized in this section. The projections at future colliders are taken mainly from corresponding collider collaborations (HL-LHC/ILC/CLIC/FCC-ee/CEPC/MuC) as well as the reports compiled by Energy Frontier Topical Groups (EF01/03/04) [14–16]. Collider scenarios considered in this work are summarized in Tab. 2. In a few places where the needed inputs are missing, we carried out our own analysis to give consistent projections for all colliders. The details are explained in the following.

4.1 Electroweak Precision Measurements

The observables related to precision measurements of Z properties include following: mass (m_Z), total width (Γ_Z), left-right asymmetry (A_f) as defined in Eq. 16 for $f = b, c, e, \mu, \tau$, partial decay width relative to the total hadronic width (R_f), and the total hadronic cross section of $e^+e^- \rightarrow Z \rightarrow hadrons$ (σ_{had}^0). The projections of their uncertainties now at future e^+e^- are listed in Tab. 3, broken down into statistical error and experimental systematic error in most cases. The numbers for FCC-ee, CEPC and ILC-GigaZ are based on a dedicated Z -pole run, while the ones for ILC250 and CLIC380 are based on radiative return events available at 250 GeV and 380 GeV run respectively. Note that the consistency on common systematic errors has improved significantly comparing to the numbers for ESG; see more details in the EF04 report. The observables W mass (m_W), W total width (Γ_W), Higgs mass (m_H) and fine-structure constant ($\alpha(m_Z)^{-1}$) are also listed in Tab. 3. The other useful observables related to W branching ratios are implicitly included in the optimal observables

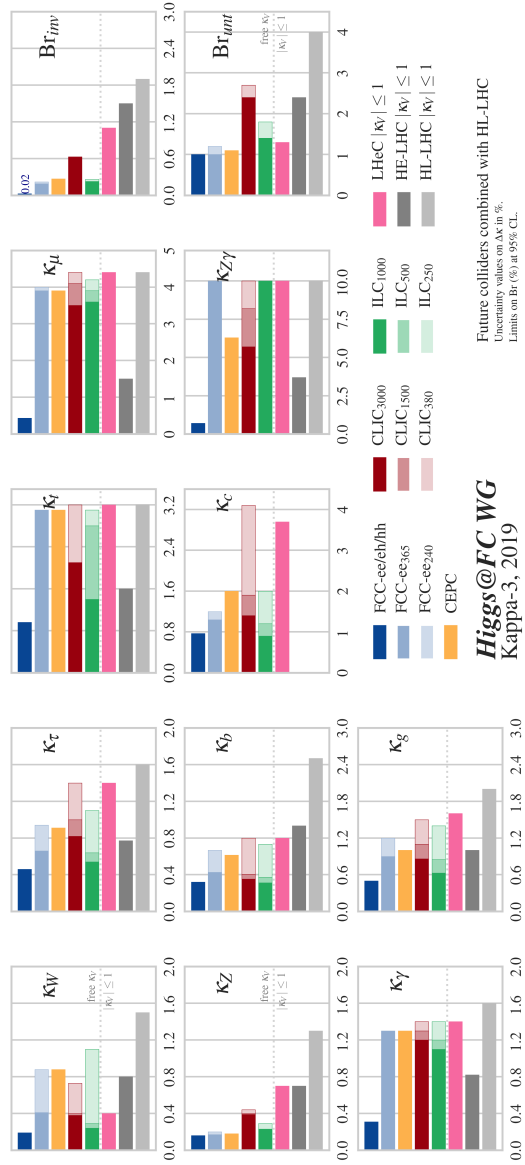


Figure 1: Expected relative precision (%) of the κ parameters in the kappa-3 scenario

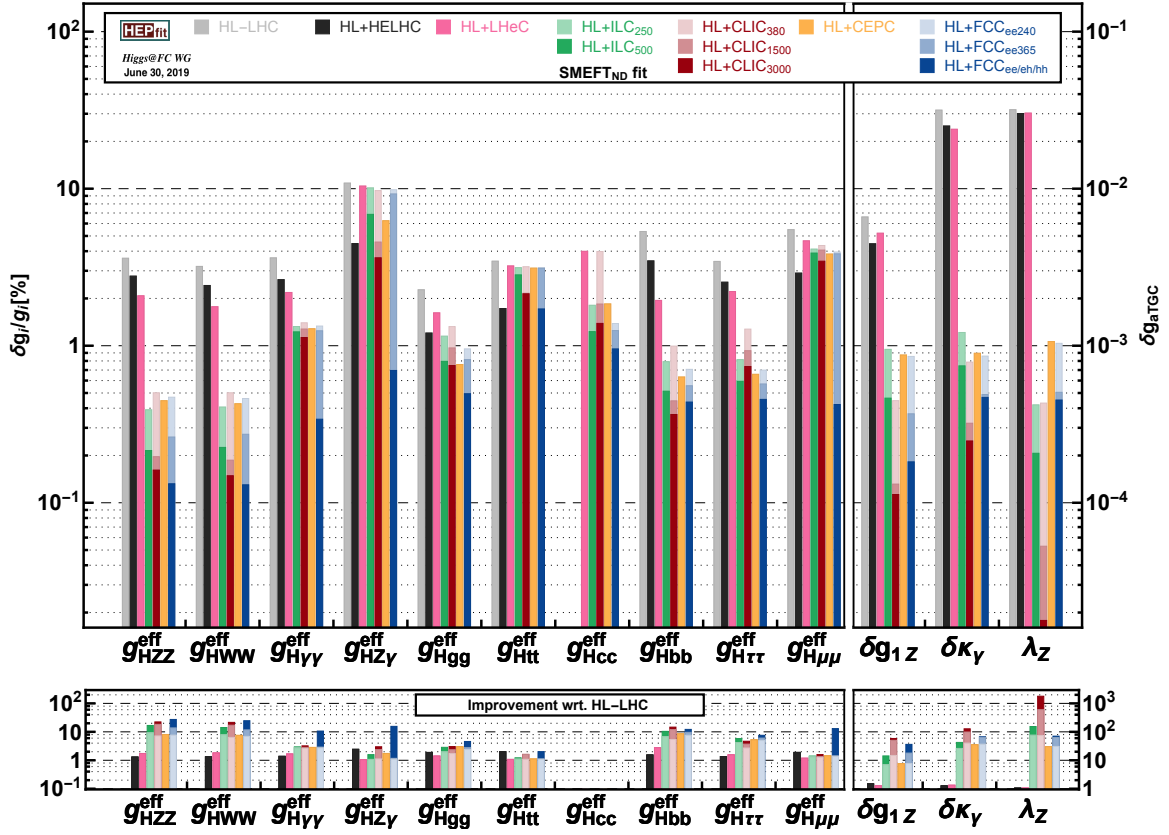


Figure 2: Sensitivity at 68% probability to deviations in the different effective Higgs couplings and aTGC from a global fit to the projections available at each future collider project.

Machine	Pol. (e^-, e^+)	Energy	Luminosity	Reference
HL-LHC	Unpolarised	14 TeV	3 ab ⁻¹	[17]
ILC	($\mp 80\%$, $\pm 30\%$)	250 GeV	2 ab ⁻¹	[18]
		350 GeV	0.2 ab ⁻¹	
	500 GeV	4 ab ⁻¹		
	($\mp 80\%$, $\pm 20\%$)	1 TeV	8 ab ⁻¹	
CLIC	($\pm 80\%$, 0%)	380 GeV	1 ab ⁻¹	[19]
		1.5 TeV	2.5 ab ⁻¹	
		3 TeV	5 ab ⁻¹	
FCC- <i>ee</i>	Unpolarised	Z-pole	150 ab ⁻¹	[20]
		$2m_W$	10 ab ⁻¹	
		240 GeV	5 ab ⁻¹	
		350 GeV	0.2 ab ⁻¹	
		365 GeV	1.5 ab ⁻¹	
CEPC	Unpolarised	Z-pole	100 ab ⁻¹	[21]
		$2m_W$	6 ab ⁻¹	
		240 GeV	20 ab ⁻¹	
		350 GeV	0.2 ab ⁻¹	
		360 GeV	1 ab ⁻¹	
MuC	Unpolarised	125 GeV	0.02 ab ⁻¹	[22, 23]
		3 TeV	3 ab ⁻¹	
		10 TeV	10 ab ⁻¹	

Table 2: Future collider scenarios considered in this work.

Quantity	current	ILC250	ILC-GigaZ	FCC-ee	CEPC	CLIC380
$\Delta\alpha(m_Z)^{-1} (\times 10^3)$	17.8*	17.8*		3.8 (1.2)	17.8*	
Δm_W (MeV)	12*	0.5 (2.4)		0.25 (0.3)	0.35 (0.3)	
Δm_Z (MeV)	2.1*	0.7 (0.2)	0.2	0.004 (0.1)	0.005 (0.1)	2.1*
Δm_H (MeV)	170*	14		2.5 (2)	5.9	78
$\Delta\Gamma_W$ (MeV)	42*	2		1.2 (0.3)	1.8 (0.9)	
$\Delta\Gamma_Z$ (MeV)	2.3*	1.5 (0.2)	0.12	0.004 (0.025)	0.005 (0.025)	2.3*
$\Delta A_e (\times 10^5)$	190*	14 (4.5)	1.5 (8)	0.7 (2)	1.5	64
$\Delta A_\mu (\times 10^5)$	1500*	82 (4.5)	3 (8)	2.3 (2.2)	3.0 (1.8)	400
$\Delta A_\tau (\times 10^5)$	400*	86 (4.5)	3 (8)	0.5 (20)	1.2 (6.9)	570
$\Delta A_b (\times 10^5)$	2000*	53 (35)	9 (50)	2.4 (21)	3 (21)	380
$\Delta A_c (\times 10^5)$	2700*	140 (25)	20 (37)	20 (15)	6 (30)	200
$\Delta\sigma_{\text{had}}^0$ (pb)	37*			0.035 (4)	0.05 (2)	37*
$\delta R_e (\times 10^3)$	2.4*	0.5 (1.0)	0.2 (0.5)	0.004 (0.3)	0.003 (0.2)	2.7
$\delta R_\mu (\times 10^3)$	1.6*	0.5 (1.0)	0.2 (0.2)	0.003 (0.05)	0.003 (0.1)	2.7
$\delta R_\tau (\times 10^3)$	2.2*	0.6 (1.0)	0.2 (0.4)	0.003 (0.1)	0.003 (0.1)	6
$\delta R_b (\times 10^3)$	3.0*	0.4 (1.0)	0.04 (0.7)	0.0014 (< 0.3)	0.005 (0.2)	1.8
$\delta R_c (\times 10^3)$	17*	0.6 (5.0)	0.2 (3.0)	0.015 (1.5)	0.02 (1)	5.6

Table 3: EWPOs at future e^+e^- : statistical error (experimental systematic error). Δ (δ) stands for absolute (relative) uncertainty, while * indicates inputs taken from current data [24]. See Refs. [9, 18, 21, 25–27].

that will be explained in Sec. 4.5. Additional electroweak observables above or below Z -pole that are relevant to 4-fermion interactions will be explained in Sec. 6.

4.2 Higgs Measurements

The observables related to measurement of Higgs properties include mostly the production cross section times decay branching ratio ($\sigma \times BR_X$) for various production and decay channels. One exception is the inclusive production cross section measurement for $e^+e^- \rightarrow ZH$, which is enabled by recoil mass technique at lepton colliders. Observables for differential cross sections are not included. The projections of Higgs measurements are listed in Tab. 4 for HL-LHC, Tab. 5-13 for future e^+e^- , and Tab. 14-16 for muon colliders. Note that in some cases two sets of numbers are provided for each observable. Numbers without parentheses are directly provided by collider collaborations, which the final fit results will be based on. However there are often subtle inconsistency between different projections for similar observables due to different level of realism that was adopted in the relevant simulation analyses. Apparently those types of difference should not bring bias to the true capabilities of

different future colliders. In order to allow us to isolate out those differences, we also provide uncertainties in parentheses that are extrapolated from a same set of analyses, which are mostly from ILC full detector simulation studies*. This can provide us a clue to understand the difference in final results. In fact one can see from the tables that two sets of inputs are rather consistent in most cases. It often happens that the list of input observables directly provided by collaborations is not complete. Whenever that happens we try to fill out the missing inputs by extrapolations. This further helps isolate out certain biases in the comparison. One such example which plays a quantitatively important role is the branching ratio of $H \rightarrow \gamma Z$.

HL-LHC	3 ab ⁻¹ ATLAS+CMS				
Prod.	ggH	VBF	WH	ZH	ttH
σ	-	-	-	-	-
$\sigma \times BR_{bb}$	19.1	-	8.3	4.6	10.7
$\sigma \times BR_{cc}$	-	-	-	-	-
$\sigma \times BR_{gg}$	-	-	-	-	-
$\sigma \times BR_{ZZ}$	2.5	9.5	32.1	58.3	15.2
$\sigma \times BR_{WW}$	2.5	5.5	9.9	12.8	6.6
$\sigma \times BR_{\tau\tau}$	4.5	3.9	-	-	10.2
$\sigma \times BR_{\gamma\gamma}$	2.5	7.9	9.9	13.2	5.9
$\sigma \times BR_{\gamma Z}$	24.4	51.2	-	-	-
$\sigma \times BR_{\mu\mu}$	11.1	30.7	-	-	-
$\sigma \times BR_{inv.}$	-	2.5	-	-	-
Δm_H	10-20 MeV	-	-	-	-

Table 4: Projected uncertainties of Higgs observables at HL-LHC: numbers by default in %.

4.3 Light fermion pair measurements

The input observables for $e^-e^+ \rightarrow f\bar{f}$ ($f = e, \mu, \tau, c, b$) at $\sqrt{s} \gg m_Z$ are summarized in Tables 17-28, these are later used in Section 6 for the 4-fermion fit. The uncertainties for the total cross sections σ_f and the forward-backward asymmetries A_{FB}^f are obtained from a common analysis using optimal observable method for all future e^+e^- . The efficiencies used in the analysis were taken from ILD full simulation

*This doesn't mean the extrapolated uncertainties are more accurate, but provides a way of comparing the capabilities of future colliders in a more equal footing.

ILC250	0.9ab ⁻¹ (-0.8,+0.3)		0.9ab ⁻¹ (+0.8,-0.3)	
Prod.	ZH	$\nu\nu H$	ZH	$\nu\nu H$
σ	1.07	-	1.07	-
$\sigma \times BR_{bb}$	0.714	4.27	0.714	17.4
$\sigma \times BR_{cc}$	4.38	-	4.38	-
$\sigma \times BR_{gg}$	3.69	-	3.69	-
$\sigma \times BR_{ZZ}$	9.49	-	9.49	-
$\sigma \times BR_{WW}$	2.43	-	2.43	-
$\sigma \times BR_{\tau\tau}$	1.7	-	1.7	-
$\sigma \times BR_{\gamma\gamma}$	17.9	-	17.9	-
$\sigma \times BR_{\gamma Z}$	63	-	59	-
$\sigma \times BR_{\mu\mu}$	37.9	-	37.9	-
$\sigma \times BR_{inv.}$	0.336	-	0.277	-

Table 5: Projected uncertainties of Higgs observables at ILC250: numbers by default in %.

	FCCee240 5ab ⁻¹		CEPC240 20ab ⁻¹	
Prod.	ZH	$\nu\nu H$	ZH	$\nu\nu H$
σ	0.5(0.537)	-	0.26	-
$\sigma \times BR_{bb}$	0.3(0.380)	3.1(2.78)	0.14	1.59
$\sigma \times BR_{cc}$	2.2(2.08)	-	2.02	-
$\sigma \times BR_{gg}$	1.9(1.75)	-	0.81	-
$\sigma \times BR_{ZZ}$	4.4(4.49)	-	4.17	-
$\sigma \times BR_{WW}$	1.2(1.16)	-	0.53	-
$\sigma \times BR_{\tau\tau}$	0.9(0.822)	-	0.42	-
$\sigma \times BR_{\gamma\gamma}$	9(8.47)	-	3.02	-
$\sigma \times BR_{\gamma Z}$	(17*)	-	8.5	-
$\sigma \times BR_{\mu\mu}$	19(17.9)	-	6.36	-
$\sigma \times BR_{inv.}$	0.3(0.226)	-	0.07	-

Table 6: Projected uncertainties of Higgs observables at FCCee240 and CEPC240: numbers by default in %.

studies [18] all for double-tagged events. However due to insufficient input about systematic errors for all channels and the fact that the technical implementation of

CLIC380	0.5 ab ⁻¹ (-0.8,0)		0.5 ab ⁻¹ (+0.8,0)	
Prod.	ZH	$\nu\nu H$	ZH	$\nu\nu H$
σ	1.5(1.43)	-	1.8(1.43)	-
$\sigma \times BR_{bb}$	0.81(1.2)	1.4(1.47)	0.92(1.2)	4.1(4.4)
$\sigma \times BR_{cc}$	13(8.7)	19(15.3)	15(8.7)	24(46)
$\sigma \times BR_{gg}$	5.7(6.6)	3.3(6.2)	6.5(6.6)	20(18.8)
$\sigma \times BR_{ZZ}$	(19.7)	(16.1)	(19.7)	(46)
$\sigma \times BR_{WW}$	5.1(4.4)	(4.6)	(4.4)	(14)
$\sigma \times BR_{\tau\tau}$	5.9(3.2)	(12.9)	6.6(3.2)	(39)
$\sigma \times BR_{\gamma\gamma}$	(31)	(36)	(31)	(108)
$\sigma \times BR_{\mu\mu}$	(69)	(129)	(69)	(129)
$\sigma \times BR_{inv.}$	0.57(0.68)	-	0.64(0.64)	-

Table 7: Projected uncertainties of Higgs observables at CLIC380: numbers by default in %; numbers in parentheses are extrapolated from ILC350.

ILC350	0.135 ab ⁻¹ (-0.8,+0.3)		0.045 ab ⁻¹ (+0.8,-0.3)	
Prod.	ZH	$\nu\nu H$	ZH	$\nu\nu H$
σ	2.46	-	4.3	-
$\sigma \times BR_{bb}$	2.05	2.46	3.5	17.7
$\sigma \times BR_{cc}$	15	25.9	25.9	186
$\sigma \times BR_{gg}$	11.4	10.5	19.8	75
$\sigma \times BR_{ZZ}$	34	27.2	59	191
$\sigma \times BR_{WW}$	7.6	7.8	13.2	57
$\sigma \times BR_{\tau\tau}$	5.5	21.8	9.4	156
$\sigma \times BR_{\gamma\gamma}$	53	61	92	424
$\sigma \times BR_{\mu\mu}$	118	218	205	1580
$\sigma \times BR_{inv.}$	1.15	-	1.83	-

Table 8: Projected uncertainties of Higgs observables at ILC350: numbers by default in %.

systematic errors in the optimal observable method is unclear at this moment, the uncertainties given in above tables are only statistical. For the ILC uncertainties, the systematics would play a minor role. But for CEPC or FCC-ee, the uncertainties are likely significantly underestimated in particular in the lepton channels. It's worth pointing out one source of the contradictory inputs is about systematic error

	1.5 ab ⁻¹ FCC-ee365		1.0 ab ⁻¹ CEPC360	
Prod.	ZH	$\nu\nu H$	ZH	$\nu\nu H$
σ	0.9(0.84)	-	1.4(1.02)	-
$\sigma \times BR_{bb}$	0.5(0.71)	0.9(1.14)	0.90(0.86)	1.1(1.39)
$\sigma \times BR_{cc}$	6.5(5.0)	10(11.9)	8.8(6.1)	16(14.5)
$\sigma \times BR_{gg}$	3.5(3.8)	4.5(4.8)	3.4(4.7)	4.5(5.9)
$\sigma \times BR_{ZZ}$	12(11.4)	10(12.5)	20(13.9)	21(15.3)
$\sigma \times BR_{WW}$	2.6(2.55)	(3.6)	2.8(3.12)	4.4(4.4)
$\sigma \times BR_{\tau\tau}$	1.8(1.83)	8(10)	2.1(2.24)	4.2(12.2)
$\sigma \times BR_{\gamma\gamma}$	18(17.7)	22(28.1)	11(21.7)	16(34.4)
$\sigma \times BR_{\mu\mu}$	40(40)	(100)	41(48)	57(123)
$\sigma \times BR_{inv.}$	0.60(0.42)	-	(0.49)	-

Table 9: Projected uncertainties of Higgs observables at FCC-ee365 and CEPC360: numbers by default in %; numbers in parentheses are extrapolated from ILC350.

ILC500	1.6 ab ⁻¹ (-0.8,+0.3)		1.6 ab ⁻¹ (+0.8,-0.3)	
Prod.	ZH	$\nu\nu H$	ZH	$\nu\nu H$
σ	1.67	-	1.67	-
$\sigma \times BR_{bb}$	1.01	0.42	1.01	1.52
$\sigma \times BR_{cc}$	7.1	3.48	7.1	14.2
$\sigma \times BR_{gg}$	5.9	2.3	5.9	9.5
$\sigma \times BR_{ZZ}$	13.8	4.8	13.8	19
$\sigma \times BR_{WW}$	3.1	1.36	3.1	5.5
$\sigma \times BR_{\tau\tau}$	2.42	3.9	2.42	15.8
$\sigma \times BR_{\gamma\gamma}$	18.6	10.7	18.6	44
$\sigma \times BR_{\mu\mu}$	47	40	47	166
$\sigma \times BR_{inv.}$	0.83	-	0.60	-

Table 10: Projected uncertainties of Higgs observables at ILC500: numbers by default in %.

for luminosity measurement at similar \sqrt{s} . It is assumed to be 0.01% at FCCee240 while 0.1% at ILC250, one order of magnitude difference. This contradictory systematic errors couldn't get resolved in time. After all we left out systematic errors for 2-fermion observables off the Z -pole.

ILC1000	3.2 ab ⁻¹ (-0.8,+0.2)	3.2 ab ⁻¹ (+0.8,-0.2)
Prod.	$\nu\nu H$	$\nu\nu H$
$\sigma \times BR_{bb}$	0.32	1.0
$\sigma \times BR_{cc}$	1.7	6.4
$\sigma \times BR_{gg}$	1.3	4.7
$\sigma \times BR_{ZZ}$	2.3	8.4
$\sigma \times BR_{WW}$	0.91	3.3
$\sigma \times BR_{\tau\tau}$	1.7	6.4
$\sigma \times BR_{\gamma\gamma}$	4.8	17
$\sigma \times BR_{\mu\mu}$	17	64

Table 11: Projected uncertainties of Higgs observables at ILC1000: numbers by default in %.

CLIC1500	2 ab ⁻¹ (-0.8,0)	0.5 ab ⁻¹ (+0.8,0)
Prod.	$\nu\nu H$	$\nu\nu H$
$\sigma \times BR_{bb}$	0.25	1.5
$\sigma \times BR_{cc}$	3.9	24
$\sigma \times BR_{gg}$	3.3	20
$\sigma \times BR_{ZZ}$	3.6	22
$\sigma \times BR_{WW}$	0.67	4.0
$\sigma \times BR_{\tau\tau}$	2.8	17
$\sigma \times BR_{\gamma\gamma}$	10	60
$\sigma \times BR_{\gamma Z}$	28	170
$\sigma \times BR_{\mu\mu}$	24	150

Table 12: Projected uncertainties of Higgs observables at CLIC1500: numbers by default in %.

4.4 Top-quark measurements

Input observables related to top-quark sector are explained in Sec. 8.

CLIC3000	4 ab ⁻¹ (-0.8,0)	1 ab ⁻¹ (+0.8,0)
Prod.	$\nu\nu H$	$\nu\nu H$
$\sigma \times BR_{bb}$	0.17	1.0
$\sigma \times BR_{cc}$	3.7	22
$\sigma \times BR_{gg}$	2.3	14
$\sigma \times BR_{ZZ}$	2.1	13
$\sigma \times BR_{WW}$	0.33	2.0
$\sigma \times BR_{\tau\tau}$	2.3	14
$\sigma \times BR_{\gamma\gamma}$	5.0	30
$\sigma \times BR_{\gamma Z}$	16	95
$\sigma \times BR_{\mu\mu}$	13	80

Table 13: Projected uncertainties of Higgs observables at CLIC3000: numbers by default in %.

MuC3000	3 ab ⁻¹	
Prod.	$\nu\nu H$	$\mu\mu H$
$\sigma \times BR_{bb}$	0.8	2.6
$\sigma \times BR_{cc}$	12	72
$\sigma \times BR_{gg}$	2.8	14
$\sigma \times BR_{ZZ}$	11	34
$\sigma \times BR_{WW}$	1.5	7.5
$\sigma \times BR_{\tau\tau}$	3.8	21
$\sigma \times BR_{\gamma\gamma}$	6.4	23
$\sigma \times BR_{\gamma Z}$	45	-
$\sigma \times BR_{\mu\mu}$	28	-

Table 14: Projected uncertainties of Higgs observables at 3 TeV muon collider: numbers by default in %.

MuC10000	10 ab ⁻¹	
Prod.	$\nu\nu H$	$\mu\mu H$
$\sigma \times BR_{bb}$	0.22	0.77
$\sigma \times BR_{cc}$	3.6	17
$\sigma \times BR_{gg}$	0.79	3.3
$\sigma \times BR_{ZZ}$	3.2	11
$\sigma \times BR_{WW}$	0.40	1.8
$\sigma \times BR_{\tau\tau}$	1.1	4.8
$\sigma \times BR_{\gamma\gamma}$	1.7	4.8
$\sigma \times BR_{\gamma Z}$	12	-
$\sigma \times BR_{\mu\mu}$	5.7	-

Table 15: Projected uncertainties of Higgs observables at 10 TeV muon collider: numbers by default in %.

MuC125	20 fb ⁻¹
Prod.	$\mu\mu \rightarrow H$
$\sigma \times BR_{bb}$	0.49
$\sigma \times BR_{cc}$	12
$\sigma \times BR_{gg}$	5.3
$\sigma \times BR_{ZZ}$	2.9
$\sigma \times BR_{WW}$	0.67
$\sigma \times BR_{\tau\tau}$	2.4
$\sigma \times BR_{\gamma\gamma}$	94
$\sigma \times BR_{\gamma Z}$	-
$\sigma \times BR_{\mu\mu}$	-

Table 16: Projected uncertainties of Higgs observables at 125 GeV muon collider: numbers by default in %.

ILC \sqrt{s} [GeV]	Pol. (e^-, e^+)	\mathcal{L} [fb $^{-1}$]	σ_e [fb]	A_{FB}^e	$[c_\theta^{\min}, c_\theta^{\max}]$	ϵ
250	(-80%, -30%)	100	64510.2 \pm 25.29	0.956 \pm 0.0001156	[-0.9, 0.9]	0.98
	(-80%, +30%)	900	68282.6 \pm 8.69	0.962 \pm 0.0000348	[-0.9, 0.9]	0.98
	(+80%, -30%)	900	66455.6 \pm 8.28	0.999 \pm 0.00000595	[-0.9, 0.9]	0.98
	(+80%, +30%)	100	86359.7 \pm 28.93	0.933 \pm 0.0001202	[-0.9, 0.9]	0.98
500	(-80%, -30%)	400	15566.2 \pm 6.22	0.956 \pm 0.0001176	[-0.9, 0.9]	0.98
	(-80%, +30%)	1600	19081.8 \pm 3.45	0.965 \pm 0.0000474	[-0.9, 0.9]	0.98
	(+80%, -30%)	1600	16326.7 \pm 3.1	0.982 \pm 0.0000362	[-0.9, 0.9]	0.98
	(+80%, +30%)	400	23477.5 \pm 7.57	0.929 \pm 0.0001196	[-0.9, 0.9]	0.98
1000	(-80%, -20%)	800	4084.86 \pm 2.253	0.958 \pm 0.0001582	[-0.9, 0.9]	0.98
	(-80%, +20%)	3200	4922.72 \pm 1.238	0.966 \pm 0.0000654	[-0.9, 0.9]	0.98
	(+80%, -20%)	3200	4429.19 \pm 1.15	0.963 \pm 0.0000701	[-0.9, 0.9]	0.98
	(+80%, +20%)	800	5828.42 \pm 2.67	0.934 \pm 0.000164	[-0.9, 0.9]	0.98

Table 17: Projections for $e^-e^+ \rightarrow e^-e^+$ at ILC, where the last column is the total selection efficiency.

ILC \sqrt{s} [GeV]	Pol. (e^-, e^+)	\mathcal{L} [fb $^{-1}$]	σ_μ [fb]	A_{FB}^μ	$[c_\theta^{\min}, c_\theta^{\max}]$	ϵ
250	(-80%, -30%)	100	1396.06 \pm 3.74	0.53 \pm 0.00227	[-0.95, 0.95]	0.98
	(-80%, +30%)	900	2329.5 \pm 1.61	0.535 \pm 0.000584	[-0.95, 0.95]	0.98
	(+80%, -30%)	900	1929.12 \pm 1.464	0.494 \pm 0.00066	[-0.95, 0.95]	0.98
	(+80%, +30%)	100	1214.07 \pm 3.484	0.5 \pm 0.002485	[-0.95, 0.95]	0.98
500	(-80%, -30%)	400	336.28 \pm 0.917	0.492 \pm 0.002374	[-0.95, 0.95]	0.98
	(-80%, +30%)	1600	559.91 \pm 0.592	0.597 \pm 0.000917	[-0.95, 0.95]	0.98
	(+80%, -30%)	1600	472.88 \pm 0.544	0.4535 \pm 0.001025	[-0.95, 0.95]	0.98
	(+80%, +30%)	400	296.72 \pm 0.861	0.46 \pm 0.00258	[-0.95, 0.95]	0.98
1000	(-80%, -20%)	800	92.65 \pm 0.34	0.484 \pm 0.003214	[-0.95, 0.95]	0.98
	(-80%, +20%)	3200	129.58 \pm 0.2012	0.487 \pm 0.001356	[-0.95, 0.95]	0.98
	(+80%, -20%)	3200	110.43 \pm 0.1858	0.445 \pm 0.001507	[-0.95, 0.95]	0.98
	(+80%, +20%)	800	81.16 \pm 0.3185	0.449 \pm 0.00351	[-0.95, 0.95]	0.98

Table 18: Projections for $e^-e^+ \rightarrow \mu^-\mu^+$ at ILC, where the last column is the total selection efficiency.

ILC \sqrt{s} [GeV]	Pol. (e^-, e^+)	\mathcal{L} [fb $^{-1}$]	σ_τ [fb]	A_{FB}^τ	$[c_\theta^{\min}, c_\theta^{\max}]$	ϵ
250	(-80%, -30%)	100	1185.87 \pm 3.444	0.515 \pm 0.00249	[-0.9, 0.9]	0.9
	(-80%, +30%)	900	1978.78 \pm 1.483	0.519 \pm 0.00064	[-0.9, 0.9]	0.9
	(+80%, -30%)	900	1638.57 \pm 1.35	0.48 \pm 0.000723	[-0.9, 0.9]	0.9
	(+80%, +30%)	100	1031.22 \pm 3.21	0.4855 \pm 0.00272	[-0.9, 0.9]	0.9
500	(-80%, -30%)	400	285.63 \pm 0.845	0.477 \pm 0.0026	[-0.9, 0.9]	0.9
	(-80%, +30%)	1600	475.59 \pm 0.545	0.482 \pm 0.001004	[-0.9, 0.9]	0.9
	(+80%, -30%)	1600	401.64 \pm 0.501	0.44 \pm 0.00112	[-0.9, 0.9]	0.9
	(+80%, +30%)	400	252.02 \pm 0.794	0.446 \pm 0.00282	[-0.9, 0.9]	0.9
1000	(-80%, -20%)	800	78.69 \pm 0.3136	0.47 \pm 0.00352	[-0.9, 0.9]	0.9
	(-80%, +20%)	3200	110.07 \pm 0.1855	0.473 \pm 0.001485	[-0.9, 0.9]	0.9
	(+80%, -20%)	3200	93.8 \pm 0.1712	0.432 \pm 0.001646	[-0.9, 0.9]	0.9
	(+80%, +20%)	800	68.93 \pm 0.2935	0.436 \pm 0.00383	[-0.9, 0.9]	0.9

Table 19: Projections for $e^-e^+ \rightarrow \tau^-\tau^+$ at ILC, where the last column is the total selection efficiency.

ILC \sqrt{s} [GeV]	Pol. (e^-, e^+)	\mathcal{L} [fb $^{-1}$]	σ_c [fb]	A_{FB}^c	$[c_\theta^{\min}, c_\theta^{\max}]$	ϵ
250	(-80%, -30%)	100	81.79 \pm 0.904	0.599 \pm 0.00886	[-0.9, 0.9]	0.03
	(-80%, +30%)	900	143.08 \pm 0.399	0.594 \pm 0.00224	[-0.9, 0.9]	0.03
	(+80%, -30%)	900	68.5 \pm 0.276	0.662 \pm 0.00302	[-0.9, 0.9]	0.03
	(+80%, +30%)	100	47.89 \pm 0.692	0.646 \pm 0.01103	[-0.9, 0.9]	0.03
500	(-80%, -30%)	400	18.88 \pm 0.2173	0.57 \pm 0.00946	[-0.9, 0.9]	0.03
	(-80%, +30%)	1600	32.93 \pm 0.1435	0.565 \pm 0.003594	[-0.9, 0.9]	0.03
	(+80%, -30%)	1600	16.52 \pm 0.1016	0.629 \pm 0.00478	[-0.9, 0.9]	0.03
	(+80%, +30%)	400	11.42 \pm 0.169	0.614 \pm 0.01168	[-0.9, 0.9]	0.03
1000	(-80%, -20%)	800	5.21 \pm 0.0807	0.561 \pm 0.01282	[-0.9, 0.9]	0.03
	(-80%, +20%)	3200	7.5 \pm 0.0484	0.559 \pm 0.00535	[-0.9, 0.9]	0.03
	(+80%, -20%)	3200	3.88 \pm 0.03484	0.618 \pm 0.00705	[-0.9, 0.9]	0.03
	(+80%, +20%)	800	3.037 \pm 0.0616	0.609 \pm 0.0161	[-0.9, 0.9]	0.03

Table 20: Projections for $e^-e^+ \rightarrow c\bar{c}$ at ILC, where the last column is the total selection efficiency.

ILC \sqrt{s} [GeV]	Pol. (e^-, e^+)	\mathcal{L} [fb $^{-1}$]	σ_b [fb]	A_{FB}^b	$[c_\theta^{\min}, c_\theta^{\max}]$	ϵ
250	(-80%, -30%)	100	268.77 \pm 1.64	0.648 \pm 0.00464	[-0.9, 0.9]	0.15
	(-80%, +30%)	900	483.56 \pm 0.733	0.66 \pm 0.001138	[-0.9, 0.9]	0.15
	(+80%, -30%)	900	134.94 \pm 0.387	0.351 \pm 0.002687	[-0.9, 0.9]	0.15
	(+80%, +30%)	100	110.32 \pm 1.05	0.4585 \pm 0.00846	[-0.9, 0.9]	0.15
500	(-80%, -30%)	400	58.18 \pm 0.3814	0.641 \pm 0.00503	[-0.9, 0.9]	0.15
	(-80%, +30%)	1600	104.77 \pm 0.256	0.649 \pm 0.00186	[-0.9, 0.9]	0.15
	(+80%, -30%)	1600	28.58 \pm 0.1336	0.446 \pm 0.00419	[-0.9, 0.9]	0.15
	(+80%, +30%)	400	23.55 \pm 0.2426	0.517 \pm 0.00882	[-0.9, 0.9]	0.15
1000	(-80%, -20%)	800	15.94 \pm 0.141	0.64 \pm 0.0068	[-0.9, 0.9]	0.15
	(-80%, +20%)	3200	23.44 \pm 0.0856	0.645 \pm 0.00279	[-0.9, 0.9]	0.15
	(+80%, -20%)	3200	6.68 \pm 0.0457	0.4755 \pm 0.00602	[-0.9, 0.9]	0.15
	(+80%, +20%)	800	5.88 \pm 0.0857	0.518 \pm 0.01248	[-0.9, 0.9]	0.15

Table 21: Projections for $e^-e^+ \rightarrow b\bar{b}$ at ILC, where the last column is the total selection efficiency.

CLIC \sqrt{s} [GeV]	Pol. (e^-, e^+)	\mathcal{L} [fb $^{-1}$]	σ_e [fb]	A_{FB}^e	$[c_\theta^{\min}, c_\theta^{\max}]$	ϵ
380	(-80%, 0%)	500	29422.4 \pm 7.65	0.96 \pm 0.0000727	[-0.9, 0.9]	0.98
	(+80%, 0%)	500	33886.8 \pm 8.06	0.954 \pm 0.0000713	[-0.9, 0.9]	0.98
1500	(-80%, 0%)	2000	2024.97 \pm 1.004	0.963 \pm 0.0001345	[-0.9, 0.9]	0.98
	(+80%, 0%)	500	2298.87 \pm 2.11	0.945 \pm 0.000299	[-0.9, 0.9]	0.98
3000	(-80%, 0%)	4000	510.3 \pm 0.3565	0.963 \pm 0.0001888	[-0.9, 0.9]	0.98
	(+80%, 0%)	1000	578.04 \pm 0.749	0.945 \pm 0.000424	[-0.9, 0.9]	0.98

Table 22: Projections for $e^-e^+ \rightarrow e^-e^+$ at CLIC, where the last column is the total selection efficiency.

CLIC \sqrt{s} [GeV]	Pol. (e^-, e^+)	\mathcal{L} [fb $^{-1}$]	σ_μ [fb]	A_{FB}^μ	$[c_\theta^{\min}, c_\theta^{\max}]$	ϵ
380	(-80%, 0%)	500	782.38 \pm 1.25	0.504 \pm 0.00138	[-0.95, 0.95]	0.98
	(+80%, 0%)	500	669.18 \pm 1.157	0.465 \pm 0.00153	[-0.95, 0.95]	0.98
1500	(-80%, 0%)	2000	49.31 \pm 0.157	0.484 \pm 0.002786	[-0.95, 0.95]	0.98
	(+80%, 0%)	500	42.54 \pm 0.2917	0.445 \pm 0.00614	[-0.95, 0.95]	0.98
3000	(-80%, 0%)	4000	12.32 \pm 0.0555	0.483 \pm 0.003945	[-0.95, 0.95]	0.98
	(+80%, 0%)	1000	10.63 \pm 0.1031	0.444 \pm 0.00869	[-0.95, 0.95]	0.98

Table 23: Projections for $e^-e^+ \rightarrow \mu^-\mu^+$ at CLIC, where the last column is the total selection efficiency.

CLIC \sqrt{s} [GeV]	Pol. (e^-, e^+)	\mathcal{L} [fb $^{-1}$]	σ_τ [fb]	A_{FB}^τ	$[c_\theta^{\min}, c_\theta^{\max}]$	ϵ
380	(-80%, 0%)	500	664.57 \pm 1.153	0.489 \pm 0.001513	[-0.9, 0.9]	0.9
	(+80%, 0%)	500	568.38 \pm 1.066	0.4515 \pm 0.001674	[-0.9, 0.9]	0.9
1500	(-80%, 0%)	2000	41.89 \pm 0.1447	0.47 \pm 0.00305	[-0.9, 0.9]	0.9
	(+80%, 0%)	500	36.13 \pm 0.269	0.432 \pm 0.00671	[-0.9, 0.9]	0.9
3000	(-80%, 0%)	4000	10.46 \pm 0.0511	0.469 \pm 0.00432	[-0.9, 0.9]	0.9
	(+80%, 0%)	1000	9.03 \pm 0.095	0.431 \pm 0.0095	[-0.9, 0.9]	0.9

Table 24: Projections for $e^-e^+ \rightarrow \tau^-\tau^+$ at CLIC, where the last column is the total selection efficiency.

CLIC \sqrt{s} [GeV]	Pol. (e^-, e^+)	\mathcal{L} [fb $^{-1}$]	σ_c [fb]	A_{FB}^c	$[c_\theta^{\min}, c_\theta^{\max}]$	ϵ
380	(-80%, 0%)	500	45.7 \pm 0.3023	0.574 \pm 0.00542	[-0.9, 0.9]	0.03
	(+80%, 0%)	500	24.41 \pm 0.221	0.631 \pm 0.00702	[-0.9, 0.9]	0.03
1500	(-80%, 0%)	2000	2.81 \pm 0.0375	0.558 \pm 0.01106	[-0.9, 0.9]	0.03
	(+80%, 0%)	500	1.534 \pm 0.0554	0.613 \pm 0.02854	[-0.9, 0.9]	0.03
3000	(-80%, 0%)	4000	0.7 \pm 0.01323	0.558 \pm 0.01568	[-0.9, 0.9]	0.03
	(+80%, 0%)	1000	0.383 \pm 0.01956	0.612 \pm 0.0404	[-0.9, 0.9]	0.03

Table 25: Projections for $e^-e^+ \rightarrow c\bar{c}$ at CLIC, where the last column is the total selection efficiency.

CLIC \sqrt{s} [GeV]	Pol. (e^-, e^+)	\mathcal{L} [fb $^{-1}$]	σ_b [fb]	A_{FB}^b	$[c_\theta^{\min}, c_\theta^{\max}]$	ϵ
380	(-80%, 0%)	500	145.83 \pm 0.54	0.649 \pm 0.00282	[-0.9, 0.9]	0.15
	(+80%, 0%)	500	46.81 \pm 0.306	0.46 \pm 0.0058	[-0.9, 0.9]	0.15
1500	(-80%, 0%)	2000	8.69 \pm 0.0659	0.643 \pm 0.00581	[-0.9, 0.9]	0.15
	(+80%, 0%)	500	2.77 \pm 0.0744	0.498 \pm 0.0233	[-0.9, 0.9]	0.15
3000	(-80%, 0%)	4000	2.16 \pm 0.02325	0.642 \pm 0.00824	[-0.9, 0.9]	0.15
	(+80%, 0%)	1000	0.689 \pm 0.02625	0.5 \pm 0.033	[-0.9, 0.9]	0.15

Table 26: Projections for $e^-e^+ \rightarrow b\bar{b}$ at CLIC, where the last column is the total selection efficiency.

FCC-ee \sqrt{s} [GeV]	Final state	\mathcal{L} [fb $^{-1}$]	σ [fb]	A_{FB}	$[c_{\theta}^{\min}, c_{\theta}^{\max}]$	ϵ
240	$e^{-}e^{+}$	5000	77330.4 ± 3.87	0.96 ± 0.00001388	$[-0.9, 0.9]$	0.98
	$\mu^{-}\mu^{+}$		1870.84 ± 0.612	0.521 ± 0.000279	$[-0.95, 0.95]$	0.98
	$\tau^{-}\tau^{+}$		1589.15 ± 0.564	0.506 ± 0.000306	$[-0.9, 0.9]$	0.9
	$c\bar{c}$		93.38 ± 0.1367	0.62 ± 0.00115	$[-0.9, 0.9]$	0.03
	$b\bar{b}$		275.64 ± 0.235	0.592 ± 0.000687	$[-0.9, 0.9]$	0.15
365	$e^{-}e^{+}$	1500	34221.5 ± 4.72	0.957 ± 0.0000399	$[-0.9, 0.9]$	0.98
	$\mu^{-}\mu^{+}$		787.74 ± 0.725	0.488 ± 0.000803	$[-0.95, 0.95]$	0.98
	$\tau^{-}\tau^{+}$		669.11 ± 0.668	0.473 ± 0.00088	$[-0.9, 0.9]$	0.9
	$c\bar{c}$		38.11 ± 0.1594	0.595 ± 0.00336	$[-0.9, 0.9]$	0.03
	$b\bar{b}$		105.12 ± 0.2647	0.603 ± 0.00201	$[-0.9, 0.9]$	0.15

Table 27: Projections for $e^{-}e^{+} \rightarrow f\bar{f}$ at FCC-ee, where the last column is the total selection efficiency.

CEPC \sqrt{s} [GeV]	Final state	\mathcal{L} [fb $^{-1}$]	σ [fb]	A_{FB}	$[c_{\theta}^{\min}, c_{\theta}^{\max}]$	ϵ
240	$e^{-}e^{+}$	5000	77330.4 ± 1.937	0.96 ± 0.00000694	$[-0.9, 0.9]$	0.98
	$\mu^{-}\mu^{+}$		1870.84 ± 0.306	0.521 ± 0.0001395	$[-0.95, 0.95]$	0.98
	$\tau^{-}\tau^{+}$		1589.15 ± 0.282	0.506 ± 0.000153	$[-0.9, 0.9]$	0.9
	$c\bar{c}$		93.38 ± 0.0683	0.62 ± 0.000574	$[-0.9, 0.9]$	0.03
	$b\bar{b}$		275.64 ± 0.1174	0.592 ± 0.0003434	$[-0.9, 0.9]$	0.15
360	$e^{-}e^{+}$	1500	35147.9 ± 5.85	0.957 ± 0.0000482	$[-0.9, 0.9]$	0.98
	$\mu^{-}\mu^{+}$		810.18 ± 0.9	0.4885 ± 0.00097	$[-0.95, 0.95]$	0.98
	$\tau^{-}\tau^{+}$		688.17 ± 0.83	0.474 ± 0.001061	$[-0.9, 0.9]$	0.9
	$c\bar{c}$		39.22 ± 0.198	0.596 ± 0.004056	$[-0.9, 0.9]$	0.03
	$b\bar{b}$		108.33 ± 0.329	0.602 ± 0.002425	$[-0.9, 0.9]$	0.15

Table 28: Projections for $e^{-}e^{+} \rightarrow f\bar{f}$ at CEPC, where the last column is the total selection efficiency.

4.5 Diboson measurements

The diboson ($e^+e^- \rightarrow W^+W^-$) measurements provide important constraints on a set of operator coefficients that are essential to the Higgs + EW fit. Conventionally, the new physics effects are parameterized in terms of three CP-even anomalous triple gauge couplings (aTGCs). This was for instance done by the LEP collaboration [28] and also in the ILC analysis [29]. Considering the tree-level contributions of SMEFT CP-even dimension-6 operators, and omitting those that only contribute to the W -boson decay rate, a total number of 7 independent parameters contribute to the $e^+e^- \rightarrow W^+W^-$ process. Among them, one degree of freedom can be associated with the modification of the W -boson mass, which we discard here due to the strong constraints from the W -mass measurements. In the language of the effective Lagrangian in Section 2.2, the remaining 6 parameters are*

$$\delta g_{1,Z}, \delta \kappa_\gamma, \lambda_Z, \delta g_{Z,L}^{ee}, \delta g_{Z,R}^{ee} \text{ and } \delta g_W^{e\nu}, \quad (19)$$

where $\delta g_{1,Z}$, $\delta \kappa_\gamma$, λ_Z are the familiar aTGCs, and $\delta g_{Z,L}^{ee}$, $\delta g_{Z,R}^{ee}$, $\delta g_W^{e\nu}$ correspond to modifications in the $Ze_L\bar{e}_L$, $Ze_R\bar{e}_R$ and $We\nu$ couplings. The latter are particularly relevant if the measurement precision of the diboson process is comparable or even better than those of Z-pole measurements. All 6 parameters are included in our global SMEFT analysis.

While several studies of the diboson measurements already exist from various collider collaborations (such as the ILC one [29]), not all projections for future lepton colliders are available, and many of the available ones uses the 3-aTGC framework which is not directly applicable in the global SMEFT framework. Furthermore, these parameters are very sensitive to the multi-dimensional differential distribution of the $e^+e^- \rightarrow W^+W^-$ process, which is practically difficult to be fully utilized in an analysis with binned-distributions. To efficiently extract information from the measurements, and for a consistent treatment among various different colliders, we perform a simplified phenomenological analysis based on Optimal Observables [30, 31] for all collider scenarios to extract the likelihood (or χ^2) of the six parameters in Eq. (19). The optimal observable analysis assumes that the new physics contributions enter observables only at the linear level. This is a good approximation for the very precise diboson measurements that are expected at future lepton colliders, and is also consistent with the SMEFT treatment in our analysis. More explicitly, the differential cross section is parameterized as

$$\frac{d\sigma}{d\Omega} = S_0 + \sum_i S_{1,i} g_i, \quad (20)$$

where $g_{i=1,\dots,6}$ are the six parameters in Eq. (19), and S_0 , $S_{1,i}$ are functions of the differential observables. In the narrow width approximation, each event can be de-

*Here we assume that the initial particles are e^+e^- . For $\mu^+\mu^-$, one needs to replace the last three parameters by the corresponding muon couplings.

scribed by five independent observables, which are the production polar angle θ and two decay angles for each W . $S_0 = \frac{d\sigma_{\text{SM}}}{d\Omega}$ is the SM differential cross section. It can be shown that the best possible reaches on the g_i are given by the inverse covariance matrix

$$c_{ij}^{-1} = \int d\Omega \frac{S_{1,i} S_{1,j}}{S_0} \cdot \mathcal{L}, \quad (21)$$

where \mathcal{L} is the total integrated luminosity. The c_{ij}^{-1} can be obtained by measuring the optimal observables, defined as $\mathcal{O}_i = \frac{S_{1,i}}{S_0}$, and is simply given by the covariance matrix V_{ij} of the \mathcal{O}_i , $c_{ij}^{-1} = nV_{ij}$ where n is the number of events.

It should be noted that the diboson process also receives contributions from (four) additional operators that modify the W branching ratios. While an optimal observable analysis could be done for each diboson decay channel including these additional parameters, it is more convenient to separate the information in the rate measurements of $e^+e^- \rightarrow W^+W^-$ from the differential ones, as the latter depend only on the parameters in Eq. (19). It is straightforward to subtract from c_{ij}^{-1} the contribution from the total rate measurement, which we treat separately with possible modifications in the W branching ratios. For the differential analysis, several assumptions are made: We consider only the statistical uncertainties of the signal and assume a conservative selection efficiency of 45% in all WW events, chosen to agree with the results from the ILC full simulation analysis of the semi-leptonic channel at 500 GeV. We include all decay channels of the WW pairs. For the hadronic decay, one could not distinguish the two quarks, and the corresponding angular distributions are ‘‘folded.’’ This effect is implemented in the optimal observables. The τ channel is treated in the same way as the lepton channels, assuming a good τ reconstruction can be achieved at the future lepton colliders. For the dilepton channels, the momenta of the two missing neutrinos cannot be directly reconstructed. They could be obtained by imposing the conditions of the W on-shell mass and the center of mass energies, which gives a set of quadratic equations that can be solved. We assume that the correct solution is always chosen for each event. The optimal observable analysis is performed for each WW channel, and the resultant likelihoods are combined in the end. For jets and leptons we use detector acceptance cuts on the polar angle of $|\cos\theta| < 0.9$ and 0.95 , respectively. We have checked that the effects of detector acceptance and smearing have only a small impact on the results, reducing the precision reaches by at most $\sim 10\text{-}15\%$. It was also shown in Ref. [29] that, with appropriate selection cuts, most backgrounds can be removed with a signal efficiency of around 70%.

For the rate measurements of the WW process, the following treatment is implemented. The decay of a single W can be separated into four channels, $e\nu$, $\mu\nu$, $\tau\nu$ and jj . For each possible decay channel of the WW pair, we estimate the precision of the rate measurement (in terms of $\sigma_{e^+e^- \rightarrow W^+W^-} \times \text{BR}_{W^+} \times \text{BR}_{W^-}$), considering only the statistical uncertainties of the signal and the above-mentioned selection efficiency of 45% in all WW events. We also assume that the W has no exotic decay, so that the

relation

$$\text{BR}_{W^- \rightarrow e\nu} + \text{BR}_{W^- \rightarrow \mu\nu} + \text{BR}_{W^- \rightarrow \tau\nu} + \text{BR}_{W^- \rightarrow jj} = 1, \quad (22)$$

is imposed. With this condition, one could extract the precision of the total cross section σ_{WW} and the W branching ratios from the measurements of all the WW channels. Additional measurements of the W -boson width (*e.g.* the ones from threshold scan) as listed in [Table 3](#), as well as the projected reach of the HL-LHC are also included in the global analysis. With these measurements, the total cross section and branching ratios can be determined even without imposing [Eq. \(22\)](#). From the projections on total cross section σ_{WW} and the W branching ratios, the likelihood (χ^2) of the operator coefficients can be obtained, which is combined with the one from the differential analysis.

5 Higgs + EW fit

In this section we report the results of a global analysis of the Higgs and EW measurements in the dimension-6 SMEFT framework. The following measurements are included in the analysis:

- The Higgs rate measurements listed in [Table 4-13](#). In particular, the results for all future colliders are assumed to be combined with the HL-LHC Higgs measurements.
- The electroweak precision observables in [Table 3](#). Here we assume as a baseline the current set of precisions for EWPO, but with SM central values. * This is combined with all future collider scenarios.
- The diboson measurements in [Section 4.5](#). For lepton colliders, this include the W branching ratio measurements and the differential analysis using optimal observables; for the HL-LHC, we implement the results from Ref. [\[32\]](#).
- For the high energy muon collider only, we also consider the $\gamma\gamma \rightarrow W^+W^-$ process for the measurements of the W branching ratios. The cross section [\[33\]](#) for this process is much larger than the one of $\mu^+\mu^- \rightarrow W^+W^-$ at very high energy. This mainly improves the reach on the operator coefficients that modify the W branching ratios.

For the study, we perform a series of fits of the dimension-6 SMEFT to the above-mentioned measurements for the different colliders scenarios in [Table 2](#). These fits

*We exclude the recent measurement of the W mass from CDF.

were performed with the `HEPfit` code [10] and using a Bayesian approach. An independent cross check of the results was performed using a χ^2 fit constructed with all the relevant measurements. In Fig. 3 and Table 29, we present the result of the fits in terms of the 68% probability sensitivity* to modifications to the effective couplings introduced in Section 2.2 [9, 25, 34],

$$\delta g_X^Y = \frac{g_{XY}^{\text{eff}}}{g_{XY}^{\text{eff,SM}}} - 1, \quad (23)$$

for the various collider scenarios listed in Table 2. For the e^+e^- colliders, the runs are considered to be staged, i.e. the high energy runs are always combined with the low energy ones. For the muon collider, three separate scenarios are considered: operating at 3 TeV, at 10 TeV, and the latter combined with a run at 125 GeV. (In Fig. 3 we also show results of these three scenarios in combination with the information of FCCee.)

Two sets of results are shown for each scenario: one assumes that the Higgs decay channels are only the ones in the SM; the other assumes the total Higgs width is not constrained by the previous condition, and the Higgs can decay into non-SM states. (This is modeled in the fits by introducing a new parameter, $\text{BR}_{\text{Exo}} \geq 0$, for the non-SM branching ratio.) These two scenarios are represented by the wide and narrow bars, respectively. They will be denoted as the constrained- Γ_H fit and the free- Γ_H fit later on. For the ILC results, we consider an additional scenario with a Giga-Z run included, which is illustrated by the triangle marks. We also impose a $U(2)$ symmetry for the electroweak gauge couplings of the first two generation quarks, which can be written explicitly as $\delta g_{Z,L/R}^{uu} = \delta g_{Z,L/R}^{cc}$ and $\delta g_{Z,L/R}^{dd} = \delta g_{Z,L/R}^{ss}$. As such, the results for $\delta g_{Z,L/R}^{cc}$ and $\delta g_{Z,L/R}^{ss}$ are not explicitly shown. This assumption is necessary in our framework to remove a flat direction among these parameters, as the asymmetry observables using jet-charge could not be measured for the first generation quarks at lepton colliders[†]. Note that the LHC could measure a similar asymmetry observable and lift this flat direction [35], in which case our $U(2)$ assumption could be removed. Since there is no official HL-LHC projection for this specific measurement, we do not consider it in our analysis. We will however illustrate the impact of these asymmetry observables later in Section 5.2. In the leptonic sector, on the other hand, we do not impose any “universality” condition, and couplings to electrons, muons and taus are assumed to be independent. Higgs couplings are also assumed to be diagonal but independent for the different fermion families. With the exception of the possibility of having possible non-SM decays of the Higgs boson, and thus Γ_H effectively as an independent parameter, this is similar to the SMEFT_{ND} fit scenario considered in [9]. As in that reference, dimension-6 SMEFT contributions are including at leading

*This is estimated as the square root of the variance of the posterior predictive distribution of the corresponding parameter from the fits.

[†]The measurement of R_{uc} as included in the next section, which can measure the electric-charge asymmetry using final state photon radiation effects, can help to relax this assumption.

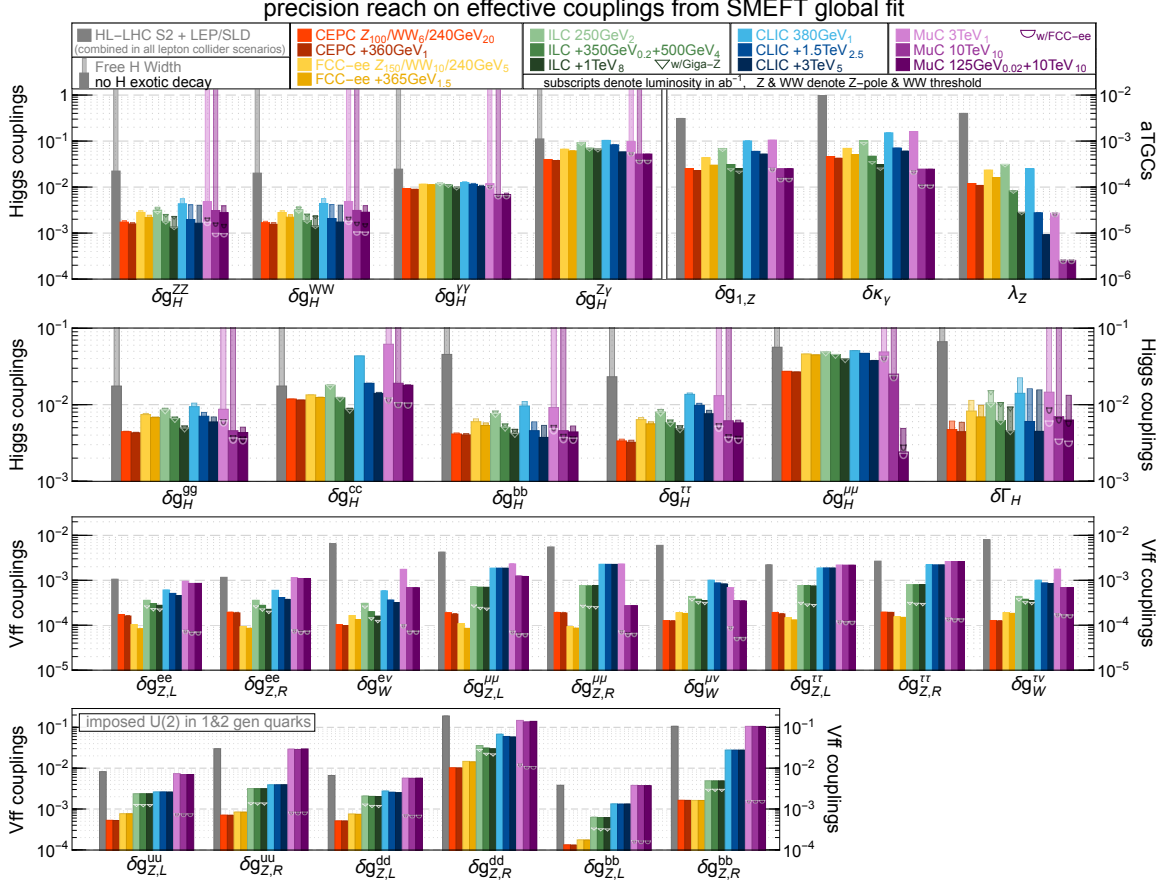


Figure 3: Precision reach on effective couplings from a SMEFT global analysis of the Higgs and EW measurements at various future colliders listed in Table 2. The wide (narrow) bars correspond to the results from the constrained- Γ_H (free- Γ_H) fit. The HL-LHC and LEP/SLD measurements are combined with all lepton collider scenarios. For e^+e^- colliders, the high energy runs are always combined with the low energy ones. For the ILC scenarios, the (upper edge of the) triangle mark shows the results for which a Giga-Z run is also included. For the muon collider, 3 separate scenarios are considered. The subscripts in the collider scenarios denote the corresponding integrated luminosity of the run in ab^{-1} .

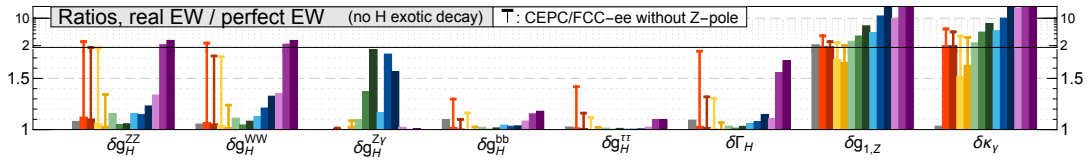


Figure 4: Ratios of the measurement precision (shown in Fig. 3) to the one assuming perfect EW measurements in the constrained- Γ_H fit. See text for details. Results are only shown for Higgs couplings and aTGCs with ratios noticeably larger than one. For CEPC/FCC-ee, we also show (with the thin “T” lines) the results without the improved measurements of the EWPO that would be possible at the future Z-pole runs.

order and SM predictions are computed including the future projected uncertainties associated to the SM input parameters in the $\{\alpha, M_Z, G_F, m_t, m_H\}$ scheme. See [Section 5.1](#) for more details on the latter and a discussion on the impact of other SM uncertainties.

For the constrained- Γ_H fit, the outcome of this analysis is similar to that presented in Ref. [25], with the exception of the CEPC results where one observes the expected improvement in the sensitivity to Higgs couplings derived from the increase in the luminosity at 240 GeV, together with the addition of the new set of measurements that would be possible at 360 GeV. The sensitivity to the aTGC via the optimal observable analysis presented in [Section 4.5](#) is also different compared to Ref. [25], as we now use all W decay channels (as opposed to only the semi-leptonic channel), but we also use a slightly more conservative selection efficiency, consider cuts not included in [25], and account for systematic effects associated to the knowledge of the effective beam polarization or the luminosity.

For the free- Γ_H fit, it is essential to have a model independent determination of the Higgs width, without which the Higgs couplings could not be constrained. Clearly, the e^+e^- colliders have the advantage of the inclusive HZ measurements, while a 125 GeV muon collider is able to directly measure the Higgs width with a threshold scan.

It is worth noting that, in a global SMEFT framework, the EW measurements are also relevant for the Higgs coupling determination, since they constrain many EW parameters that could also enter the Higgs processes. To illustrate this, we show in [Fig. 4](#) the ratios of the measurement precision to the one obtained assuming *perfect EW* measurements for the Higgs couplings and aTGCs. This *perfect EW* scenario assumes that the experimental precision of the EWPO sensitive to the Z and W couplings of fermions is so high that these can be assumed to be exactly SM like, i.e. $\delta g_{Z,L/R}^f, \delta g_W^{ff'} \equiv 0$. The results are only shown for the constrained- Γ_H fit, and for those with this ratio significantly larger than one. This ratio is generally very close to one for the Higgs couplings at CEPC and FCC-ee, which benefit from the future Z-pole runs. For comparison, we also show the results for CEPC and FCC-ee with such future Z-pole measurements removed, and much larger ratios are observed for many of the couplings. On the other hand, the lack of better EW measurements could be a limiting factor for the determination of the HWW and HZZ couplings at a muon collider. For the aTGCs the situation is different, and we observe a deterioration by a factor ~ 2 in $\delta g_{1,Z}$ and $\delta \kappa_\gamma$ at the 240/250 GeV e^+e^- Higgs/EW factories, which gets significantly worse at high energy lepton colliders (e^+e^- and $\mu^-\mu^-$). Interestingly, our results also suggest that the determination of the $HZ\gamma$ coupling at the linear colliders at high energies could be significantly improved with better EW measurements. This is due to its capability of probing the $HZ\gamma$ coupling via the Higgstrahlung process

with polarized beams.*

5.1 Impact of the Standard Model uncertainties on the results

The previous results have been obtained from a fit to the experimental predictions presented in Section 4. On the theory side, we considered the observable predictions from the SM, complemented with the dimension-6 SMEFT operators. For the SM predictions, and as it was done in [9], we include the effects associated to the projected experimental uncertainties on the SM input parameters, the so-called *parametric uncertainties*. Apart from these, one needs to take into account that the current precision of SM theory calculations, e.g. known in general at the 2-loop level for the EWPO, may not be enough to match the projected experimental precision of the different future measurements, i.e. the uncertainty associated to missing higher-order corrections, typically referred as *intrinsic theory uncertainties* may be a limiting factor. A lot of work has been dedicated to establish the theory requirements that would be needed so the theory calculations do not hinder the interpretation of the different precision measurements at a future e^+e^- EW/Higgs factories. (See, e.g., [37].) In this subsection we quantify the impact of such intrinsic uncertainties from both *current* calculations and those projected to be available by the time a future e^+e^- collider operates.

A summary of the current and future intrinsic uncertainties for EWPO are given in Table 30. These estimates have been obtained in [38–40]. Parametric errors are also shown in that table for a benchmark of precision for the SM inputs. In the actual fits, these are assigned to each observable at each collider according to the uncertainty of the corresponding SM input in Table 3. For the strong coupling constant at the Z pole and the Top mass, both missing in that table, we assume the following: a) an independent determination of $\alpha_s(M_Z)$ from lattice QCD will bring up a determination with an uncertainty ~ 0.0002 ; b) the HL-LHC will be able to measure m_t with an uncertainty of the order of 400 MeV, which would be reduced at a future e^+e^- factory running at the $t\bar{t}$ threshold down to ~ 20 MeV.

For single Higgs production, following [40], we assume the current theory uncertainty for $e^+e^- \rightarrow ZH$ and $e^+e^- \rightarrow \bar{\nu}H$ via W boson fusion is of $O(1\%)$, due to the missing 2-loop effects.† With the full 2-loop calculation for the ZH process, the uncertainty is expected to be reduced to $\lesssim 0.3\%$, whereas in the more complicated case of W boson fusion, a partial result could bring the uncertainty below 1%. The uncertainties for Higgs decays, also from [40], are summarized in table 31.

Finally, for the $e^+e^- \rightarrow W^+W^-$ process, we used our own projections obtained

*For unpolarized beams, the contribution of the $HZ\gamma$ coupling to the Higgstrahlung process is accidentally suppressed. See e.g. Ref. [36].

†The two-loop corrections to $e^+e^- \rightarrow ZH$ have been recently computed in [41, 42].

in %	HL-LHC	CEPC		FCC-ee		ILC						CLIC			muon-collider		
		240	+360	240	+365	250		+500		+1TeV		380	+1.5TeV	+3TeV	3TeV	10TeV	10TeV
		+Z/WW		+Z/WW		Giga-Z		Giga-Z		Giga-Z							
δg_H^{ZZ}	2.2	0.17	0.16	0.28	0.22	0.31	0.29	0.18	0.18	0.13	0.13	0.43	0.19	0.16	0.48	0.31	0.28
	–	0.19	0.17	0.31	0.25	0.37	0.35	0.26	0.25	0.23	0.23	0.56	0.41	0.4	–	–	0.39
δg_H^{WW}	2.	0.17	0.15	0.28	0.22	0.32	0.31	0.19	0.18	0.14	0.14	0.44	0.21	0.17	0.49	0.31	0.28
	–	0.18	0.17	0.31	0.25	0.37	0.36	0.26	0.26	0.24	0.23	0.56	0.42	0.41	–	–	0.39
$\delta g_H^{\gamma\gamma}$	2.5	0.91	0.89	1.2	1.1	1.2	1.2	1.1	1.1	0.98	0.97	1.2	1.1	1.	1.2	0.7	0.69
	–	0.91	0.9	1.2	1.1	1.2	1.2	1.1	1.1	1.	1.	1.3	1.2	1.1	–	–	0.74
$\delta g_H^{Z\gamma}$	11.	4.	3.8	6.7	6.1	9.3	9.1	7.	6.8	6.7	6.6	10.	8.3	5.8	9.7	5.2	5.2
	–	4.	3.8	6.7	6.1	9.3	9.1	7.	6.8	6.7	6.6	10.	8.3	5.8	–	–	5.2
$\delta g_{1,Z}$	0.31	0.025	0.023	0.044	0.03	0.069	0.067	0.031	0.025	0.025	0.022	0.1	0.06	0.052	0.1	0.025	0.025
	0.31	0.025	0.023	0.043	0.03	0.069	0.067	0.031	0.025	0.025	0.022	0.1	0.06	0.052	0.1	0.025	0.025
$\delta\kappa_\gamma$	0.97	0.046	0.042	0.069	0.05	0.1	0.092	0.047	0.036	0.031	0.026	0.15	0.071	0.06	0.16	0.025	0.024
	0.97	0.046	0.043	0.069	0.05	0.1	0.092	0.047	0.036	0.031	0.026	0.15	0.071	0.061	0.16	0.025	0.025
λ_Z	0.4	0.012	0.011	0.023	0.016	0.031	0.031	0.0082	0.0082	0.0028	0.0028	0.025	0.0028	0.00092	0.0027	0.00026	0.00025
	0.4	0.012	0.011	0.023	0.016	0.031	0.031	0.0083	0.0082	0.0028	0.0028	0.025	0.0028	0.00092	0.0027	0.00026	0.00026
δg_H^{gg}	1.8	0.44	0.43	0.74	0.68	0.85	0.85	0.66	0.66	0.49	0.49	0.94	0.71	0.59	0.87	0.46	0.43
	–	0.45	0.44	0.77	0.69	0.9	0.89	0.69	0.69	0.53	0.53	1.1	0.79	0.69	–	–	0.51
δg_H^{cc}	1.8	1.2	1.1	1.3	1.2	1.8	1.8	1.2	1.2	0.87	0.87	4.3	1.9	1.4	6.2	1.9	1.8
	–	1.2	1.1	1.4	1.3	1.8	1.8	1.2	1.2	0.9	0.9	4.3	1.9	1.5	–	–	1.8
δg_H^{bb}	4.5	0.41	0.4	0.6	0.53	0.77	0.77	0.5	0.51	0.42	0.42	0.96	0.46	0.37	0.92	0.46	0.44
	–	0.43	0.42	0.66	0.58	0.83	0.83	0.56	0.56	0.48	0.47	1.1	0.6	0.54	–	–	0.53
$\delta g_H^{\tau\tau}$	2.3	0.34	0.32	0.64	0.56	0.8	0.8	0.58	0.58	0.49	0.48	1.4	0.98	0.76	1.3	0.62	0.58
	–	0.36	0.34	0.68	0.6	0.87	0.86	0.63	0.63	0.53	0.53	1.4	1.	0.84	–	–	0.63
$\delta g_H^{\mu\mu}$	5.6	2.7	2.7	4.6	4.5	4.9	4.9	4.5	4.5	4.	4.	5.1	4.7	3.8	4.9	2.5	0.24
	–	2.7	2.7	4.6	4.5	4.9	4.9	4.5	4.5	4.	4.	5.1	4.7	3.8	–	–	0.49
$\delta\Gamma_H$	6.7	0.47	0.44	0.82	0.69	1.1	1.	0.62	0.62	0.46	0.46	1.4	0.6	0.45	1.5	0.7	0.63
	–	0.61	0.59	1.1	0.98	1.5	1.5	1.1	1.1	0.94	0.93	2.3	1.6	1.6	–	–	1.3
$\delta g_{Z,L}^e$	0.11	0.017	0.016	0.01	0.0083	0.036	0.027	0.03	0.023	0.028	0.023	0.061	0.051	0.046	0.095	0.085	0.085
	0.11	0.017	0.016	0.01	0.0083	0.036	0.027	0.03	0.024	0.028	0.023	0.061	0.051	0.046	0.095	0.085	0.086
$\delta g_{Z,R}^e$	0.12	0.019	0.019	0.0092	0.0085	0.036	0.027	0.028	0.023	0.023	0.02	0.06	0.041	0.037	0.11	0.11	0.11
	0.12	0.02	0.019	0.0092	0.0085	0.036	0.027	0.028	0.023	0.023	0.02	0.06	0.041	0.038	0.11	0.11	0.11
δg_W^e	0.65	0.01	0.0097	0.016	0.013	0.031	0.027	0.02	0.015	0.016	0.013	0.058	0.036	0.032	0.17	0.068	0.068
	0.65	0.01	0.0097	0.016	0.013	0.031	0.027	0.02	0.015	0.016	0.013	0.058	0.036	0.032	0.18	0.068	0.068
$\delta g_{Z,L}^{\mu\mu}$	0.42	0.019	0.018	0.011	0.0085	0.071	0.028	0.07	0.025	0.07	0.024	0.19	0.19	0.19	0.23	0.12	0.12
	0.42	0.019	0.018	0.011	0.0085	0.071	0.028	0.07	0.025	0.07	0.024	0.19	0.19	0.19	0.23	0.12	0.12
$\delta g_{Z,R}^{\mu\mu}$	0.55	0.019	0.019	0.0093	0.0086	0.076	0.028	0.075	0.026	0.075	0.026	0.23	0.23	0.23	0.23	0.027	0.027
	0.55	0.019	0.019	0.0091	0.0086	0.076	0.028	0.075	0.026	0.075	0.026	0.23	0.23	0.23	0.23	0.027	0.027
$\delta g_W^{\mu\mu}$	0.6	0.013	0.012	0.019	0.018	0.044	0.039	0.038	0.033	0.035	0.032	0.1	0.087	0.083	0.068	0.035	0.034
	0.6	0.013	0.012	0.019	0.018	0.044	0.039	0.038	0.033	0.035	0.032	0.1	0.087	0.083	0.069	0.035	0.035
$\delta g_{Z,L}^{\tau\tau}$	0.22	0.019	0.018	0.015	0.013	0.076	0.032	0.075	0.03	0.074	0.029	0.19	0.19	0.19	0.22	0.22	0.22
	0.22	0.019	0.018	0.014	0.013	0.076	0.033	0.075	0.03	0.075	0.029	0.19	0.19	0.19	0.22	0.22	0.22
$\delta g_{Z,R}^{\tau\tau}$	0.27	0.019	0.019	0.015	0.015	0.08	0.032	0.079	0.031	0.079	0.03	0.22	0.22	0.22	0.26	0.26	0.26
	0.27	0.02	0.02	0.015	0.015	0.081	0.032	0.079	0.031	0.079	0.031	0.22	0.22	0.22	0.26	0.26	0.26
$\delta g_W^{\tau\tau}$	0.79	0.013	0.012	0.019	0.018	0.044	0.039	0.038	0.033	0.035	0.032	0.1	0.087	0.083	0.18	0.068	0.068
	0.79	0.013	0.013	0.019	0.018	0.044	0.039	0.038	0.033	0.035	0.032	0.1	0.087	0.083	0.18	0.068	0.068
$\delta g_{Z,L}^{\nu\nu}$	0.82	0.052	0.052	0.077	0.076	0.24	0.13	0.24	0.13	0.24	0.13	0.26	0.26	0.26	0.73	0.7	0.7
	0.83	0.052	0.052	0.077	0.076	0.24	0.13	0.24	0.13	0.24	0.13	0.26	0.26	0.26	0.73	0.7	0.7
$\delta g_{Z,R}^{\nu\nu}$	3.	0.071	0.071	0.084	0.084	0.32	0.14	0.31	0.14	0.31	0.14	0.39	0.39	0.39	2.9	2.9	2.9
	3.	0.071	0.071	0.084	0.084	0.32	0.14	0.31	0.14	0.31	0.14	0.39	0.39	0.39	2.9	2.9	2.9
$\delta g_{Z,L}^{\mu\mu}$	0.66	0.051	0.051	0.075	0.074	0.21	0.13	0.2	0.12	0.2	0.12	0.28	0.26	0.25	0.56	0.56	0.56
	0.66	0.051	0.051	0.075	0.074	0.21	0.13	0.2	0.12	0.2	0.12	0.28	0.26	0.25	0.56	0.56	0.56
$\delta g_{Z,R}^{\mu\mu}$	19.	1.	1.	1.5	1.4	3.6	2.9	3.1	2.3	3.	2.2	6.8	6.	5.8	15.	14.	14.
	19.	1.	1.	1.5	1.4	3.6	2.9	3.1	2.3	3.	2.2	6.8	6.	5.8	15.	14.	14.
$\delta g_{Z,L}^{\tau\tau}$	0.38	0.013	0.013	0.017	0.017	0.063	0.034	0.062	0.033	0.062	0.033	0.13	0.13	0.13	0.38	0.37	0.37
	0.38	0.013	0.013	0.017	0.017	0.063	0.034	0.062	0.033	0.062	0.033	0.13	0.13	0.13	0.38	0.37	0.37
$\delta g_{Z,R}^{\tau\tau}$	11.	0.16	0.16	0.16	0.16	0.49	0.3	0.49	0.3	0.49	0.3	2.8	2.8	2.8	11.	10.	10.
	11.	0.16	0.16	0.16	0.16	0.49	0.3	0.49	0.3	0.49	0.3	2.8	2.8	2.8	11.	10.	10.

Table 29: Precision reach (in percentage) on effective couplings from a SMEFT global analysis of the Higgs and EW measurements at various future colliders listed in Table 2. For each coupling, the first (second) row shows the results from the constrained- Γ_H (free- Γ_H) fit. The results match those in Fig. 3.

Table 30: Current and future (absolute) theory uncertainties in the SM predictions for different EWPO. Future parametric uncertainties correspond to $\Delta m_H = 10$ MeV, $\Delta m_t = 20$ MeV, $\Delta\alpha_s(m_Z) = 0.0002$, $\Delta m_Z = 0.1$ MeV and two uncertainties for $\Delta\alpha(m_Z)^{-1} = 17.8/3.2$. The latter has a particular impact in the uncertainties of the W mass and the effective weak mixing angle. Current parametric uncertainties from [43].

EWPO	current unc. ΔO		future unc. ΔO	
	Th _{Intr}	Th _{Par}	Th _{Intr}	Th _{Par}
M_W [MeV]	4	4.2	1	2.4/0.6
$\sin^2 \theta_W$	$5 \cdot 10^{-5}$	$4 \cdot 10^{-3}$	$1.5 \cdot 10^{-5}$	$4.5 \cdot 10^{-5}/10^{-5}$
Γ_Z [MeV]	0.4	0.6	0.15	0.16/0.1
σ_{had}^0 [pb]	6	5.3	n/a	1/1
R_ℓ^0	$6 \cdot 10^{-3}$	$6.3 \cdot 10^{-3}$	$1.5 \cdot 10^{-3}$	$1.5 \cdot 10^{-3}/1.2 \cdot 10^{-3}$
R_c^0	$5 \cdot 10^{-5}$	$2 \cdot 10^{-5}$	n/a	$4.7 \cdot 10^{-6}/3.9 \cdot 10^{-6}$
R_b^0	$11 \cdot 10^{-5}$	$2 \cdot 10^{-5}$	$5 \cdot 10^{-5}$	$2.8 \cdot 10^{-6}/2.3 \cdot 10^{-6}$

via the optimal observable method. Unfortunately, there are no estimates available for the SM theory uncertainties in this case.

In order to quantify the impact of these SM uncertainties we consider the results derived from a series of fits analogous to the one presented above in different scenarios:

- (a) including only the SM parametric uncertainties, denoted as $\text{SM}_{\text{Param.}}$;
- (b) including the SM parametric and *future* intrinsic uncertainties, denoted as $\text{SM}_{\text{Full(Future)}}$;
- (c) including the SM parametric and *current* intrinsic uncertainties, denoted as $\text{SM}_{\text{Full(Current)}}$.

These are to be compared with another scenario:

- (d) *ignoring all* the SM theory uncertainties, which we denote as the *No Error* scenario.

In Figure 5, we show the deterioration of the results with respect to last scenario without any SM uncertainty, by presenting the ratios of the uncertainties $\delta g^{(a,b,c)}/\delta g_{\text{No Error}}$ for the different Higgs and electroweak couplings, respectively. Given

Table 31: Current and future (relative) uncertainties in the SM predictions for the different Higgs decay channels. The future parametric uncertainties correspond to an assumed precision of $\Delta m_b = 13$ MeV, $\Delta m_c = 7$ MeV, $\Delta m_t = 50$ MeV, $\Delta \alpha_s = 0.0002$ and $\Delta m_H = 10$ MeV.

Decay	current unc. $\delta\Gamma$ [%]				future unc. $\delta\Gamma$ [%]			
	Th _{Intr}	Th _{Par} ^{<i>m_q</i>}	Th _{Par} ^{α_s}	Th _{Par} ^{<i>m_H</i>}	Th _{Intr}	Th _{Par} ^{<i>m_q</i>}	Th _{Par} ^{α_s}	Th _{Par} ^{<i>m_H</i>}
$H \rightarrow b\bar{b}$	< 0.4	1.4	0.4	—	0.2	0.6	< 0.1	—
$H \rightarrow \tau^+\tau^-$	< 0.3	—	—	—	< 0.1	—	—	—
$H \rightarrow c\bar{c}$	< 0.4	4.0	0.4	—	0.2	1.0	< 0.1	—
$H \rightarrow \mu^+\mu^-$	< 0.3	—	—	—	< 0.1	—	—	—
$H \rightarrow W^+W^-$	0.5	—	—	2.6	0.3	—	—	0.1
$H \rightarrow gg$	3.2	< 0.2	3.7	—	1.0	—	0.5	—
$H \rightarrow ZZ$	0.5	—	—	3.0	0.3	—	—	0.1
$H \rightarrow \gamma\gamma$	< 1.0	< 0.2	—	—	< 1.0	—	—	—
$H \rightarrow Z\gamma$	5.0	—	—	2.1	1.0	—	—	0.1

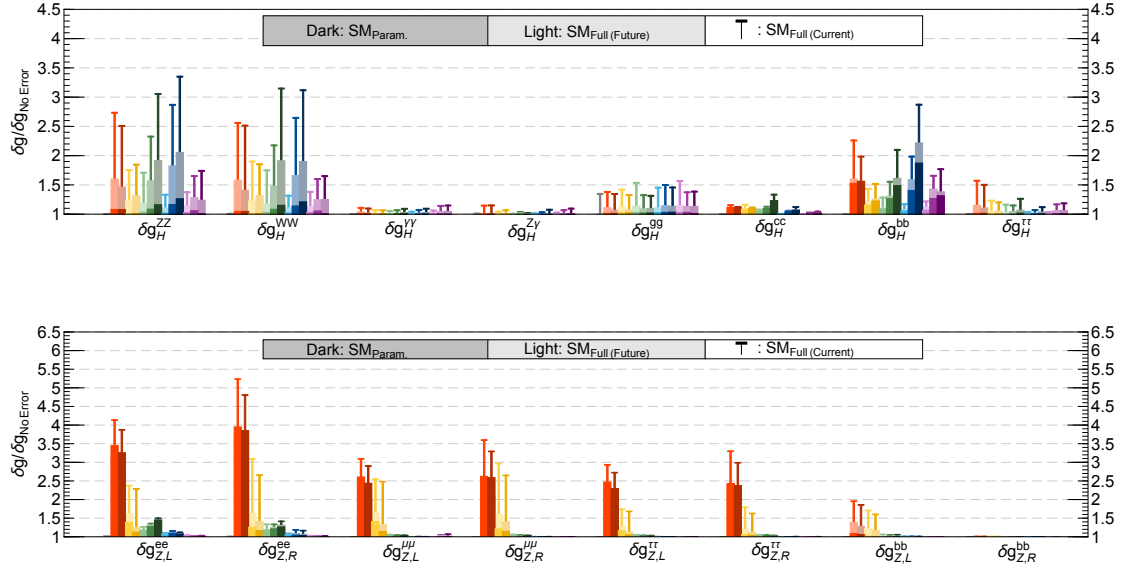


Figure 5: Impact of the parametric and intrinsic theory errors on the determination of the effective Higgs and EW couplings from the SMEFT fit. The impact is plotted in terms of the ratio between the uncertainties, δg , obtained when a given source of SM theory errors is included in the global fit and the ones derived in the case when these are not included, $\delta g_{\text{No Error}}$. The results indicated by the dark bars assume only parametric errors are included; in the light bars both parametric and intrinsic errors as projected in the future are included; finally, the thin “T” lines denote the case when future parametric errors and *current* intrinsic theory uncertainties are included.

the lack of estimates for the SM theory uncertainties in $e^+e^- \rightarrow W^+W^-$ we chose not to show the results for the aTGC. One must note that, due to the connection between aTGC and the Higgs in the dimension-6 SMEFT formalism, the results for the determination of the Higgs couplings to vector bosons may also be affected by extra uncertainties in the W^+W^- process, and therefore, the numbers presented here should be taken as an optimistic estimate of the effect of the theory uncertainties.

As it is apparent from the results in the top panel of Figure 5, and comparing with the uncertainties in Table 29 assuming the future theory calculations would be sufficient for a determination of the couplings to vector bosons at the level of 0.2-0.3 percent. Below this level of precision, the determination of the HZZ and HWW couplings would be somewhat limited by the theory uncertainties. As also noted in [9], the effect of parametric errors is relatively small, with perhaps the exception of m_b . Focusing the attention in the bottom panel of Figure 5, and looking at the case of circular colliders, we observe that, in particular, the inclusion of the SM uncertainties has a strong impact on the determination of the electroweak couplings of leptons, especially if no progress in the theory calculations is made. This is due to the higher precision that is expected for these couplings coming from the measurements at the

future Z -pole runs, which then also requires of higher theoretical precision to take advantage of such experimental measurements. The second thing that is noticeable is the large impact of parametric uncertainties on the CEPC results compared to the FCCee ones. In this case, this is mostly attributed to the different expected precision for $\alpha(m_Z)$, where the FCCee plans to run slightly below and above the Z pole to determine this parameter with improved accuracy [44]. Assuming similar measurements are performed at the CEPC would reduce significantly the impact of the parametric errors in the determination of the leptonic electroweak couplings.

5.2 Relaxing $U(2)$ assumption

As mentioned at the beginning of this section, using the future projections for the EWPO available in the literature, there is very little discriminating power between contributions from the electroweak couplings of the first family of quarks. Hence, in the fits presented here we assumed a $U(2)$ symmetry that effectively sets the first and second family quark couplings to the same value, allowing to close the fits without any flat direction. Indeed, as shown in [35], even though current Z -pole observables provide measurements that can be sensitive to the charm and even strange quark couplings separately, the traditional LEP/SLD EWPO are blind to a particular combination of up and down- quark couplings. To break this assumption we need to use an observable measurement that can be particularly sensitive to contributions from the lighter quark families. (Note also that there are currently no future Z pole projections for strange quark observables, which complicates giving sensible estimates for the sensitivity to modifications of the corresponding couplings.) In [35] it was shown that such observable can be provided by the LHC measurement of the forward-backward asymmetry in the Drell-Yan process around the Z pole, as a function of the rapidity of the dilepton system. This by itself cannot constrain all the Zqq interactions but is able to do so in combination with Z -pole measurements.

HL-LHC projections for measurements using the Drell-Yan process are available as estimates for the sensitivity to the effective weak mixing angle $\sin^2 \theta_{\text{Eff}}^{\text{lept}}$ [45, 46], in which the projections of the forward-backward asymmetry (A_{FB}) measurements are also presented. Here we use the ATLAS projections [45] of the A_{FB} measurements in the e^+e^- channel, which are divided into three sets with different rapidity ($|Y_{ee}| = [0.8 - 1.2], [2.4 - 2.8], [3.2 - 3.6]$), each presented for an invariant mass (m_{ee}) range of 60-200 GeV. We include all three rapidity sets in our analysis, and use only the two invariant mass bins of 80-90 GeV and 90-100 GeV for each set, in order to focus on the Z -pole effects and avoid large contamination from possible 4-fermion interactions. For simplicity, we consider only the contributions from $g_{Z,L/R}^{uu,dd}$, assuming all other contributions of the dimension-6 operators are sufficiently well constrained by the Z -pole measurements at lepton colliders, following the treatment in [35].

In Fig. 6 we illustrate the impact of this hadron-collider measurement on the de-

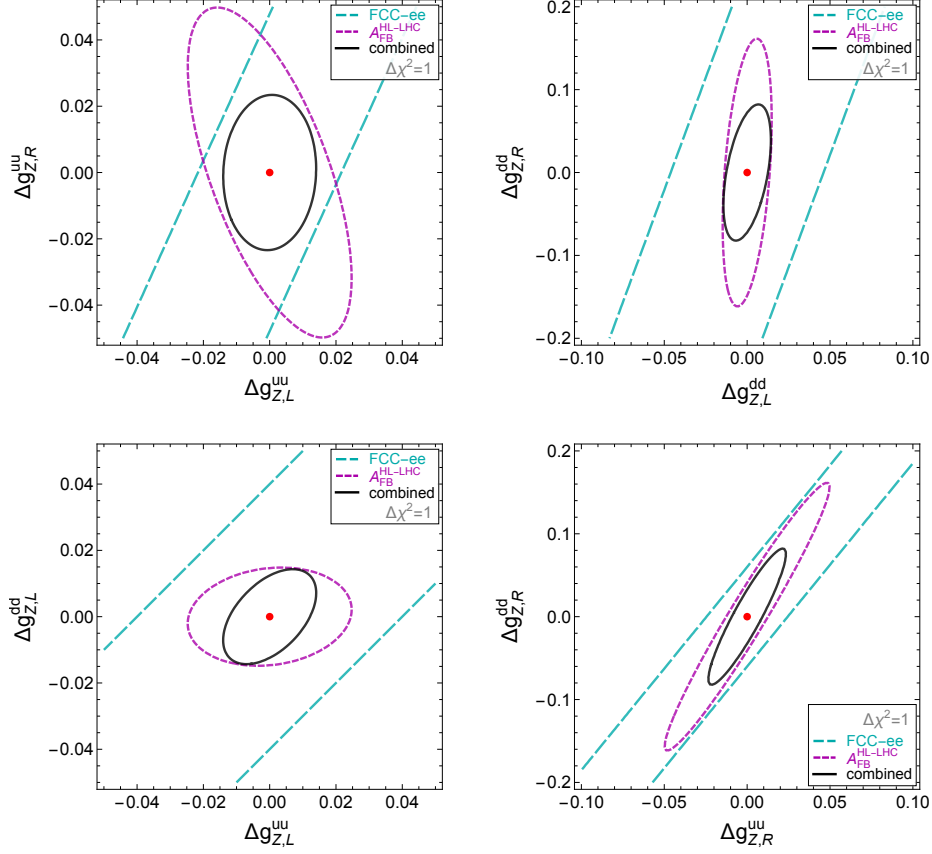


Figure 6: Marginalized $\Delta\chi^2 = 1$ bounds for $\Delta g_{Z,L/R}^{uu,dd}$ from the A_{FB} measurements at HL-LHC with ATLAS projection [45] and the FCC-ee-only Higgs + EW fit. Note that the couplings are not normalized to SM values.

termination of the up and down quark coupling by showing the $\Delta\chi^2 = 1$ bounds on different planes of the $g_{Z,L/R}^{uu,dd}$ space from the FCC-ee fit, with and without our estimate for the sensitivity to the forward-backward asymmetry at the HL-LHC. Indeed, in the FCC-ee alone fit one observes the presence of the flat direction. Using the A_{FB} measurement across 3 rapidity sets and 2 invariant mass bins, one can close this in the global fit. Furthermore, given the different correlations of the Z -pole flat direction and the A_{FB} constraints, the combined bound can significantly improve the sensitivity beyond that which would be possible using the asymmetry alone, as shown in the upper-left panel. As discussed at the beginning, however, we prefer to leave this observable outside of the main fit presented in this section until proper HL-LHC estimates from ATLAS and/or CMS are available.

$2\ell 2q$ operators ($p, r = 1, 2, 3$)	4ℓ operators ($p < r = 1, 2, 3$)
Chirality conserving	Two flavors
$[\mathcal{O}_{\ell q}]_{pprr} = (\bar{\ell}_p \bar{\sigma}_\mu \ell_p)(\bar{q}_r \bar{\sigma}^\mu q_r)$	$[\mathcal{O}_{\ell\ell}]_{pprr} = (\bar{\ell}_p \bar{\sigma}_\mu \ell_p)(\bar{\ell}_r \bar{\sigma}^\mu \ell_r)$
$[\mathcal{O}_{\ell q}^{(3)}]_{pprr} = (\bar{\ell}_p \bar{\sigma}_\mu \sigma^i \ell_p)(\bar{q}_r \bar{\sigma}^\mu \sigma^i q_r)$	$[\mathcal{O}_{\ell\ell}]_{pprr} = (\bar{\ell}_p \bar{\sigma}_\mu \ell_p)(\bar{\ell}_r \bar{\sigma}^\mu \ell_r)$
$[\mathcal{O}_{\ell u}]_{pprr} = (\bar{\ell}_p \bar{\sigma}_\mu \ell_p)(u_r^c \sigma^\mu \bar{u}_r^c)$	$[\mathcal{O}_{\ell e}]_{pprr} = (\bar{\ell}_p \bar{\sigma}_\mu \ell_p)(e_r^c \sigma^\mu \bar{e}_r^c)$
$[\mathcal{O}_{\ell d}]_{pprr} = (\bar{\ell}_p \bar{\sigma}_\mu \ell_p)(d_r^c \sigma^\mu \bar{d}_r^c)$	$[\mathcal{O}_{\ell e}]_{rrpp} = (\bar{\ell}_r \bar{\sigma}_\mu \ell_r)(e_p^c \sigma^\mu \bar{e}_p^c)$
$[\mathcal{O}_{e q}]_{pprr} = (e_p^c \sigma_\mu \bar{e}_p^c)(\bar{q}_r \bar{\sigma}^\mu q_r)$	$[\mathcal{O}_{\ell e}]_{pprr} = (\bar{\ell}_p \bar{\sigma}_\mu \ell_p)(e_r^c \sigma^\mu \bar{e}_p^c)$
$[\mathcal{O}_{e u}]_{pprr} = (e_p^c \sigma_\mu \bar{e}_p^c)(u_r^c \sigma^\mu \bar{u}_r^c)$	$[\mathcal{O}_{e e}]_{pprr} = (e_p^c \sigma_\mu \bar{e}_p^c)(e_r^c \sigma^\mu \bar{e}_r^c)$
$[\mathcal{O}_{e d}]_{pprr} = (e_p^c \sigma_\mu \bar{e}_p^c)(d_r^c \sigma^\mu \bar{d}_r^c)$	
Chirality violating	One flavor
$[\mathcal{O}_{\ell e q u}]_{pprr} = (\bar{\ell}_p^j \bar{e}_p^c) \epsilon_{jk} (\bar{q}_r^k \bar{u}_r^c)$	$[\mathcal{O}_{\ell\ell}]_{pppp} = \frac{1}{2} (\bar{\ell}_p \bar{\sigma}_\mu \ell_p)(\bar{\ell}_p \bar{\sigma}^\mu \ell_p)$
$[\mathcal{O}_{\ell e q u}^{(3)}]_{pprr} = (\bar{\ell}_p^j \bar{\sigma}_{\mu\nu} \bar{e}_p^c) \epsilon_{jk} (\bar{q}_r^k \bar{\sigma}_{\mu\nu} \bar{u}_r^c)$	$[\mathcal{O}_{\ell e}]_{pppp} = (\bar{\ell}_p \bar{\sigma}_\mu \ell_p)(e_p^c \sigma^\mu \bar{e}_p^c)$
$[\mathcal{O}_{\ell e d q}]_{pprr} = (\bar{\ell}_p^j \bar{e}_p^c)(d_r^c q_r^j)$	$[\mathcal{O}_{e e}]_{pppp} = \frac{1}{2} (e_p^c \sigma_\mu \bar{e}_p^c)(e_p^c \sigma^\mu \bar{e}_p^c)$

Table 32: 4-fermion operators included in this study. We use the notations in [5] but rename \mathcal{O}_{qe} as \mathcal{O}_{eq} so the lepton bilinear product always appears first. In each operator, p, r represent the flavor indices and j, k the isospin indices.

6 Four-fermion operators

In this section we focus our attention on the sector of electroweak interactions, but extend the fit beyond electroweak precision measurements, considering $2 \rightarrow 2$ fermion processes above the pole as well as measurements at low energy experiments. In the SMEFT, describing such a set of observables requires to consider not only the operators modifying the fermion electroweak couplings, as in the previous section, but also the corresponding set of four-fermion operators modifying these processes. For the different (projected) measurements, described in what follows, we will need to include the leptonic and semi-leptonic four-fermion operators in Eq. (5) and summarized again in Table 32.

6.1 Observables

6.1.1 Z - and W -pole observables

The Z - and W -pole observables that are sensitive to the electroweak vertex corrections in Eq. (13) have been studied in [47] without any flavor assumption. We summarize the numerical results for these pole observables in Table 33 with all the SM predictions

taken from the best fit values from GFitter [48] except that the leptonic branching ratios for W are taken from [28]. For the experimental results, we use the data and the corresponding correlation matrices, whenever possible, from LEP-1 [49] for the Z -pole observables. We also include A_s from SLD [50] and the very precise observable R_{uc} from PDG [51] in our fit. While for the W -pole observables, we use the data from LEP-2 [28] for the leptonic W branching ratios. The W mass is taken from [52] by CDF and D0, and with averaged W boson decay width from [51]. For W couplings to quarks, we also include R_{Wc} from [51] and R_σ from the CMS collaboration [53]. In particular, the latter observable can be used to constrain $\delta g_{Z,L}^{tt}$, while $\delta g_{Z,R}^{tt}$ would remain free until top data is included as done in Section 8. In addition, two well-known flat directions exist for a global fit using only these pole observables. These flat directions can be lifted by less well-measured observables. To that end, we choose the model-independent Z -quark coupling measurements from D0 [54] as well as the forward-backward asymmetry measurements (projection) from the LHC (HL-LHC).

6.1.2 High-energy observables for 4-fermion operators

To go beyond the vertex shifts, observables off the Z pole need to be included. LEP-2 [28, 55] reported fermion pair production above the Z pole, with a center of mass energy \sqrt{s} scan ranging from 130 GeV to 209 GeV. For the leptonic final state, the production cross sections and the forward-backward asymmetries were measured for $\mu^+\mu^-$ and $\tau^+\tau^-$ final states, and the differential cross section for the e^+e^- final state was reported. In contrast, for the quark final state, only the total production cross sections and the forward-backward asymmetries were measured. Note that since the LEP-2 experiment was run below the top pair threshold, the $t\bar{t}$ final state would not be produced on-shell. For reference, all these observables are summarized in Table 34, where we generically use $f(s)$ to reflect the fact that the corresponding observable is s -dependent, and the angle θ for Bhabha is the scattering angle with respect to the incoming e^- . These channels receive contributions from both the vertex shifts discussed above, and the 4-fermion operators enumerated in Table 32. As noticed in [56, 57], the energy scan of LEP-2 only provides 5 distinct observables, i.e., $\sum_{q \neq t} \sigma(q\bar{q})$, $\sigma(b\bar{b})$, $\sigma(c\bar{c})$, $\sigma_{\text{FB}}(b\bar{b})/\sum_{q \neq t} \sigma(q\bar{q})$, $\sigma_{\text{FB}}(c\bar{c})/\sum_{q \neq t} \sigma(q\bar{q})$, which would allow to probe only four different combinations of the $2\ell 2q$ operators. For this reason, less precise measurements of the total cross sections and the forward-backward asymmetries of $c\bar{c}$ and $b\bar{b}$ at $\sqrt{s} = 58$ GeV from VENUS [58] and TOPAZ [59] are also included in our fit.

Observable	Experimental value	Ref.	SM prediction
Γ_Z [GeV]	2.4952 ± 0.0023	[49]	2.4950
σ_{had} [nb]	41.541 ± 0.037	[49]	41.484
R_e	20.804 ± 0.050	[49]	20.743
R_μ	20.785 ± 0.033	[49]	20.743
R_τ	20.764 ± 0.045	[49]	20.743
$A_{\text{FB}}^{0,e}$	0.0145 ± 0.0025	[49]	0.0163
$A_{\text{FB}}^{0,\mu}$	0.0169 ± 0.0013	[49]	0.0163
$A_{\text{FB}}^{0,\tau}$	0.0188 ± 0.0017	[49]	0.0163
R_b	0.21629 ± 0.00066	[49]	0.21578
R_c	0.1721 ± 0.0030	[49]	0.17226
A_b^{FB}	0.0992 ± 0.0016	[49]	0.1032
A_c^{FB}	0.0707 ± 0.0035	[49]	0.0738
A_e	0.1516 ± 0.0021	[49]	0.1472
A_μ	0.142 ± 0.015	[49]	0.1472
A_τ	0.136 ± 0.015	[49]	0.1472
A_e	0.1498 ± 0.0049	[49]	0.1472
A_τ	0.1439 ± 0.0043	[49]	0.1472
A_b	0.923 ± 0.020	[49]	0.935
A_c	0.670 ± 0.027	[49]	0.668
A_s	0.895 ± 0.091	[50]	0.935
R_{uc}	0.166 ± 0.009	[51]	0.1724
m_W [GeV]	80.385 ± 0.015	[52]	80.364
Γ_W [GeV]	2.085 ± 0.042	[51]	2.091
$\text{Br}(W \rightarrow e\nu)$	0.1071 ± 0.0016	[28]	0.1083
$\text{Br}(W \rightarrow \mu\nu)$	0.1063 ± 0.0015	[28]	0.1083
$\text{Br}(W \rightarrow \tau\nu)$	0.1138 ± 0.0021	[28]	0.1083
R_{Wc}	0.49 ± 0.04	[51]	0.50
R_σ	0.998 ± 0.041	[53]	1.000

Table 33: Z and W -pole observables used in the fit. $A_{e,\tau}$ appear twice in the above table: The first numbers are from SLC, and the second ones are from τ polarization at LEP-1.

Observable	Experimental value	Ref.	SM prediction
$\sigma(\mu^+\mu^-)$	$f(s)$	[28]	$f(s)$ [28]
$\sigma(\tau^+\tau^-)$	$f(s)$	[28]	$f(s)$ [28]
$\sum_{q \neq t} \sigma(q\bar{q})$	$f(s)$	[28, 58, 59]	$f(s)$ [28, 58, 59]
$\sigma(b\bar{b})$	$f(s)$	[55, 58, 59]	$f(s)$ [55, 58, 59]
$\sigma(c\bar{c})$	$f(s)$	[55, 58, 59]	$f(s)$ [55, 58, 59]
$\frac{\sigma_{\text{FB}}(b\bar{b})}{\sum_{q \neq t} \sigma(q\bar{q})}$	$f(s)$	[55, 58, 59]	$f(s)$ [55, 58, 59]
$\frac{\sigma_{\text{FB}}(c\bar{c})}{\sum_{q \neq t} \sigma(q\bar{q})}$	$f(s)$	[55, 58, 59]	$f(s)$ [55, 58, 59]
$A_{\text{FB}}(\mu^+\mu^-)$	$f(s)$	[28]	$f(s)$ [28]
$A_{\text{FB}}(\tau^+\tau^-)$	$f(s)$	[28]	$f(s)$ [28]
$\frac{d\sigma}{d\cos\theta}(\text{Bhabha})$	$f(s, \cos\theta)$	[28]	$f(s, \cos\theta)$ [28]

Table 34: Observables for fermion-pair production at lepton colliders. Here, we use $f(s)$ and $f(s, \cos\theta)$ to reflect the fact that the corresponding observables depend on the center of mass energy \sqrt{s} and the scattering angle θ that is with respect to the incoming e^- .

6.1.3 Low-energy precision observables

On the other hand, well below the Z pole, various precision observables can also be utilized to constrain these 4-fermion operators. These observables, together the corresponding processes and the relevant experiments, are summarized in Table 35. As implied in the table, these observables are conventionally parameterized using the low-energy EFT (LEFT). We adopt the notations in [57] and parameterize the LEFT

Process	Observable	Experimental value	Ref.	SM prediction
$\nu_{\mu}^{-} - e^{-}$ scattering	$g_{LV}^{\nu_{\mu}e}$	-0.035 ± 0.017	CHARM-II [60]	-0.0396 [61]
	$g_{LA}^{\nu_{\mu}e}$	-0.503 ± 0.017		-0.5064 [61]
τ decay	$\frac{G_F^2}{G_F^2}$	1.0029 ± 0.0046	PDG2014 [62]	1
	$\frac{G_F^2}{G_F^2}$	0.981 ± 0.018		
	$\frac{G_F^2}{G_F^2}$			
Neutrino scattering	$R_{\nu_{\mu}}$	0.3093 ± 0.0031	CHARM ($r = 0.456$) [63]	0.3156 [63]
	$R_{\bar{\nu}_{\mu}}$	0.390 ± 0.014		0.370 [63]
	$R_{\nu_{\mu}}$	0.3072 ± 0.0033	CDHS ($r = 0.393$) [64]	0.3091 [64]
	$R_{\bar{\nu}_{\mu}}$	0.382 ± 0.016		0.380 [64]
	κ	0.5820 ± 0.0041	CCFR [65]	0.5830 [65]
$R_{\nu_e \bar{\nu}_e}$	$0.406^{+0.145}_{-0.135}$	CHARM [66]	0.33 [67]	
Parity-violating scattering	$(s_w^2)^{\text{Møller}}$	0.2397 ± 0.0013	SLAC-E158 [68]	0.2381 ± 0.0006 [69]
	$Q_W^{Cs}(55, 78)$	-72.62 ± 0.43	PDG2016 [67]	-73.25 ± 0.02 [67]
	$Q_W^p(1, 0)$	0.064 ± 0.012	QWEAK [70]	0.0708 ± 0.0003 [67]
	A_1	$(-91.1 \pm 4.3) \times 10^{-6}$	PVDIS [71]	$(-87.7 \pm 0.7) \times 10^{-6}$ [71]
	A_2	$(-160.8 \pm 7.1) \times 10^{-6}$		$(-158.9 \pm 1.0) \times 10^{-6}$ [71]
	$g_{VA}^{e\nu} - g_{VA}^{e\ell}$	-0.042 ± 0.057	SAMPLE ($\sqrt{Q^2} = 200$ MeV) [72]	-0.0360 [67]
		-0.12 ± 0.074	SAMPLE ($\sqrt{Q^2} = 125$ MeV) [72]	0.0265 [67]
b_{SPS}	$-(1.47 \pm 0.42) \times 10^{-4} \text{ GeV}^{-2}$ $-(1.74 \pm 0.81) \times 10^{-4} \text{ GeV}^{-2}$	SPS ($\lambda = 0.81$) [73] SPS ($\lambda = 0.66$) [73]	$-1.56 \times 10^{-4} \text{ GeV}^{-2}$ [73] $-1.57 \times 10^{-4} \text{ GeV}^{-2}$ [73]	
τ polarization	\mathcal{P}_{τ}	0.012 ± 0.058	VENUS [74]	0.028 [74]
	$\mathcal{A}_{\mathcal{P}}$	0.029 ± 0.057		0.021 [74]
Neutrino trident production	$\frac{\sigma}{\sigma_{\text{SM}}}(\nu_{\mu}\gamma^* \rightarrow \nu_{\mu}\mu^+\mu^-)$	0.82 ± 0.28	CCFR [75–77]	1
$d_I \rightarrow u_j \ell \bar{\nu}_I(\gamma)$	$\epsilon_{L,R,S,P,T}^{deI}$	See text	[78]	0
$e^+e^- \rightarrow f\bar{f}$	δA_{LR}^e	2.0%	SuperKEKB [79]	0.00015
	δA_{LR}^{μ}	1.5%		-0.0006
	δA_{LR}^{τ}	2.4%		-0.0006
	δA_{LR}^c	0.5%		-0.005
	δA_{LR}^b	0.4%		-0.020

Table 35: Low-energy observables included in the global fit to break possible degeneracies for the 4ℓ and $2\ell 2q$ operators listed in Table 32. The last entry for A_{LR}^f is taken from [79] for SuperKEKB that would operate at 10.58 GeV with 40 ab^{-1} integrated luminosity and a beam polarization of $(70 \pm 0.3)\%$.

as

$$\begin{aligned}
\mathcal{L}_{\text{LEFT}} \supset & - \sum_{I,J=1,2} \frac{2\tilde{V}_{ud_I}^{e_J}}{v^2} \left[\left(1 + \epsilon_L^{d_I e_J}\right) (\bar{e}_J \bar{\sigma}_\mu \nu_J) (\bar{u} \bar{\sigma}^\mu d_I) + \epsilon_R^{d_I e_J} (\bar{e}_J \bar{\sigma}_\mu \nu_J) \left(u^c \sigma^\mu \bar{d}_I^c\right) \right. \\
& + \frac{\epsilon_S^{d_I e_J} + \epsilon_P^{d_I e_J}}{2} (e_J^c \nu_J) (u^c d_I) + \frac{\epsilon_S^{d_I e_J} - \epsilon_P^{d_I e_J}}{2} (e_J^c \nu_J) \left(\bar{u} \bar{d}_I^c\right) \\
& \left. + \epsilon_T^{d_I e_J} (e_J^c \sigma_{\mu\nu} \nu_J) (u^c \sigma_{\mu\nu} d_I) + h.c. \right] \\
& - \sum_{q=u,d} \frac{2}{v^2} (\bar{\nu}_J \bar{\sigma}^\mu \nu_J) (g_{LL}^{\nu J q} \bar{q} \sigma_\mu q + g_{LR}^{\nu J q} q^c \sigma_\mu \bar{q}^c) \\
& + \sum_{q=u,d} \frac{1}{2v^2} [g_{AV}^{e_J q} (\bar{e}_J \gamma_\mu \gamma_5 e_J) (\bar{q} \gamma_\mu q) + g_{VA}^{e_J q} (\bar{e}_J \gamma_\mu e_J) (\bar{q} \gamma_\mu \gamma_5 q) \\
& + g_{VV}^{e_J q} (\bar{e}_J \gamma_\mu e_J) (\bar{q} \gamma_\mu q) + g_{AA}^{e_J q} (\bar{e}_J \gamma_\mu \gamma_5 e_J) (\bar{q} \gamma_\mu \gamma_5 q)] \\
& - \sum_{I,J=1,2} \frac{1}{v^2} (\bar{\nu}_J \bar{\sigma}_\mu \nu_J) [(g_{LV}^{\nu J e_I} + g_{LA}^{\nu J e_I}) (\bar{e}_I \bar{\sigma}_\mu e_I) + (g_{LV}^{\nu J e_I} - g_{LA}^{\nu J e_I}) (e_I^c \sigma_\mu \bar{e}_I^c)],
\end{aligned} \tag{24}$$

where the first (second) term is usually referred to as the charge- (neutral-) current neutrino non-standard interactions (NSIs), and the third (last) term is the 4-fermion operators of $2\ell 2q$ (4ℓ) types. Note also that the SMEFT framework we adopt in this study forces $\epsilon_R^{de} = \epsilon_R^{d\mu}$ up to $\mathcal{O}(1/\Lambda^4)$ as a result of the $SU(2)_L \times U(1)_Y$ invariance [80–82].

Due to the presence of the SMEFT operators, the weak currents will be modified and as a result, the W couplings to quarks will no longer be unitary. An overall $\tilde{V}_{ud_I}^{e_J}$ is factored out to reflect this fact and its “11” element would be related to the actual V_{ud}^e through $V_{ud}^e = \tilde{V}_{ud}^e (1 + \delta V_{ud}^e)$ with δV_{ud}^e chosen such that $\epsilon_L^{de} = -\epsilon_R^{de}$. As a consequence, δV_{ud}^e effectively only depends on ϵ_S^{de} . Note that corrections from ϵ_S^{de} can not always be absorbed away from a redefinition of the hadronic form factors for a generic process, the nuclear or the neutron beta decay for example. For this reason, one shall take \tilde{V}_{ud}^e as a free parameter in the fit to be consistent. In practice, \tilde{V}_{ud}^e can be precisely measured from the superallowed nuclear beta decay [83], which in turn allows one to perform a unitarity test of the first row of the CKM matrix, via a combined analysis of the $K_{e3(\gamma)}$ decay rates to extract \tilde{V}_{us}^e . Calculations of the decay rates, on the other hand, rely on a global fit to the kinematic distributions of the decay, as well as extra observables, such as the lepton-universality ratios $R_{\pi,K}$, from the (inclusive) (semi)leptonic decays of pions and kaons, plus nuclear, neutron and hyperon beta decays in order to lift the flat directions in the fit [78]. A global fit on the ϵ parameters has been done in [78], with the full correlation matrix provided. One can thus readily reconstruct the χ^2 from their results and add it to the global fit in a larger framework, the SMEFT for example, as long as the matching and running

effects are properly included.

We have independently performed the matching between the LEFT in Eq. (24) and the SMEFT in the Higgs basis, perfect agreement has been found with those in [57]. Note that the validity of EFTs requires the LEFT and the SMEFT to be defined at very different energy scales, thus this matching procedure is only meaningful at the weak scale. Therefore, to consistently combine the low-energy observables with the high-energy ones, we evolve the LEFT Wilson coefficients, typically defined at 2 GeV, up to the weak scale through the renormalization group equations. While the running effects are generically small at the percent level and can be neglected for our purpose, it is not quite accurate for the $2\ell 2q$ type operators, where higher-loop QCD effects were found to be significant [57, 84]. For this reason, one-loop QED and electroweak [85–87], as well as three-loop QCD [88] including b and t threshold effects [89, 90] are included in our analysis, but Yukawa suppressed corrections in [91] are generically ignored.

Following the prescription discussed above, the χ^2 for the high- and low-energy processes is then constructed from these observables summarized in Table 33, Table 34, and Table 35, with the exception for the muon neutrino scattering and the $d_I \rightarrow u_J \ell \bar{\nu}_\ell(\gamma)$ ($I, J = 1, 2$) processes.* For the former, due to the strong and non-Gaussian correlations between $g_{LL}^{\nu Jq}$ and $g_{LR}^{\nu Jq}$, we use the PDG fit in [67] using the $g_{L,R}^{\nu\mu}$ and $\theta_{L,R}^{\nu\mu}$ parameterization. These variables are related to our notations in Eq. (24) through

$$\left(g_{L/R}^{\nu J}\right)^2 \equiv \frac{\left(g_{LL/LR}^{\nu Ju}\right)^2 + \left(g_{LL/LR}^{\nu Jd}\right)^2}{\left(1 + \epsilon_L^{deJ}\right)^2}, \quad \theta_{L/R}^{\nu J} \equiv \arctan\left(\frac{g_{LL/LR}^{\nu Ju}}{g_{LL/LR}^{\nu Jd}}\right), \quad (25)$$

and are expanded consistently to the linear order in terms of the dimension-six SMEFT operators in practice. While for the latter, a global fit for the ϵ parameters in Eq. (24) has been performed in [78] taking into account both inclusive and exclusive (semi)leptonic decay of pions and kaons, as well as nuclear, neutron and hyperon decays. We reconstruct the full χ^2 from their results with the full correlations taken into account, and then marginalize over \tilde{V}_{ud}^e and the effective couplings of the strange quark.†

6.2 Flat directions

The observables discussed in previous subsections, however, are not sufficient enough to separately constrain all the Wilson coefficients involved for the following

*As an intermediate step, we derive all the analytical results for all the observables used in our fit, and find agreement with those in [47, 57]. Results from our global fit also agree those in [47, 57].

†Inclusion of the strange couplings will introduce the dependence on off-diagonal flavor couplings, which will not be covered in this study.

reasons:

- Since LEP was run below the top-pair threshold, flat directions will thus show up for the 4-fermion operators of the $2\ell 2q$ type, which we denote by **Flat**[top]. These flat directions may be lifted at future lepton colliders by running above the top-pair threshold, see [Section 8](#).
- Though the total cross section and the forward-backward asymmetry for $c\bar{c}$ are included using the experimental results from VENUS and TOPAZ, the corresponding information for the strange quark is missing. As a result, similar flat directions as **Flat**[top], i.e., **Flat**[strange], arise. These flat directions could be lifted when σ_s and A_{FB}^s becomes available at future lepton colliders.
- The parity-conserving $(\bar{e}\gamma_\mu\gamma_5e)(\bar{q}_1\gamma_\mu\gamma_5q_1)$ and the axial vector neutrino-quark $(\bar{\nu}_L\gamma_\mu\nu_L)(\bar{q}_1\gamma_\mu\gamma_5q_1)$ operators remain unconstrained at the low-energy parity-violating scattering experiments or LEP. We denote these flat directions as **Flat**[parity]. These flat directions could possibly be eliminated by future low-energy parity-violating electron-nucleus scattering experiments, the P2 experiment as MESA [\[92\]](#), for example.
- The muon scattering off the Carbon target at CERN SPS is insufficient to disentangle the contributions from $\mathcal{O}_{eq,eu,ed}$. We denote the resultant flat directions as **Flat**[SPS]. Varying the muon beam polarization λ alone will not help in lifting this flat direction, but precision measurements of the neutral-current charged-lepton and quark interactions would, light quark pair production at a future muon collider for example.
- The trident process is the only low-energy channel sensitive to the four-muon operators $\mathcal{O}_{\ell\ell,\ell e}$, we denote this flat direction by **Flat**[trident]. We note that the $Z \rightarrow 4\mu$ branching ratio has been measured at the LHC [\[93–95\]](#) and can thus be used to probe these operators.* However, this branching ratio is also dependent on \mathcal{O}_{ee} . Therefore, to eventually close the fit, one could, for example, measure the cross section and the asymmetry of muon pair production at a future muon collider. Note in particular that the muon beam polarization would be expected to help improve the fit significantly in this respect.
- The $\pi_{\mu 2}$ decay rate only provides one constraint on $\epsilon_P^{d\mu}$ from the flavor observable R_π . Interpreting in the SMEFT, $\epsilon_P^{d\mu}$ is sourced from both \mathcal{O}_{ledq} and \mathcal{O}_{lequ} . The lack of additional flavor observables sensitive to $\epsilon_P^{d\mu}$ results in an additional flat direction, which we call **Flat**[flavor].

To separate these flat directions, we define [\[57\]](#)

*We thank Radja Boughezal for pointing this observable to us.

- **Flat**[top]:

$$\left[\hat{c}_{\ell q}^{(3)}\right]_{1133} = \left[c_{\ell q}^{(3)}\right]_{1133} + [c_{\ell q}]_{1133}. \quad (26)$$

- **Flat**[strange]:

$$\begin{aligned} \left[\hat{c}_{\ell q}^{(3)}\right]_{1122} &= \left[c_{\ell q}^{(3)}\right]_{1122} - [c_{\ell q}]_{1122}, \\ \left[\hat{c}_{\ell d}\right]_{1122} &= [c_{\ell d}]_{1122} + \left(5 - \frac{3g^2}{g'^2}\right) [c_{\ell q}]_{1122} - [\hat{c}_{eq}]_{1111}, \\ \left[\hat{c}_{ed}\right]_{1122} &= [c_{ed}]_{1122} - \left(3 - \frac{3g^2}{g'^2}\right) [c_{\ell q}]_{1122} - [\hat{c}_{eq}]_{1111}. \end{aligned} \quad (27)$$

- **Flat**[parity]:

$$\begin{aligned} [\hat{c}_{eq}]_{1111} &= [c_{eq}]_{1111} + [c_{\ell q}]_{1111}, \\ [\hat{c}_{\ell u}]_{1111} &= [c_{\ell u}]_{1111} + [c_{\ell q}]_{1111} - [\hat{c}_{eq}]_{1111}, \\ [\hat{c}_{\ell d}]_{1111} &= [c_{\ell d}]_{1111} + [c_{\ell q}]_{1111} - [\hat{c}_{eq}]_{1111}, \\ [\hat{c}_{eu}]_{1111} &= [c_{eu}]_{1111} - [c_{\ell q}]_{1111}, \\ [\hat{c}_{ed}]_{1111} &= [c_{ed}]_{1111} - [c_{\ell q}]_{1111}, \end{aligned} \quad (28)$$

- **Flat**[SPS]:

$$[\hat{c}_{eq}]_{2211} = [c_{eq}]_{2211} + [c_{ed}]_{2211} - 2[c_{eu}]_{2211}, \quad (29)$$

- **Flat**[trident]:

$$[\hat{c}_{\ell\ell}]_{2222} = [c_{\ell\ell}]_{2222} + \frac{2g'^2}{g^2 + 3g'^2} [c_{\ell e}]_{2222}, \quad (30)$$

- **Flat**[flavor]:

$$\epsilon_P^{d\mu}[2\text{ GeV}] = 0.86 [c_{\ell edq}]_{2211} - 0.86 [c_{\ell equ}]_{2211} + 0.012 \left[c_{\ell edq}^{(3)}\right]_{2211}. \quad (31)$$

It is worth pointing out that the numbers on the right hand side are directly from the renormalization group evolution, based on [84], from $\mu = 2\text{ GeV}$ to $\mu = m_Z$, where the matching between the LEFT and the SMEFT is performed. The coefficient of $\left[c_{\ell edq}^{(3)}\right]_{2211}$ is much smaller than the other two since it only indirectly matches onto $\epsilon_P^{d\mu}[2\text{ GeV}]$ through the renormalization group evolution.

6.3 SMEFT global fit results

Results for the vertex and the 4-fermion operators are reported in this subsection based on inputs summarized in Section 4. The numerical 1σ bounds from the global fit are summarized in Table 36, and also pictorially in Fig. 7, Fig. 8 and Fig. 9 at various lepton colliders. As for the Higgs and electroweak fit presented in last section, the relative (absolute) 1σ errors are always reported whenever their corresponding SM predictions are non-vanishing (vanishing). Several comments are in order:

- While one can implement special flavor structures, such as the $U(3)^5$ global symmetry [96, 97] and the Minimal Flavor Violation symmetry [98], to reduce the number of parameters in the fit, we do not make any flavor assumptions except for focusing on flavor diagonal operators only in this study.
- For ILC running at different energies and luminosities, a horizontal white line is drawn in Fig. 7, Fig. 8 and Fig. 9 to indicate the alternative results if the pole observables from the GigaZ option in Table 3 is adopted for the fit.
- At future circular lepton colliders, we find $\delta g_Z^{\ell\ell}$ would be constrained about one order of magnitude better than δg_Z^{qq} . Projections on the R_{uc} parameter are expected to improve the sensitivity to δg_Z^{qq} .
- The right-handed coupling between W and the first-generation quark only contributes at the quadratic order to high-energy observables, and their corrections to the SM predictions are thus suppressed and ignored. In contrast, the low-energy flavor observables, neutral-current electron-neutrino scattering off nuclei and the CKM unitarity test specifically, have a linear dependence on it. These low-energy flavor observables dominate the constraint on $\hat{\delta}g_R^{Wq_1}$.
- Measurements of the average τ polarization and its forward-backward asymmetry at VENUS help eliminate the flat direction existed in τ pair production at LEP. However, results from the VENUS collaboration are not yet very precise and are expected to be surpassed by SuperKEKB [79] and future e^+e^- [99] results.
- With polarized beams probing different combinations of the Wilson coefficients at future linear lepton colliders, constraints on some of the 4-fermion operators turn out to be several orders of magnitude better than those at the future circular colliders, $[c_{eq}]_{1122}$ and $[c_{eu}]_{1122}$ for example. This largely seeds in the fact that beam polarizations help reduce the correlations among multiple Wilson coefficients significantly.

in %	LEP + SLC + SLD + D0 + LHC	HL-LHC 14 TeV	ILC						CLIC			FCC-ee		CEPC	
			250		+500		+1 TeV		380	+1.5 TeV	+3 TeV	240	+365	240	+360
			Giga-Z		Giga-Z		Giga-Z								
$\delta g_W^{\nu\nu}$	0.64	0.233	0.046	0.043	0.042	0.0465	0.042	0.0404	0.091	0.085	0.083	0.0185	0.018	0.012	0.0119
$\delta g_W^{\mu\nu}$	0.59	0.58	0.047	0.043	0.042	0.047	0.043	0.041	0.1	0.091	0.089	0.0184	0.018	0.0119	0.0118
$\delta g_W^{\nu\nu}$	0.79	0.62	0.047	0.043	0.042	0.047	0.043	0.041	0.1	0.092	0.089	0.0184	0.018	0.0119	0.0118
$\delta g_{ZL}^{\nu\nu}$	0.102	0.098	0.0286	0.0153	0.0121	0.0212	0.013	0.01	0.053	0.046	0.044	0.0077	0.0076	0.0053	0.0053
$\delta g_{ZL}^{\mu\nu}$	0.45	0.13	0.064	0.058	0.054	0.028	0.026	0.025	0.094	0.09	0.09	0.008	0.008	0.0075	0.0075
$\delta g_{ZL}^{\nu\nu}$	0.22	0.22	0.073	0.066	0.062	0.033	0.031	0.03	0.15	0.14	0.137	0.0127	0.0127	0.008	0.008
$\delta g_{ZR}^{\nu\nu}$	0.116	0.113	0.029	0.015	0.0118	0.0213	0.0128	0.01	0.058	0.051	0.049	0.0077	0.0076	0.0053	0.0053
$\delta g_{ZR}^{\mu\nu}$	0.58	0.157	0.07	0.064	0.06	0.028	0.026	0.0253	0.11	0.106	0.105	0.008	0.008	0.0076	0.0076
$\delta g_{ZR}^{\nu\nu}$	0.266	0.265	0.078	0.072	0.068	0.033	0.031	0.03	0.174	0.163	0.16	0.0146	0.0145	0.0084	0.0084
$\delta g_{ZL}^{\mu\nu}$	6.65	1.29	0.67	0.66	0.65	0.56	0.56	0.56	0.86	0.84	0.84	0.55	0.55	0.55	0.55
$\delta g_{ZL}^{\nu\nu}$	1.06	1.05	0.22	0.198	0.183	0.144	0.138	0.132	0.24	0.233	0.23	0.076	0.076	0.052	0.051
$\delta g_{ZR}^{\mu\nu}$	11.92	11.92	11.91	11.91	11.91	11.91	11.91	11.91	11.91	11.91	11.91	11.91	11.91	11.91	11.91
$\delta g_{ZR}^{\nu\nu}$	18.1	7.36	7.05	7.05	7.05	7.04	7.03	7.03	7.1	7.09	7.09	7.03	7.03	7.03	7.03
$\delta g_{ZR}^{\mu\nu}$	3.42	3.4	0.32	0.3	0.28	0.16	0.153	0.148	0.4	0.39	0.39	0.084	0.084	0.068	0.068
$\delta g_{ZL}^{\mu\nu}$	8.05	1.61	1.46	1.46	1.46	1.44	1.44	1.44	1.5	1.49	1.49	1.44	1.44	1.44	1.44
$\delta g_{ZL}^{\nu\nu}$	6.03	2.29	1.35	1.35	1.35	1.35	1.34	1.34	1.42	1.41	1.41	1.33	1.33	1.33	1.33
$\delta g_{ZR}^{\mu\nu}$	0.4	0.395	0.061	0.055	0.051	0.042	0.04	0.038	0.094	0.09	0.089	0.0173	0.0173	0.0124	0.0124
$\delta g_{ZR}^{\nu\nu}$	153.85	45.75	44.02	44.	43.99	43.98	43.97	43.96	44.19	44.18	44.17	43.91	43.91	43.91	43.91
$\delta g_{ZR}^{\mu\nu}$	63.14	53.5	18.48	18.34	18.24	18.06	17.79	17.69	24.02	23.37	23.16	16.46	16.45	16.35	16.35
$\delta g_{ZR}^{\nu\nu}$	11.19	11.07	0.46	0.43	0.4	0.374	0.356	0.34	1.32	1.18	1.16	0.16	0.16	0.16	0.16
$\delta g_R^{Wq_1}$	1.69	1.69	1.69	1.69	1.69	1.69	1.69	1.69	1.69	1.69	1.69	1.69	1.69	1.69	1.69
$[c_{\ell}]_{1111}$	0.4	0.28	0.0051	0.0017	0.00061	0.005	0.00167	0.00059	0.0059	0.0007	0.00023	0.064	0.063	0.063	0.063
$[c_{\ell}]_{1111}$	0.22	0.074	0.0062	0.00216	0.00077	0.0048	0.00207	0.00076	0.005	0.0013	0.00044	0.00385	0.0031	0.00203	0.00195
$[c_{\ell}]_{1111}$	0.404	0.39	0.0065	0.00217	0.00083	0.006	0.0021	0.00082	0.0086	0.00195	0.00066	0.067	0.066	0.066	0.065
$[c_{\ell}]_{1221}$	1.63	1.23	0.162	0.155	0.152	0.177	0.166	0.16	0.32	0.3	0.29	0.057	0.056	0.0385	0.038
$[c_{\ell}]_{1122}$	1.82	1.81	0.162	0.154	0.152	0.176	0.165	0.16	0.32	0.3	0.29	1.66	1.2	1.66	1.21
$[c_{\ell}]_{1122}$	1.87	1.86	0.0089	0.0029	0.00101	0.0085	0.0028	0.001	0.0088	0.0011	0.00037	1.71	1.23	1.71	1.24
$[c_{\ell}]_{2211}$	1.8	1.8	0.0089	0.0029	0.00102	0.0086	0.0028	0.001	0.0089	0.0021	0.00072	1.71	1.23	1.71	1.24
$[c_{\ell}]_{1122}$	2.38	1.91	0.0067	0.00224	0.0008	0.0063	0.00215	0.00078	0.0069	0.00164	0.00056	1.79	1.29	1.79	1.3
$[c_{\ell}]_{1331}$	1.34	1.32	0.49	0.49	0.48	0.49	0.49	0.49	0.56	0.55	0.55	0.46	0.46	0.46	0.46
$[c_{\ell}]_{1133}$	11.29	5.32	0.49	0.49	0.48	0.49	0.49	0.49	0.56	0.55	0.55	5.17	1.82	5.17	1.86
$[c_{\ell}]_{1133}$	7.22	5.32	0.01	0.00324	0.00114	0.0096	0.00315	0.00112	0.0101	0.00124	0.000416	5.3	1.81	5.3	1.86
$[c_{\ell}]_{3311}$	7.22	5.32	0.01	0.00324	0.00115	0.0097	0.0032	0.00113	0.01	0.0024	0.00081	5.3	1.81	5.3	1.86
$[c_{\ell}]_{1133}$	12.16	5.59	0.0074	0.00247	0.00088	0.007	0.00237	0.00086	0.0077	0.0018	0.00062	5.56	1.89	5.56	1.94
$[\hat{c}_{\ell}]_{2222}$	22.92	22.92	22.84	22.84	22.84	22.84	22.84	22.84	22.84	22.84	22.84	22.84	22.84	22.84	22.84
$[c_{\ell}]_{2332}$	2.25	1.96	1.81	1.81	1.81	1.81	1.81	1.81	1.83	1.83	1.83	1.8	1.8	1.8	1.8
$[c_{\ell}^{(3)}]_{1111}$	2.9	1.8	1.78	1.78	1.78	1.78	1.78	1.78	1.79	1.79	1.79	1.78	1.78	1.78	1.78
$[\hat{c}_{\ell}]_{1111}$	179.61	178.79	178.74	178.74	178.74	178.74	178.74	178.74	178.75	178.75	178.75	178.74	178.74	178.74	178.74
$[\hat{c}_{\ell}]_{1111}$	8.75	7.68	7.65	7.65	7.65	7.65	7.65	7.65	7.66	7.66	7.66	7.65	7.65	7.65	7.65
$[\hat{c}_{\ell}]_{1111}$	17.92	11.61	11.56	11.56	11.56	11.56	11.56	11.56	11.57	11.57	11.57	11.56	11.56	11.56	11.56
$[\hat{c}_{\ell}]_{1111}$	9.38	7.86	7.84	7.84	7.84	7.84	7.84	7.84	7.84	7.84	7.84	7.83	7.83	7.83	7.83
$[\hat{c}_{\ell}]_{1111}$	17.11	11.55	11.51	11.51	11.51	11.51	11.51	11.51	11.52	11.52	11.52	11.51	11.51	11.51	11.51
$[c_{\ell}^{(3)}]_{1122}$	28.94	13.43	0.0245	0.0081	0.0028	0.023	0.0077	0.0027	0.023	0.0029	0.00097	10.83	0.29	10.83	0.283
$[c_{\ell}]_{1122}$	7.76	7.59	0.034	0.011	0.0039	0.0335	0.0108	0.00385	0.0335	0.00415	0.0014	6.76	0.185	6.76	0.172
$[\hat{c}_{\ell}]_{1122}$	121.45	86.39	44.68	44.68	44.68	44.68	44.68	44.68	44.7	44.69	44.69	75.47	44.7	75.47	44.7
$[c_{\ell}]_{1122}$	26.26	25.75	0.061	0.017	0.0058	0.061	0.0168	0.0058	0.054	0.012	0.0041	18.89	0.46	18.89	0.47
$[c_{\ell}]_{1122}$	41.3	19.08	0.023	0.0078	0.0028	0.022	0.0076	0.00276	0.024	0.0058	0.002	15.16	0.4	15.16	0.395
$[\hat{c}_{\ell}]_{1122}$	128.73	86.56	25.43	25.43	25.43	25.43	25.43	25.43	25.45	25.44	25.44	69.8	25.48	69.8	25.47
$[c_{\ell}^{(3)}]_{1133}$	7.57	1.44	0.0107	0.0035	0.00122	0.0102	0.0034	0.0012	0.0104	0.00128	0.00043	0.42	0.082	0.42	0.082
$[c_{\ell}]_{1133}$	9.54	6.65	0.0228	0.007	0.0024	0.0225	0.0069	0.0024	0.022	0.0026	0.00087	3.55	0.103	3.55	0.11
$[c_{\ell}]_{1133}$	4.74	3.37	0.0122	0.0044	0.00165	0.012	0.0044	0.00164	0.0136	0.0035	0.0012	2.26	0.073	2.26	0.071
$[c_{\ell}]_{1133}$	18.57	3.05	0.0122	0.004	0.00144	0.0118	0.00395	0.00142	0.0135	0.00305	0.00103	1.	0.19	1.	0.19
$[c_{\ell}^{(3)}]_{2211}$	3.57	2.76	2.02	2.02	2.01	2.02	2.02	2.02	2.05	2.05	2.04	2.01	2.01	2.	2.
$[c_{\ell}]_{2211}$	5.93	2.77	2.68	2.68	2.68	2.67	2.67	2.67	2.7	2.7	2.7	2.67	2.67	2.67	2.67
$[c_{\ell}]_{2211}$	8.11	6.22	6.13	6.13	6.13	6.13	6.13	6.13	6.14	6.14	6.14	6.13	6.13	6.13	6.13
$[c_{\ell}]_{2211}$	26.34	13.11	12.96	12.96	12.96	12.96	12.96	12.96	12.98	12.97	12.97	12.96	12.96	12.96	12.96
$[\hat{c}_{\ell}]_{2211}$	40.71	38.89	38.88	38.88	38.88	38.88	38.88	38.88	38.88	38.88	38.88	38.88	38.88	38.88	38.88
$[c_{\ell}]_{1111}$	0.076	0.076	0.076	0.076	0.076	0.076	0.076	0.076	0.076	0.076	0.076	0.076	0.076	0.076	0.076
$[c_{\ell}]_{1111}$	0.076	0.076	0.076	0.076	0.076	0.076	0.076	0.076	0.076	0.076	0.076	0.076	0.076	0.076	0.076
$[c_{\ell}^{(3)}]_{1111}$	0.194	0.194	0.194	0.194	0.194	0.194	0.194	0.194	0.194	0.194	0.194	0.194	0.194	0.194	0.194
$c_{\ell}^{(3)} [2 \text{ GeV}]$	0.144	0.141	0.13	0.13	0.13	0.13	0.13	0.13	0.13	0.13	0.13	0.13	0.13	0.13	0.13

Table 36: Precision reach (in percentage) on the effective couplings from a SMEFT global analysis of the 4-fermion operators at various future lepton colliders.

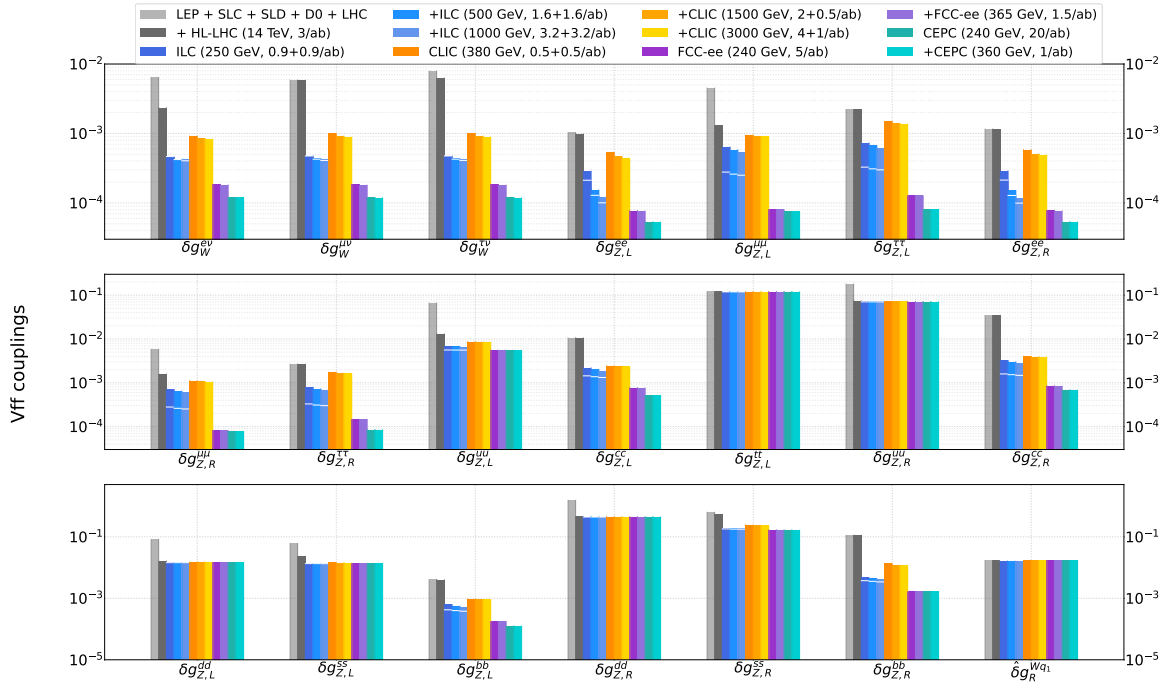


Figure 7: Precision reach on the effective couplings from a SMEFT global analysis of the 4-fermion operators at various future lepton colliders. The horizontal white line for ILC suggests the global fit results when applying the pole observables from its GigaZ option.

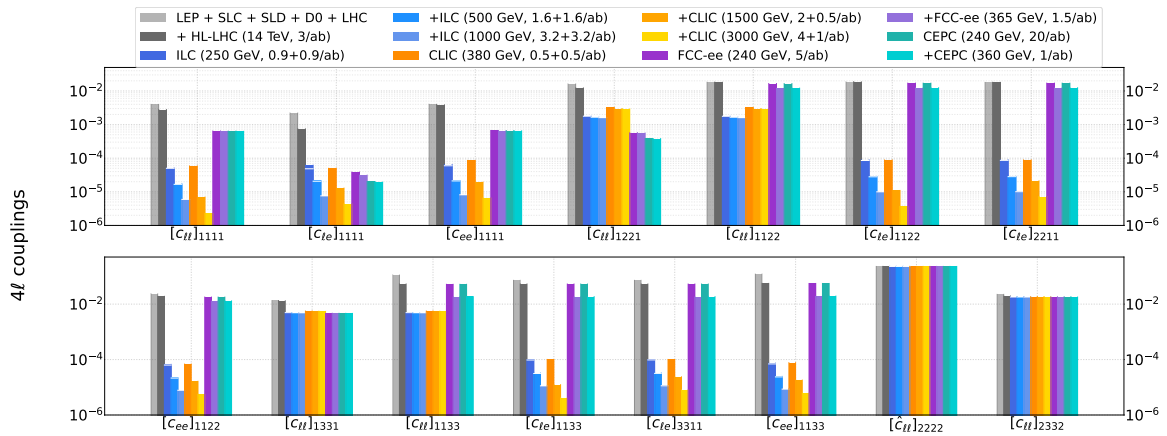


Figure 8: Fig. 7 continued.

6.4 Implication on some benchmark UV models

We discuss the implication of the global 4-fermion fit on specific UV models in this section. To that end, we focus on two specific models in the following: (1) The Y-Universal Z' model, and (2) the leptoquark model with two colored scalar leptoquarks, $(\mathbf{\bar{3}}, \mathbf{1})_{\frac{1}{3}}$ and $(\mathbf{\bar{3}}, \mathbf{3})_{\frac{1}{3}}$.

6.4.1 The Y-Universal Z' model

The Y-Universal Z' model is interesting since its couplings to the SM are flavor-diagonal, avoiding stringent flavor constraints. Our discussion on this model [100] is similar to that in [101]: We first translate the results for the 4-fermion fit into a global fit for the oblique parameters by marginalizing over all the other Wilson coefficients. We then perform an individual fit for $\mathcal{O}_{2W,2B}$ operators as defined in [102]. The results are shown in Fig. 10. Then, given that the Y-Universal Z' model only matches onto the \mathcal{O}_{2B} operator, the bound on this operator can thus be straightforwardly transferred onto the parameter space of this model for various colliders. This is shown in Fig. 11. We comment on that, for the hadron colliders, the difference between our result and that in [101] comes from the fact that we only consider the neutral Drell-Yan processes for the 4-fermion fit in this work. For future lepton colliders, our results are generically improved due to the updated inputs used in this study.

6.4.2 The scalar leptoquark model

This model is obtained by extending the SM with two colored scalar leptoquarks, $(\mathbf{\bar{3}}, \mathbf{1})_{\frac{1}{3}}$ and $(\mathbf{\bar{3}}, \mathbf{3})_{\frac{1}{3}}$, and the relevant part in the Lagrangian for our discussion below can be written as

$$\mathcal{L}_{\text{LQ}}^{\text{Yukawa}} \supset (\lambda_{i\alpha}^{1L} \bar{q}_i^c \ell_\alpha + \lambda_{i\alpha}^{1R} \bar{u}_i^c e_\alpha) S_1 + \lambda_{i\alpha}^{3L} \bar{q}_i^c \epsilon \sigma^I \ell_\alpha S_3^I + \text{h.c.} \quad (32)$$

At tree level, the full model only matches onto the following operators with the matching relations given by [103, 104]

$$\left[c_{lq}^{(1)} \right]_{\alpha\beta ij} = \frac{\lambda_{i\alpha}^{1L*} \lambda_{j\beta}^{1L} v^2}{4M_1^2} + \frac{3\lambda_{i\alpha}^{3L*} \lambda_{j\beta}^{3L} v^2}{4M_3^2}, \quad \left[c_{lq}^{(3)} \right]_{\alpha\beta ij} = -\frac{\lambda_{i\alpha}^{1L*} \lambda_{j\beta}^{1L} v^2}{4M_1^2} + \frac{\lambda_{i\alpha}^{3L*} \lambda_{j\beta}^{3L} v^2}{4M_3^2}, \quad (33)$$

$$\left[c_{lequ}^{(1)} \right]_{\alpha\beta ij} = \frac{\lambda_{j\beta}^{1R} \lambda_{i\alpha}^{1L*} v^2}{2M_1^2}, \quad \left[c_{lequ}^{(3)} \right]_{\alpha\beta ij} = -\frac{\lambda_{j\beta}^{1R} \lambda_{i\alpha}^{1L*} v^2}{8M_1^2}, \quad [c_{eu}]_{\alpha\beta ij} = \frac{\lambda_{i\alpha}^{1R*} \lambda_{j\beta}^{1R} v^2}{2M_1^2}. \quad (34)$$

For simplicity, we will work in the universal Yukawa scenario for the following discussion. As a result, these five Wilson coefficients will only depend on two ratios: λ_1/M_1 and λ_3/M_3 . Constraints on this model from our global fit are then shown

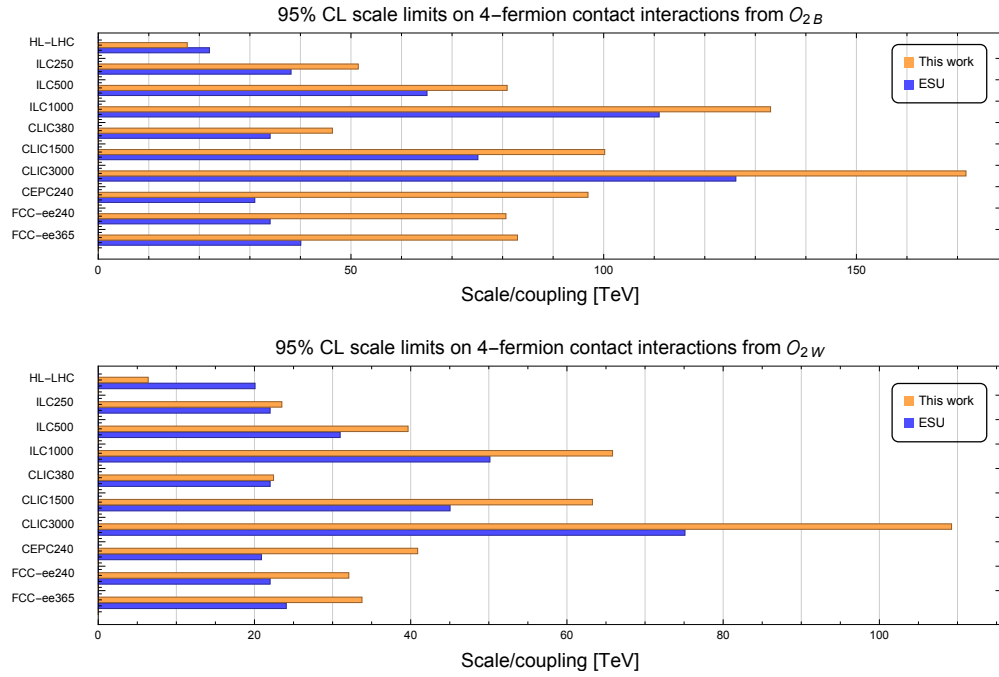


Figure 10: Constraints on the $O_{2W,2B}$ from the global 4-fermion fit and the comparison with ESU.

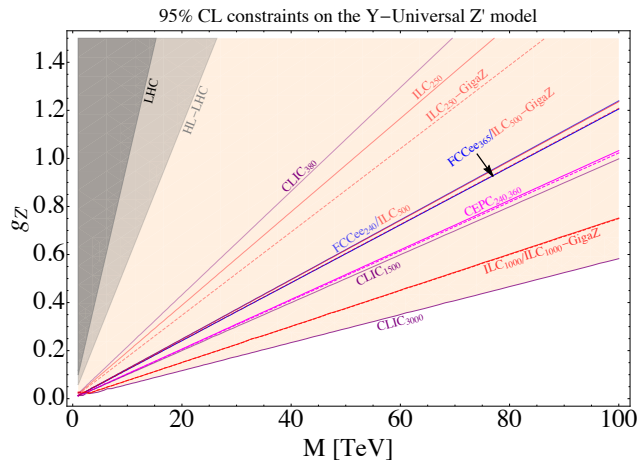


Figure 11: Constraints on the Y-Universal Z' model from the global 4-fermion fit.

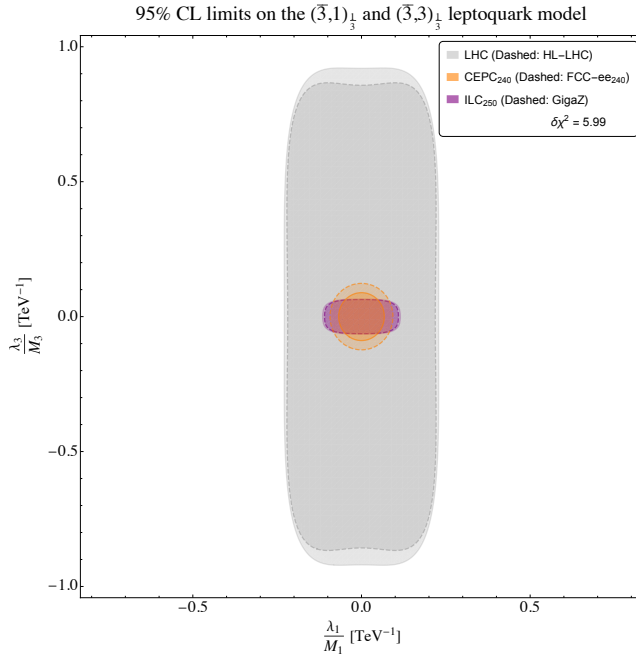


Figure 12: Constraints on the scalar leptoquark model from the global 4-fermion fit.

in Fig. 12, marginalizing over the other Wilson coefficients that cannot be matched from this model at tree level. Since the 4-fermion global fit presented in this section does not involve any top operators, in Fig. 12, we only show these collider options running below the top pair production threshold. We conclude that future lepton colliders will surpass the LHC or its high-luminosity era significantly in exploring the parameter space of this model. In particular, due to the large luminosity of CEPC, it will be more competitive than FCC-ee in probing both ratios. In contrast, the linear colliders will be more powerful than the circular colliders in constraining λ_3/M_3 , or equivalently orders of magnitude better in constraining $\hat{c}_{\ell q}^{(3)}$, due to beam polarization.

7 CP-odd operators

All the results presented thus far pertain only to CP-even SMEFT interactions. Here we explore the constraints that CP observables can be set on the bosonic sector of the dimension-six SMEFT.

There are in total six pure bosonic CPV SMEFT operators in the Warsaw basis, which are summarized in Eq. (4). The two operators involving gluons can be very stringently constrained by neutron and chromo electronic dipole moments [105], we thus do not include them in our fit. These remaining operators will affect the triple

gauge couplings (TGCs) that are phenomenologically parameterized as [106], in the broken phase,

$$\begin{aligned}
(\mathcal{L}_{\text{CPV}}^{\text{bosonic}})^{V_1 V_2 V_3}_{\text{broken}} = ie & \left(\tilde{\kappa}_\gamma \tilde{F}_{\mu\nu} W^{+\mu} W^{-\nu} + \frac{\tilde{\lambda}_\gamma}{M_W^2} \tilde{F}^{\nu\lambda} W_{\lambda\mu}^+ W^{-\mu}_\nu \right. \\
& \left. + \cot \theta_w \tilde{\kappa}_Z \tilde{Z}_{\mu\nu} W^{+\mu} W^{-\nu} + \cot \theta_w \frac{\tilde{\lambda}_Z}{M_W^2} \tilde{Z}^{\nu\lambda} W_{\lambda\mu}^+ W^{-\mu}_\nu \right) \\
& + e \cot \theta_w \hat{\kappa}_Z (\partial^\mu Z^\nu + \partial^\nu Z^\mu) W_\mu^+ W_\nu^-. \tag{35}
\end{aligned}$$

Clearly, all the terms in the first bracket violate both \hat{P} and \widehat{CP} while conserve \hat{C} , and conversely, the last term in Eq. (35) violates both \hat{C} and \widehat{CP} while conserves \hat{P} . In contrast, all the operators in Eq. (4) conserve \hat{C} but violate \hat{P} and \widehat{CP} . Therefore, fixing our notations as in [107] in the unbroken phase,

$$\begin{aligned}
(\mathcal{L}_{\text{CPV}}^{\text{bosonic}})_{\text{unbroken}} = & + \frac{g^2 \tilde{c}_{WW}}{m_W^2} \phi^\dagger \phi W_{\mu\nu}^a \tilde{W}^{a\mu\nu} + \frac{4gg' \tilde{c}_{WB}}{m_W^2} \phi^\dagger \frac{\sigma_a}{2} \phi W_{\mu\nu}^a \tilde{B}^{\mu\nu} \\
& + \frac{g^2 \tilde{c}_{BB}}{m_W^2} \phi^\dagger \phi B_{\mu\nu} \tilde{B}^{\mu\nu} + \frac{g^3 \tilde{c}_{3W}}{m_W^2} \varepsilon_{abc} W_{\mu\nu}^a W^{b\nu}_\rho \tilde{W}^{c\rho\mu}, \tag{36}
\end{aligned}$$

one can readily obtain the matching between these two formalisms:

$$\tilde{\kappa}_\gamma = -8\tilde{c}_{WB}, \quad \tilde{\kappa}_Z = \frac{8s_w^2}{c_w^2} \tilde{c}_{WB} = -\frac{s_w^2}{c_w^2} \tilde{\kappa}_\gamma, \tag{37}$$

$$\tilde{\lambda}_\gamma = \tilde{\lambda}_Z = 6g^2 \tilde{c}_{3W}, \quad \hat{\kappa}_Z = 0. \tag{38}$$

Note that all results are in perfect agreement with those in [108, 109] after a notation transformation.

The OPAL collaboration has reported their measurements of $\tilde{\lambda}_Z = -0.18_{-0.16}^{+0.24}$ and $\tilde{\kappa}_Z = -0.20_{-0.07}^{+0.10}$ in [110], which can thus be used to constrain \tilde{c}_{WB} and \tilde{c}_{3W} in Eq. (36). While these bounds are weak, it is essential to include them to lift the flat directions. On the other hand, these operators also modify the production and the decay of the Higgs at the LHC [111–113]. As a result, stringent bounds on these operators have been obtained from the $h \rightarrow 4\ell$ channel, which are included in our fit. In addition, for future lepton colliders, we also utilize the angular asymmetries $\mathcal{A}_\phi^{(1)}$ and $\mathcal{A}_\phi^{(2)}$ from $e^+e^- \rightarrow ZH$ production [114] and their projections at both future circular lepton colliders [115] and linear ones [116]. Recall that these angular asymmetric observables in [115] are parameterized using the mass eigenstates

$$(\mathcal{L}_{\text{CPV}}^{\text{bosonic}})^{hV_1V_2}_{\text{broken}} = \frac{\hat{\alpha}_{Z\tilde{Z}}}{v} h Z_{\mu\nu} \tilde{Z}^{\mu\nu} + \frac{\hat{\alpha}_{A\tilde{Z}}}{v} h A_{\mu\nu} \tilde{Z}^{\mu\nu}, \tag{39}$$

one can readily match these $\hat{\alpha}$'s onto those in our notations in Eq. (35) and find

- For circular colliders:

$$\widehat{\alpha}_{Z\tilde{Z}} = \frac{4}{c_w^2} \widetilde{c}_{BB}, \quad (40)$$

$$\widehat{\alpha}_{A\tilde{Z}} = \frac{8s_w}{c_w} \widetilde{c}_{WW}. \quad (41)$$

- For polarized linear colliders with the subscripts indicating the beam polarization:

$$(\widehat{\alpha}_{Z\tilde{Z}})_{e_L^- e_R^+} = \frac{8\widetilde{c}_{BB}}{c_w^2} + \frac{s_w^2}{1/2 - s_w^2} \frac{s - m_Z^2}{s} 8\widetilde{c}_{WW}, \quad (42)$$

$$(\widehat{\alpha}_{Z\tilde{Z}})_{e_R^- e_L^+} = \frac{8\widetilde{c}_{BB}}{c_w^2} - \frac{s - m_Z^2}{s} 8\widetilde{c}_{WW}, \quad (43)$$

where \sqrt{s} is the center of mass energy, and we define the following variables for simplicity:

$$\widetilde{c}_{BB} \equiv c_w^4 \widetilde{c}_{WW} + s_w^4 \widetilde{c}_{BB} + 2c_w^2 s_w^2 \widetilde{c}_{WB}, \quad (44)$$

$$\widetilde{c}_{WW} \equiv c_w^2 (\widetilde{c}_{WW} - \widetilde{c}_{WB}) + s_w^2 (\widetilde{c}_{WB} - \widetilde{c}_{BB}). \quad (45)$$

Utilizing $\widetilde{\lambda}_Z$ and $\widetilde{\kappa}_Z$ from OPAL, the $h \rightarrow 4\ell$ decay channel at the HL-LHC, and the two angular asymmetries $\mathcal{A}_\phi^{(1)}$ and $\mathcal{A}_\phi^{(2)}$ from ZH production as just discussed above, the fit for the four CPV operators can then be closed. The results are shown in Fig. 13 using the notations in [111–113] to compare different colliders, and we do not combine future colliders with the HL-LHC for this purpose. The upper row of Fig. 13 is obtained by using the aTGC results from OPAL in [110], and these results are estimated to, to be conservative, get improved by a factor of 10 (100) for the HL-LHC (future lepton colliders). We then obtain the results in the second row of Fig. 13 based on this estimation. We find the HL-LHC could better constrain $g_4^{\gamma\gamma}$, while it will not be as competitive as future colliders in terms of constraining $g_4^{ZZ, Z\gamma}$. Furthermore, the linear colliders will in general surpass the circular ones due to beam polarization. Interestingly, we also find the hadron and the lepton colliders are sensitive to very different combinations of these g_4 couplings, or equivalently, $\widetilde{c}_{WW, WB, BB}$ in Eq. (36) in the Warsaw basis. This is explicitly shown in Fig. 14, where the blue region is for the HL-LHC, and the orange for ILC250. We present in the left panel the region plot with $\delta\chi^2 = 1$ from the current fit, and the right one from the future fit based on the aforementioned estimation. This complementarity between the HL-LHC and future lepton colliders helps improve the global fit for the CPV operators when they are combined together, as is shown in Fig. 15 and numerically summarized in Table 37..

Could these constraints be further improved by including others observables that are sensitive to these CPV operators? Realizing that these operators could also modify

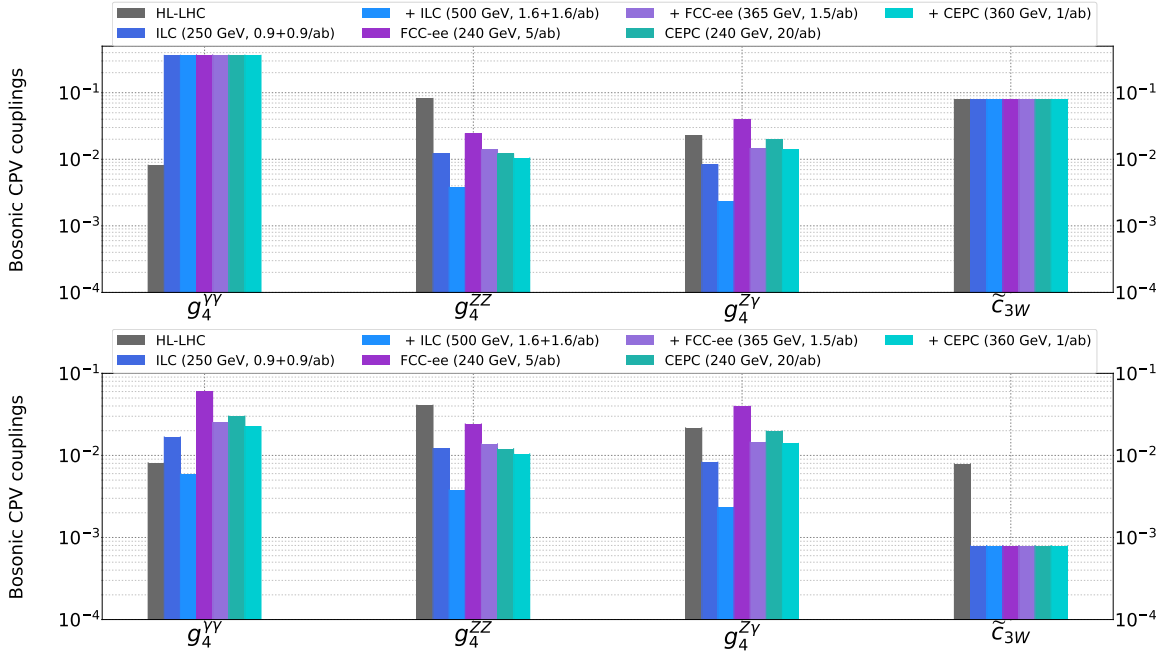


Figure 13: Global fit results for the CPV g_4 couplings. Above: Results from the current fit. Bottom: Assuming OPAL precision on aTGCs is improved by a factor of 10 (100) for HL-LHC (future colliders).

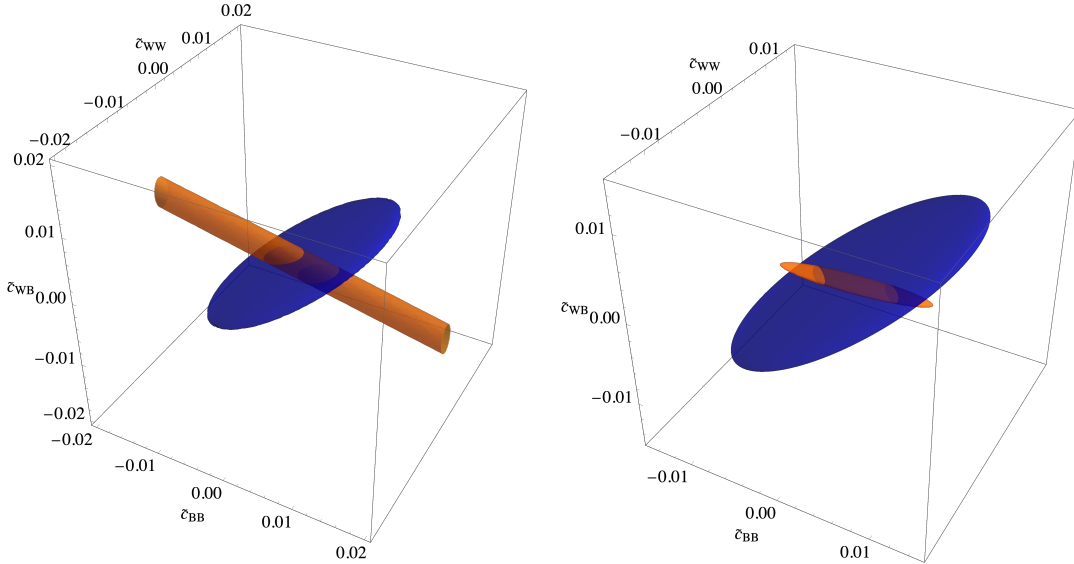


Figure 14: The 3D region plot with $\delta\chi^2 = 1$, where blue is for the HL-LHC and orange for ILC250. Left: Results from the current fit. Right: Assuming OPAL precision on aTGCs is improved by a factor of 10 (100) for HL-LHC (future colliders).

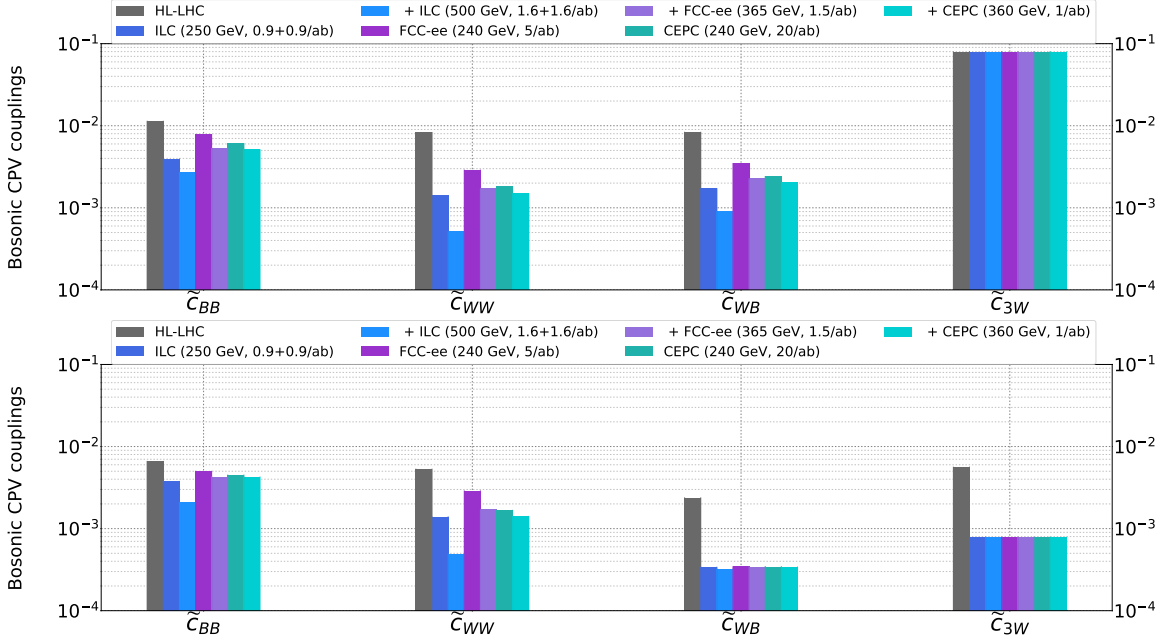


Figure 15: Global fit results for the CPV operators in the Warsaw basis. Above: Results from the current fit. Bottom: Assuming OPAL precision on aTGCs is improved by a factor of 10 (100) for HL-LHC (future colliders).

in	HL-LHC		ILC				FCC-ee				CEPC			
	14 TeV		250		+500		240		+365		240		+360	
%	est.		est.		est.		est.		est.		est.		est.	
\tilde{C}_{BB}	1.13	0.66	0.39	0.376	0.27	0.21	0.78	0.50	0.53	0.43	0.61	0.45	0.51	0.425
\tilde{C}_{WW}	0.83	0.53	0.14	0.14	0.051	0.049	0.29	0.29	0.17	0.17	0.18	0.167	0.15	0.14
\tilde{C}_{WB}	0.83	0.237	0.17	0.034	0.09	0.032	0.35	0.0344	0.225	0.034	0.24	0.034	0.203	0.034
\tilde{C}_{3W}	7.93	0.56	7.93	0.078	7.93	0.078	7.93	0.078	7.93	0.078	7.93	0.078	7.93	0.078

Table 37: Precision reach (in percentage) on the effective couplings from a SMEFT global analysis of the CPV operators at various future lepton colliders. Here “est.” means the results from the future global fit based on our estimation for the aTGC precision at the HL-LHC and future colliders. See text for details.

the $h \rightarrow \gamma\gamma$ decay rate, which would be measured at the percent level at the high-luminosity era of the LHC or future lepton colliders [9], it is natural to investigate the impact of this decay rate on possibly improving the fit. To that end, we note that, generically, the $h \rightarrow \gamma\gamma$ decay rate will receive corrections from both the CP-even and the CP-odd operators. The relevant Lagrangian in the broken phase can be expressed as

$$\mathcal{L}_{h\gamma\gamma} = \frac{1}{2v} h \zeta_A A_{\mu\nu} A^{\mu\nu} + \frac{1}{2v} h \tilde{\zeta}_A A_{\mu\nu} \tilde{A}^{\mu\nu}. \quad (46)$$

The ζ_A and $\tilde{\zeta}_A$ parameters in the broken phase can be straightforwardly matched onto those Wilson coefficients in the unbroken phase, and the former case has been investigated in [107] and independently checked to give*

$$\zeta_A = s_w^2 [8c_{WW} + 8c_{BB} - 2(8c_{WB})], \quad (47)$$

while for the latter, we find

$$\tilde{\zeta}_A = s_w^2 [8\tilde{c}_{WW} + 8\tilde{c}_{BB} - 2(8\tilde{c}_{WB})], \quad (48)$$

and both results are in perfect agreement with those in [108, 109] after a notation transformation.

Due to the different transformation properties under \widehat{CP} , the CP-even and the CP-odd sectors do not interfere with one another and the CP-odd operators would only contribute at the quadratic order. However, since the SM contribution to $h \rightarrow \gamma\gamma$ is loop suppressed, one could thus expect the CP-odd operators to contribute at the same order compared with the SM, or the leading-order interference between the SM and the CP-even operators, or the quadratic contributions from the CP-even operators. For estimation, one can ignore these contributions from the CP-even operators since their corresponding Wilson coefficients are constrained at $\mathcal{O}(10^{-5})$ from a global study on the Higgs couplings at ILC250+500 in [107]. We then find adding this rate to the global fit could further improve the 1σ bounds on these CPV operators by a factor of a few except for $W_{\mu\nu}^a W_{\rho}^{b\nu} \widetilde{W}_{\rho\mu}^c$ due to its vanishing contribution to this rate.

8 The top-quark sector in the global EFT fit

The Tevatron and LHC have characterized top-quark interactions to excellent precision. Differential measurements of top quark pair production well into the boosted regime provide a strong constraint on the $t\bar{t}$ -gluon vertex and $q\bar{q}t\bar{t}$ operators [117].

*Note the typo of an extra factor of “8” in [107].

Top quark decay, electro-weak single top-quark production and associated production with a Z - or W -boson, a photon or a Higgs boson constrain the electro-weak interactions and Yukawa coupling directly [118–120]. Four-top production and $t\bar{t}b\bar{b}$ production, finally, constrain the four-heavy-quark operators [121]. Several groups have performed fits of the top sector of the SMEFT to these data [122–125] and even explored the subtle interplay between the top sector and the Higgs/EW sectors, combining Higgs, electro-weak and top data in comprehensive SMEFT fits with several tens of parameters [126, 127].

The prospects for the complete LHC programme, including the high-luminosity phase that collects an integrated luminosity of 3 ab^{-1} , are based on an extrapolation of current run 2 results. The measurements that form the basis of our projection are listed in Table 38. For rare associated production processes the S2 scenario, also used for Higgs physics projections [17], is adopted. In this scenario, experimental systematic uncertainties, as well as statistical uncertainties, are assumed to scale with the inverse of the integrated luminosity. Theoretical and modelling uncertainties are reduced by a factor two. For top quark production, where measurements already reach a precision of a few %, the systematic uncertainty is divided by two. Further details are provided in Ref. [128].

Process	Observable	\sqrt{s}	$\int \mathcal{L}$	Experiment	SM	Ref.
$pp \rightarrow t\bar{t}$	$d\sigma/dm_{t\bar{t}}$ (15+3 bins)	13 TeV	140 fb $^{-1}$	CMS	[129]	[130]
$pp \rightarrow t\bar{t}$	$dA_C/dm_{t\bar{t}}$ (4+2 bins)	13 TeV	140 fb $^{-1}$	ATLAS	[129]	[131]
$pp \rightarrow t\bar{t}H + tHq$	σ	13 TeV	140 fb $^{-1}$	ATLAS	[132]	[133]
$pp \rightarrow t\bar{t}Z$	$d\sigma/dp_T^Z$ (7 bins)	13 TeV	140 fb $^{-1}$	ATLAS	[134]	[135]
$pp \rightarrow t\bar{t}\gamma$	$d\sigma/dp_T^\gamma$ (11 bins)	13 TeV	140 fb $^{-1}$	ATLAS	[136, 137]	[138]
$pp \rightarrow tZq$	σ	13 TeV	77.4 fb $^{-1}$	CMS	[139]	[140]
$pp \rightarrow t\gamma q$	σ	13 TeV	36 fb $^{-1}$	CMS	[141]	[141]
$pp \rightarrow t\bar{t}W$	σ	13 TeV	36 fb $^{-1}$	CMS	[132, 142]	[143]
$pp \rightarrow t\bar{b}$ (s-ch)	σ	8 TeV	20 fb $^{-1}$	LHC	[144, 145]	[146]
$pp \rightarrow tW$	σ	8 TeV	20 fb $^{-1}$	LHC	[147]	[146]
$pp \rightarrow tq$ (t-ch)	σ	8 TeV	20 fb $^{-1}$	LHC	[144, 145]	[146]
$t \rightarrow Wb$	F_0, F_L	8 TeV	20 fb $^{-1}$	LHC	[148]	[149]
$p\bar{p} \rightarrow t\bar{b}$ (s-ch)	σ	1.96 TeV	9.7 fb $^{-1}$	Tevatron	[150]	[151]
$e^-e^+ \rightarrow b\bar{b}$	R_b, A_{FBLR}^{bb}	$\sim 91 \text{ GeV}$	202.1 pb $^{-1}$	LEP/SLD	–	[49]

Table 38: Measurements included in the EFT fit of the top-quark electroweak sector. For each measurement, the process, the observable, the center-of-mass energy, the integrated luminosity and the experiment/collider are given. The last two columns list the references for the predictions and measurements that are included in the fit. LHC refers to the combination of ATLAS and CMS measurements. In a similar way, Tevatron refers to the combination of CDF and D0 results, and LEP/SLD to different experiments from those two accelerators.

A future electron-positron collider is expected to improve the measurements of the bottom EW couplings, and, when operated above the $t\bar{t}$ threshold, the top EW couplings [152–154] and provide strong bounds on $e^+e^-t\bar{t}$ operators [155].

Prospects for the $e^+e^- \rightarrow b\bar{b}$ process are included that are based on the full-simulation studies of the ILD concept [156] at $\sqrt{s} = 250$ GeV. The prospects are based on realistic estimates of efficiency and acceptance, including the signal losses required to ensure a robust calibration of the flavour tagging efficiency. The statistical uncertainties on the measurements of the cross section and forward-backward asymmetry are complemented by polarisation and flavour-tagging systematics. For the Z -pole runs we use the projections for R_b and A_{FB} provided by the FCCee and CEPC projects for their “TeraZ” runs at the Z -pole, shown in Table 3.

The $e^+e^- \rightarrow t\bar{t}$ process opens up for centre-of-mass energies that exceed twice the top mass (i.e. $\sqrt{s} \gtrsim 350$ GeV) and probes the electroweak couplings of the top quark at tree-level. Data taken with different beam polarisations at linear colliders can be used to distinguish the photon and Z -boson couplings [153–155, 157]. At circular colliders, a measurement of the final state polarisation using the semi-leptonically decaying top quarks can also be used to separate the two contributions [152]. We base our prospects on the study of statistically optimal observables defined at leading order on the $e^+e^- \rightarrow t\bar{t} \rightarrow WbWb$ differential distribution [155]. This $WbWb$ final state also receives contribution from single top production which become sizeable at high centre-of-mass energies. Realistic acceptance, identification and reconstruction efficiencies are estimated from full-simulation studies for the ILC and CLIC in Ref. [154, 158]. Since they were performed only for sub-set of centre-of-mass energies and beam polarisations, overall efficiency factors are extrapolated as a functions of the centre-of-mass energy. They drop significantly for the TeV centre-of-mass energies of ILC and CLIC since a degradation of top-selection and flavour-tagging capabilities is expected in this regime.

The top-quark Yukawa coupling can be determined in a robust manner through the tree-level dependence of the associated $e^+e^- \rightarrow t\bar{t}H$ production process. This process is accessible at centre-of-mass energy above the $t\bar{t}H$ production threshold at $\sqrt{s} = 500$ – 550 GeV. At linear colliders, where the luminosity grows with energy, there is a broad plateau up to about 1.5 TeV where $e^+e^- \rightarrow t\bar{t}H$ is accessible. We base our projections on full-simulation studies by ILC and CLIC [158–160].

Several studies have been published for an energy-frontier hadron collider [161–164], but no systematic projections have been performed of the broad top physics program and no quantitative results are presented here. For a qualitative discussion on this topic we refer to Ref. [128].

In Fig. 16 the 95% probability bounds from a fit to the current data are shown in the dark red bars, as well as the limits obtained from the extrapolations of the complete HL-LHC program, with an integrated luminosity of 3 ab^{-1} , in light red.

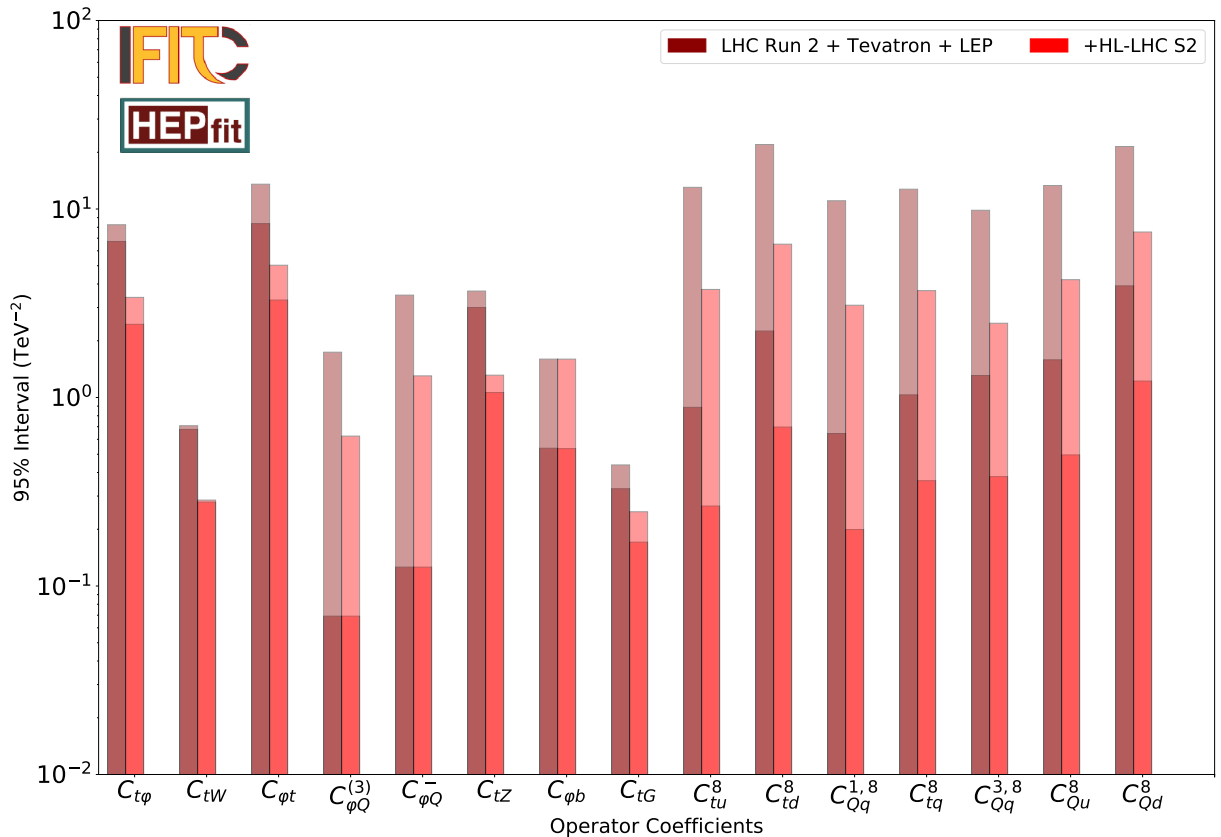


Figure 16: The 95% probability bounds on the Wilson coefficients for dimension-six operators that affect the top-quark production and decay measurements listed in Table 38 after run 2 of the LHC (in dark red) and prospects for the bounds expected after completion of the complete LHC program, including the high-luminosity stage (in light red). Only linear terms proportional to Λ^{-2} are taken into account in the dependence of the observables on the Wilson coefficients. The individual bounds obtained from a single-parameter fit are shown as solid bars, while the global or marginalised bounds obtained fitting all Wilson coefficients at once are indicated by the full bars (shaded region in each bar).

These fits, and the others of this section, have been performed using the HEPfit package [10].

Across the board, the HL-LHC program is expected to improve the bounds by a factor of two to four with respect to the current run 2 limits, both for individual bounds and global fit results. Exceptions are the individual bounds on $C_{\phi Q}^-$ and $C_{\phi Q}^3$, that continue to depend on the $Zb\bar{b}$ measurements at the Z -pole.

The marginalised bounds on the four-fermion operators remain an order of magnitude worse than the individual bounds after the HL-LHC, even if both individual and global bounds improve considerably. This is due to unresolved correlations between the coefficients. The same feature is observed in recent fits to the top sector of the SMEFT [122, 123] and in global Higgs/EW/top fits [126, 127]. Stricter limits can be obtained if the dimension-six-squared terms proportional to Λ^{-4} are included in the fit [126].

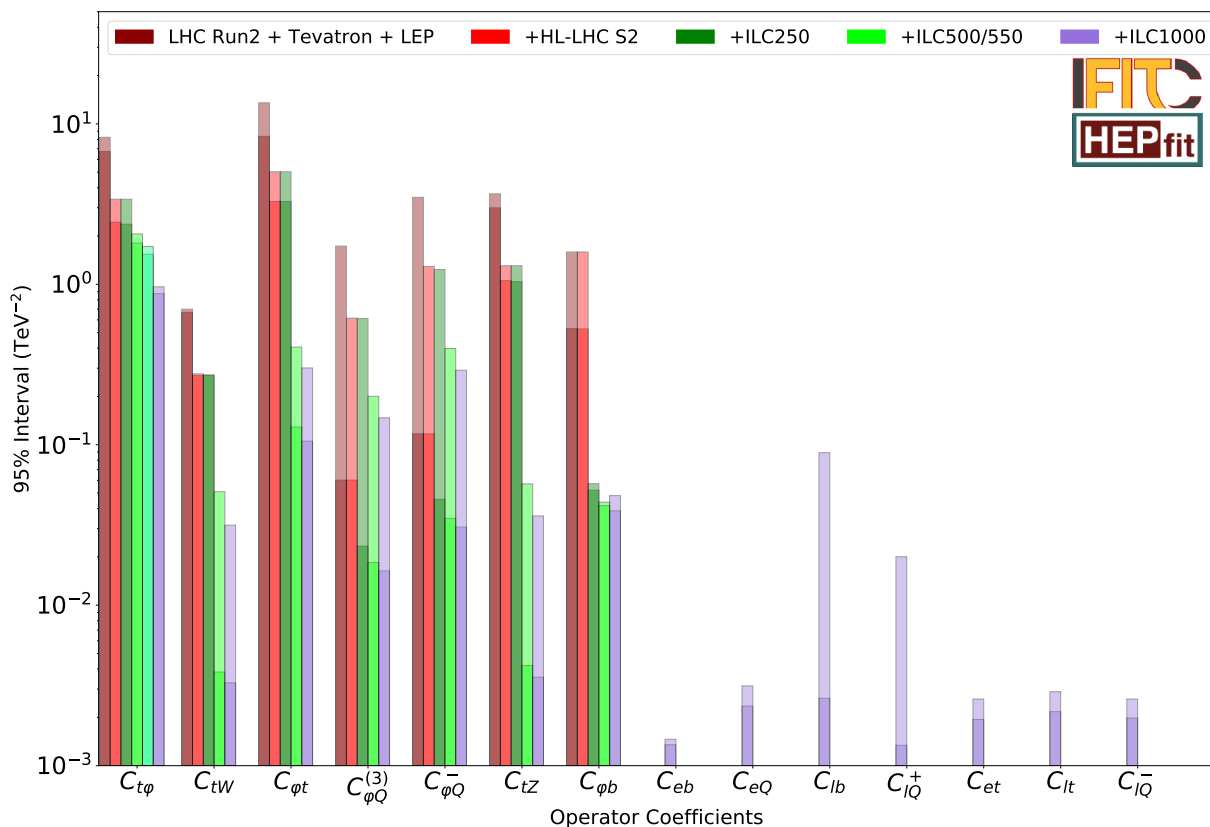


Figure 17: Comparison of current LHC constraints with HL-LHC ones, and those deriving from ILC runs at 250, 500 and 1000 GeV. The limits on the $q\bar{q}t\bar{t}$ and C_{tG} coefficients are not shown, since the e^+e^- collider measurements considered are not sensitive to them, but all operators are included in the global fit. The improvement expected from the HL-LHC on these coefficients is shown in Fig. 16. The additional bar included for $C_{t\phi}$ in light green shows the effect on this operator of ILC working at 550 GeV. The solid bars provide the individual limits of the single-parameter fit and the shaded ones the marginalised limits of the global fit.

In Fig. 17, the impact of runs of electron-positron machines at different centre-of-mass energies is illustrated. The current bounds in brown are compared to HL-LHC ones in red. The subsequent bars add data at $\sqrt{s} = 250$ GeV, 500 GeV and 1 TeV. The beam polarizations and integrated luminosities of the different ILC stages are summarised in Table 2. Only the electroweak operators are presented, as the e^+e^- data have the strongest impact there, but results corresponds to a global analysis, including also the $q\bar{q}t\bar{t}$ operators and C_{tG} .

The dark green bar shows that the ‘‘Higgs factory’’ run improves the bounds on bottom-quark operators, including $C_{\phi Q}^3$ and $C_{\phi Q}^-$ and $C_{\phi b}$. The improvement is especially pronounced for the individual bounds. As expected, data above the top-quark pair production threshold is required to improve the bounds on the top-quark operators.

Runs at two different centre-of-mass energies above the top-quark pair production threshold are required to disentangle the $e^+e^-t\bar{t}$ operator coefficients from the two-fermion operator coefficients [155]. The two sets of operators have very different scaling with energy: the sensitivity to four-fermion operators grows quadratically, while it is constant or grows only linearly for two-fermion operators. In a fit to data taken at a single centre of mass, linear combinations of their coefficients remain degenerate and form blind directions. The combination of runs at two different centre-of-mass energies effectively disentangles them and provides global fit constraints close to the individual bounds. Note that the two-quark two-lepton operators could also be probed at the LHC, although we have ignored them in our LHC and HL-LHC analysis. Dedicated signal regions, for instance with off- Z -peak dilepton invariant masses in $pp \rightarrow t\bar{t}\ell^+\ell^-$ [165–167], would increase their sensitivity.

In Fig. 18, we compare the bounds expected from the HL-LHC and from the final stages of the CEPC, FCC- ee , ILC and CLIC. The centre-of-mass energies, integrated luminosities and beam polarisations envisaged for each of these projects are given in Table 2. The circular colliders (FCC- ee and CEPC) operated at and slightly above the $t\bar{t}$ threshold are expected to improve constraints on the bottom- and top-operators by factors 5 and 2 for some two-fermion operators. Indeed, their ‘‘TeraZ’’ runs provide very competitive bounds (individual ones, in particular) on two-fermion bottom-operator coefficients. Their constraining power on four-fermion operators is, however, limited by the energy reach. Since, at these colliders, the two runs above the $t\bar{t}$ -threshold are very close the two-fermion and four-fermion operators are harder to disentangle. The global limits remain significantly above the individual bounds.

The linear colliders (ILC and CLIC), operated at two centre-of-mass energies above the $t\bar{t}$ threshold, can provide very tight bounds on all operators. The bounds on four-fermion operators take advantage of the energy-growing sensitivity and become very competitive if e^+e^- collision data at a centre-of-mass energy greater than 1 TeV is available. The ILC1000 and CLIC3000 bounds of $\mathcal{O}(10^{-3})$ on the $e^+e^-t\bar{t}$ operators

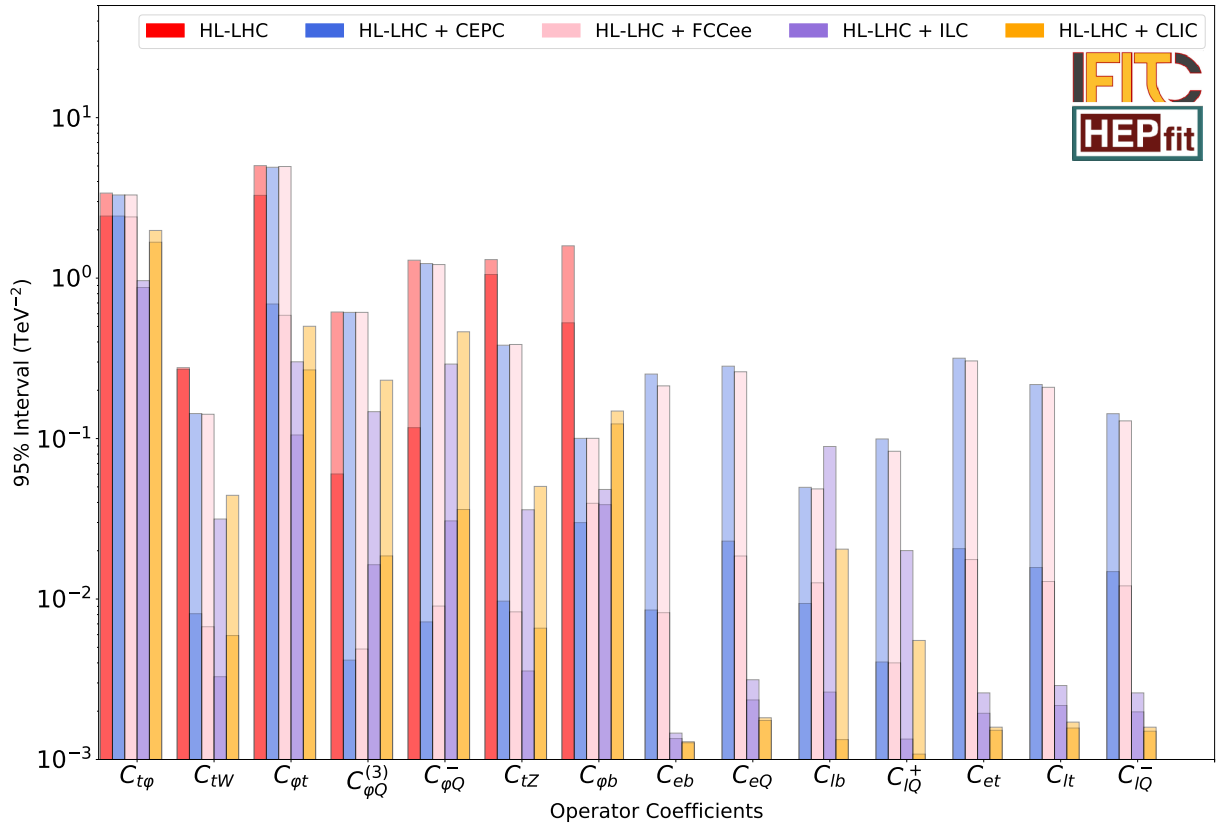


Figure 18: Comparison of the constraints expected from a combination of HL-LHC and lepton collider data. The limits on the $q\bar{q}t\bar{t}$ and C_{tG} coefficients are not shown, since the e^+e^- collider measurements considered are not sensitive to them, but all operators are included in the global fit. The improvement expected from the HL-LHC on these coefficients is shown in Fig. 16. The solid bars provide the individual limits of the single-parameter fit and the shaded ones the marginalised limits of the global fit.

are by far the tightest top-sector SMEFT constraints that can be achieved at any future collider considered in this work.*

Furthermore, operation above the $e^+e^- \rightarrow t\bar{t}H$ production threshold provides a direct probe of the top-quark Yukawa. The additional bar for $C_{t\phi}$, in Fig. 17, accounts for an ILC run at 550 GeV and shows the impact of the strongly enhanced cross section

*A muon collider or advanced linear collider have the potential to improve these bounds further, but quantitative projections for integrated luminosity and experimental performance are currently not available.

Values in % units		LHC	HL-LHC	ILC500	ILC550	ILC1000	CLIC
δy_t	Global fit	6.12	2.53	1.57	1.30	0.739	1.48
	Indiv. fit	5.08	1.85	1.41	1.17	0.705	1.26

Table 39: Uncertainties for the top-quark yukawa coupling at 68% probability for different scenarios, in percentage. The ILC500, ILC550 and CLIC scenarios also include the HL-LHC. The ILC1000 scenario includes also ILC500 and HL-LHC.

of the $e^+e^- \rightarrow t\bar{t}H$ process reaches the resonant peak boosts the sensitivity [160] to the top-quark Yukawa coupling. Also the scenarios for 1 TeV and 1.5 TeV operation considered here yield competitive constraints on this process, that help to improve the bounds on $C_{t\phi}$ with respect to the HL-LHC, as shown in Fig. 18. The limits obtained for $C_{t\phi}$ have been expressed in terms of the top-quark yukawa coupling (δy_t) in Tab. 39.

9 Conclusion and Outlook

In this work we performed a few global SMEFT fits for the Higgs and Electroweak sector, 4-fermion interactions, top-quark sector and pure bosonic CP-odd operators, each with a well defined subset of dimension-6 operators in the Warsaw basis. The focus was on the future lepton colliders with various running scenarios, that are being discussed in the process of Snowmass 2021. We conclude that future lepton colliders can advance significantly our understanding of the properties of various SM particles, by offering precise and coherent probes to new physics effects in a way that is independent of underlining UV models.

LHC will keep pushing the boundaries of precision measurements, capable of delivering 2-5% precision for many Higgs effective couplings at the end of HL-LHC. Future e^+e^- will not only be able to improve the precision by a factor of 2-10, but also provide a qualitatively new determination of the Higgs total width by treating it as a free parameter. The capabilities of all future e^+e^- colliders considered in this work are shown to be similar for Higgs coupling determinations. Muon colliders can offer comparable precisions in the cases where, either the Higgs total width is constrained (not allowing any untagged Higgs exotic decay), or the 125 GeV run is combined. There are synergies, which play important roles in the global fits, on Higgs rare decays ($H \rightarrow \gamma\gamma, \gamma Z, \mu\mu$) as well as top-Yukawa coupling between HL-LHC and future lepton colliders.

Electroweak effective couplings for W and Z can be improved by a few orders of magnitude at future e^+e^- colliders over what we know of today. Circular e^+e^- can offer better precisions with the dedicated high luminosity run at Z -pole and WW

threshold. Linear e^+e^- can offer competitive measurements on left-right asymmetries by either a dedicated Z -pole run or radiative return events at the same ZH run using polarized beams. There are important synergies between EWPOs and direct Higgs observables. The Z -pole and WW run at circular e^+e^- can help improve Higgs coupling precisions by a factor of around two. While at linear e^+e^- this improvement factor, which is much lower, already saturates after using the EWPOs by radiative events.

The 4-fermion interactions can be probed at future e^+e^- up to a scale of $O(100)$ TeV when the underlining models are strongly coupled. The reaches are significantly better at linear e^+e^- than circular e^+e^- not only because of higher collision energies but also polarized beams which help lift degeneracies. There are important synergies with low-energy measurements without which certain degeneracies can not be lift.

The measurements of top-quark mass and EW couplings will be improved significantly at future e^+e^- when the top-pair threshold and open production runs are included. The degeneracies in $eett$ contact interactions can not be lift without running at two different energies well above tt threshold. Many top-quark measurements at (HL-)LHC are helpful in the global fit for improving the precision of top-quark EW couplings.

The advance in the SM theory predictions will be indispensable in order to match the precision that will become reachable at future lepton colliders. In general beyond NNLO electroweak corrections will be needed. The requirement is in particular strong for EWPOs by the Z -pole programs at circular e^+e^- .

ACKNOWLEDGEMENTS

We would like to thank A. Belloni and A. Freitas for continuous support in coordinating the efforts for the needed inputs and facilitating discussions of this work with EF04 group members. We also would like to thank S. Dawson, A. Gribsan, J. M. Hernandez, A. Irels, Z. Liu, J. List, P. Meade, I. Ojalvo, R. Schwienhorst, C. Vernieri and D. Wacheroth for helpful discussions to this work.

The work of J.B. has been supported by the FEDER/Junta de Andalucía project grant P18-FRJ-3735. YD is supported by National Key Research and Development Program of China under Grant No. 2020YFC2201501, the National Science Foundation of China (NSFC) under Grants No. 12022514, No. 11875003 and No. 12047503, and CAS Project for Young Scientists in Basic Research YSBR-006, and the Key Research Program of the CAS Grant No. XDPB15. JG is supported by National Natural Science Foundation of China (NSFC) under grant No. 12035008. CG is supported by the Helmholtz Association through the recruitment initiative program and

by the Deutsche Forschungsgemeinschaft under Germany’s Excellence Strategy EXC 2121 “Quantum Universe” - 390833306. JT was supported by the Japan Society for the Promotion of Science (JSPS) under Grants-in-Aid for Science Research 15H02083. The work of VM has been supported by the Italian Ministry of Research (MUR) under the grant PRIN20172LNEEZ.

References

- [1] B. Henning, X. Lu, T. Melia, and H. Murayama, *2, 84, 30, 993, 560, 15456, 11962, 261485, ...: Higher dimension operators in the SM EFT*, *JHEP* **08** (2017) 016, [[arXiv:1512.03433](#)]. [Erratum: *JHEP* 09, 019 (2019)].
- [2] R. Alonso, E. E. Jenkins, and A. V. Manohar, *Geometry of the Scalar Sector*, *JHEP* **08** (2016) 101, [[arXiv:1605.03602](#)].
- [3] A. Helset, A. Martin, and M. Trott, *The Geometric Standard Model Effective Field Theory*, *JHEP* **03** (2020) 163, [[arXiv:2001.01453](#)].
- [4] T. Cohen, N. Craig, X. Lu, and D. Sutherland, *Unitarity violation and the geometry of Higgs EFTs*, *JHEP* **12** (2021) 003, [[arXiv:2108.03240](#)].
- [5] B. Grzadkowski, M. Iskrzynski, M. Misiak, and J. Rosiek, *Dimension-Six Terms in the Standard Model Lagrangian*, *JHEP* **10** (2010) 085, [[arXiv:1008.4884](#)].
- [6] D. Barducci et al., *Interpreting top-quark LHC measurements in the standard-model effective field theory*, [arXiv:1802.07237](#).
- [7] A. Falkowski, *Effective field theory approach to LHC Higgs data*, *Pramana* **87** (2016), no. 3 39, [[arXiv:1505.00046](#)].
- [8] J. de Blas, G. Durieux, C. Grojean, J. Gu, and A. Paul, *On the future of Higgs, electroweak and diboson measurements at lepton colliders*, *JHEP* **12** (2019) 117, [[arXiv:1907.04311](#)].
- [9] J. de Blas et al., *Higgs Boson Studies at Future Particle Colliders*, *JHEP* **01** (2020) 139, [[arXiv:1905.03764](#)].
- [10] J. de Blas et al., *HEPfit: a code for the combination of indirect and direct constraints on high energy physics models*, *Eur. Phys. J. C* **80** (2020), no. 5 456, [[arXiv:1910.14012](#)].
- [11] A. Caldwell, D. Kollar, and K. Kroninger, *BAT: The Bayesian Analysis Toolkit*, *Comput. Phys. Commun.* **180** (2009) 2197–2209, [[arXiv:0808.2552](#)].

- [12] A. C. Caldwell, D. Kollar, and K. Kroninger, *BAT: The Bayesian analysis toolkit*, *J. Phys. Conf. Ser.* **219** (2010) 032013.
- [13] F. Beaujean, A. Caldwell, D. Kollar, and K. Kroninger, *BAT: The Bayesian analysis toolkit*, *J. Phys. Conf. Ser.* **331** (2011) 072040.
- [14] S. Dawson et al., *Report of the Topical Group on Higgs Physics for Snowmass 2021: The Case for Precision Higgs Physics*, in *2022 Snowmass Summer Study*, 9, 2022. [arXiv:2209.07510](#).
- [15] K. Agashe et al., *Report of the Topical Group on Top quark physics and heavy flavor production for Snowmass 2021*, [arXiv:2209.11267](#).
- [16] A. Belloni et al., *Report of the Topical Group on Electroweak Precision Physics and Constraining New Physics for Snowmass 2021*, [arXiv:2209.08078](#).
- [17] M. Cepeda et al., *Report from Working Group 2: Higgs Physics at the HL-LHC and HE-LHC*, *CERN Yellow Rep. Monogr.* **7** (2019) 221–584, [[arXiv:1902.00134](#)].
- [18] **ILC International Development Team** Collaboration, I. Adachi et al., *The International Linear Collider: Report to Snowmass 2021*. 3, 2022. [arXiv:2203.07622](#).
- [19] A. Robson and P. Roloff, *Updated CLIC luminosity staging baseline and Higgs coupling prospects*, [arXiv:1812.01644](#).
- [20] G. Bernardi et al., *The Future Circular Collider: a Summary for the US 2021 Snowmass Process*, [arXiv:2203.06520](#).
- [21] H. Cheng et al., *The Physics potential of the CEPC. Prepared for the US Snowmass Community Planning Exercise (Snowmass 2021)*. 5, 2022. [arXiv:2205.08553](#).
- [22] M. Forsslund and P. Meade, *High Precision Higgs from High Energy Muon Colliders*, [arXiv:2203.09425](#).
- [23] J. de Blas, J. Gu, and Z. Liu, *Higgs Precision at a 125 GeV Muon Collider*, [arXiv:2203.04324](#).
- [24] **Particle Data Group** Collaboration, P. Zyla et al., *Review of particle physics*, to be published in *Prog. Theor. Exp. Phys.* **2020** (2020) 083C01.
- [25] J. de Blas, G. Durieux, C. Grojean, J. Gu, and A. Paul, *On the future of Higgs, electroweak and diboson measurements at lepton colliders*, *JHEP* **12** (2019) 117, [[arXiv:1907.04311](#)].

- [26] **LCC Physics Working Group** Collaboration, K. Fujii et al., *Tests of the Standard Model at the International Linear Collider*, [arXiv:1908.11299](#).
- [27] A. Blondel and P. Janot, *FCC-ee overview: new opportunities create new challenges*, *Eur. Phys. J. Plus* **137** (2022), no. 1 92, [[arXiv:2106.13885](#)].
- [28] **ALEPH, DELPHI, L3, OPAL, LEP Electroweak** Collaboration, S. Schael et al., *Electroweak Measurements in Electron-Positron Collisions at W-Boson-Pair Energies at LEP*, *Phys. Rept.* **532** (2013) 119–244, [[arXiv:1302.3415](#)].
- [29] I. Marchesini, *Triple gauge couplings and polarization at the ILC and leakage in a highly granular calorimeter*. PhD thesis, Hamburg U., 2011.
- [30] M. Diehl and O. Nachtmann, *Optimal observables for the measurement of three gauge boson couplings in $e^+ e^- \rightarrow W^+ W^-$* , *Z. Phys. C* **62** (1994) 397–412.
- [31] J. F. Gunion, B. Grzadkowski, and X.-G. He, *Determining the top - anti-top and Z Z couplings of a neutral Higgs boson of arbitrary CP nature at the NLC*, *Phys. Rev. Lett.* **77** (1996) 5172–5175, [[hep-ph/9605326](#)].
- [32] C. Grojean, M. Montull, and M. Riemann, *Diboson at the LHC vs LEP*, *JHEP* **03** (2019) 020, [[arXiv:1810.05149](#)].
- [33] T. Han, Y. Ma, and K. Xie, *Quark and gluon contents of a lepton at high energies*, *JHEP* **02** (2022) 154, [[arXiv:2103.09844](#)].
- [34] T. Barklow, K. Fujii, S. Jung, R. Karl, J. List, T. Ogawa, M. E. Peskin, and J. Tian, *Improved Formalism for Precision Higgs Coupling Fits*, *Phys. Rev. D* **97** (2018), no. 5 053003, [[arXiv:1708.08912](#)].
- [35] V. Bresó-Pla, A. Falkowski, and M. González-Alonso, *A_{FB} in the SMEFT: precision Z physics at the LHC*, *JHEP* **08** (2021) 021, [[arXiv:2103.12074](#)].
- [36] G. Durieux, C. Grojean, J. Gu, and K. Wang, *The leptonic future of the Higgs*, *JHEP* **09** (2017) 014, [[arXiv:1704.02333](#)].
- [37] A. Blondel, A. Freitas, J. Gluza, T. Riemann, S. Heinemeyer, S. Jadach, and P. Janot, *Theory Requirements and Possibilities for the FCC-ee and other Future High Energy and Precision Frontier Lepton Colliders*, [arXiv:1901.02648](#).
- [38] M. Awramik, M. Czakon, A. Freitas, and G. Weiglein, *Precise prediction for the W boson mass in the standard model*, *Phys. Rev. D* **69** (2004) 053006, [[hep-ph/0311148](#)].

- [39] I. Dubovyk, A. Freitas, J. Gluza, T. Riemann, and J. Usovitsch, *Electroweak pseudo-observables and Z-boson form factors at two-loop accuracy*, *JHEP* **08** (2019) 113, [[arXiv:1906.08815](#)].
- [40] A. Freitas et al., *Theoretical uncertainties for electroweak and Higgs-boson precision measurements at FCC-ee*, [arXiv:1906.05379](#).
- [41] A. Freitas and Q. Song, *Two-Loop Electroweak Corrections with Fermion Loops to $e^+e^- \rightarrow ZH$* , [arXiv:2209.07612](#).
- [42] X. Chen, X. Guan, C.-Q. He, Z. Li, X. Liu, and Y.-Q. Ma, *Complete two-loop electroweak corrections to $e^+e^- \rightarrow HZ$* , [arXiv:2209.14953](#).
- [43] J. de Blas, M. Ciuchini, E. Franco, A. Goncalves, S. Mishima, M. Pierini, L. Reina, and L. Silvestrini, *Global analysis of electroweak data in the Standard Model*, *Phys. Rev. D* **106** (2022), no. 3 033003, [[arXiv:2112.07274](#)].
- [44] P. Janot, *Direct measurement of $\alpha_{QED}(m_Z^2)$ at the FCC-ee*, *JHEP* **02** (2016) 053, [[arXiv:1512.05544](#)]. [Erratum: *JHEP* 11, 164 (2017)].
- [45] **ATLAS** Collaboration, *Prospect for a measurement of the Weak Mixing Angle in $pp \rightarrow Z/\gamma^* \rightarrow e^+e^-$ events with the ATLAS detector at the High Luminosity Large Hadron Collider*, .
- [46] **CMS** Collaboration, *A proposal for the measurement of the weak mixing angle at the HL-LHC*, .
- [47] A. Efrati, A. Falkowski, and Y. Soreq, *Electroweak constraints on flavorful effective theories*, *JHEP* **07** (2015) 018, [[arXiv:1503.07872](#)].
- [48] **Gfitter Group** Collaboration, M. Baak, J. Cúth, J. Haller, A. Hoecker, R. Kogler, K. Mönig, M. Schott, and J. Stelzer, *The global electroweak fit at NNLO and prospects for the LHC and ILC*, *Eur. Phys. J. C* **74** (2014) 3046, [[arXiv:1407.3792](#)].
- [49] **ALEPH, DELPHI, L3, OPAL, SLD, LEP Electroweak Working Group, SLD Electroweak Group, SLD Heavy Flavour Group** Collaboration, S. Schael et al., *Precision electroweak measurements on the Z resonance*, *Phys. Rept.* **427** (2006) 257–454, [[hep-ex/0509008](#)].
- [50] **SLD** Collaboration, K. Abe et al., *First direct measurement of the parity violating coupling of the Z0 to the s quark*, *Phys. Rev. Lett.* **85** (2000) 5059–5063, [[hep-ex/0006019](#)].
- [51] **Particle Data Group** Collaboration, J. Beringer et al., *Review of Particle Physics (RPP)*, *Phys. Rev. D* **86** (2012) 010001.

- [52] **CDF, D0** Collaboration, T. E. W. Group, *2012 Update of the Combination of CDF and D0 Results for the Mass of the W Boson*, [arXiv:1204.0042](#).
- [53] **CMS** Collaboration, V. Khachatryan et al., *Measurement of the t-channel single-top-quark production cross section and of the $|V_{tb}|$ CKM matrix element in pp collisions at $\sqrt{s} = 8$ TeV*, *JHEP* **06** (2014) 090, [[arXiv:1403.7366](#)].
- [54] **D0** Collaboration, V. M. Abazov et al., *Measurement of $\sin^2 \theta_{\text{eff}}^{\ell}$ and Z-light quark couplings using the forward-backward charge asymmetry in $p\bar{p} \rightarrow Z/\gamma^* \rightarrow e^+e^-$ events with $\mathcal{L} = 5.0 \text{ fb}^{-1}$ at $\sqrt{s} = 1.96$ TeV*, *Phys. Rev. D* **84** (2011) 012007, [[arXiv:1104.4590](#)].
- [55] **ALEPH, DELPHI, L3, OPAL, LEP Electroweak Working Group** Collaboration, J. Alcaraz et al., *A Combination of preliminary electroweak measurements and constraints on the standard model*, [hep-ex/0612034](#).
- [56] A. Falkowski and K. Mimouni, *Model independent constraints on four-lepton operators*, *JHEP* **02** (2016) 086, [[arXiv:1511.07434](#)].
- [57] A. Falkowski, M. González-Alonso, and K. Mimouni, *Compilation of low-energy constraints on 4-fermion operators in the SMEFT*, *JHEP* **08** (2017) 123, [[arXiv:1706.03783](#)].
- [58] **VENUS** Collaboration, K. Abe et al., *A Study of the charm and bottom quark production in e^+e^- annihilation at $s^{*(1/2)} = 58\text{-GeV}$ using prompt electrons*, *Phys. Lett. B* **313** (1993) 288–298.
- [59] **TOPAZ** Collaboration, Y. Inoue et al., *Measurement of the cross-section and forward - backward charge asymmetry for the b and c quark in e^+e^- annihilation with inclusive muons at $s^{*(1/2)} = 58\text{-GeV}$* , *Eur. Phys. J. C* **18** (2000) 273–282, [[hep-ex/0012033](#)].
- [60] **CHARM-II** Collaboration, P. Vilain et al., *Precision measurement of electroweak parameters from the scattering of muon-neutrinos on electrons*, *Phys. Lett. B* **335** (1994) 246–252.
- [61] J. Erler and S. Su, *The Weak Neutral Current*, *Prog. Part. Nucl. Phys.* **71** (2013) 119–149, [[arXiv:1303.5522](#)].
- [62] **Particle Data Group** Collaboration, K. A. Olive et al., *Review of Particle Physics*, *Chin. Phys. C* **38** (2014) 090001.
- [63] **CHARM** Collaboration, J. V. Allaby et al., *A Precise Determination of the Electroweak Mixing Angle from Semileptonic Neutrino Scattering*, *Z. Phys. C* **36** (1987) 611.

- [64] A. Blondel et al., *Electroweak Parameters From a High Statistics Neutrino Nucleon Scattering Experiment*, *Z. Phys. C* **45** (1990) 361–379.
- [65] **CCFR, E744, E770** Collaboration, K. S. McFarland et al., *A Precision measurement of electroweak parameters in neutrino - nucleon scattering*, *Eur. Phys. J. C* **1** (1998) 509–513, [[hep-ex/9701010](#)].
- [66] **CHARM** Collaboration, J. Dorenbosch et al., *Experimental Verification of the Universality of ν_e and ν_μ Coupling to the Neutral Weak Current*, *Phys. Lett. B* **180** (1986) 303–307.
- [67] **Particle Data Group** Collaboration, C. Patrignani et al., *Review of Particle Physics*, *Chin. Phys. C* **40** (2016), no. 10 100001.
- [68] **SLAC E158** Collaboration, P. L. Anthony et al., *Precision measurement of the weak mixing angle in Moller scattering*, *Phys. Rev. Lett.* **95** (2005) 081601, [[hep-ex/0504049](#)].
- [69] A. Czarnecki and W. J. Marciano, *Electroweak radiative corrections to polarized Moller scattering asymmetries*, *Phys. Rev. D* **53** (1996) 1066–1072, [[hep-ph/9507420](#)].
- [70] **Qweak** Collaboration, D. Androic et al., *First Determination of the Weak Charge of the Proton*, *Phys. Rev. Lett.* **111** (2013), no. 14 141803, [[arXiv:1307.5275](#)].
- [71] **PVDIS** Collaboration, D. Wang et al., *Measurement of parity violation in electron-quark scattering*, *Nature* **506** (2014), no. 7486 67–70.
- [72] E. J. Beise, M. L. Pitt, and D. T. Spayde, *The SAMPLE experiment and weak nucleon structure*, *Prog. Part. Nucl. Phys.* **54** (2005) 289–350, [[nucl-ex/0412054](#)].
- [73] A. Argento et al., *Electroweak Asymmetry in Deep Inelastic Muon - Nucleon Scattering*, *Phys. Lett. B* **120** (1983) 245.
- [74] **VENUS** Collaboration, H. Hanai et al., *Measurement of tau polarization in $e^+ e^-$ annihilation at $s^{*(1/2)} = 58\text{-GeV}$* , *Phys. Lett. B* **403** (1997) 155–162, [[hep-ex/9703003](#)].
- [75] **CHARM-II** Collaboration, D. Geiregat et al., *First observation of neutrino trident production*, *Phys. Lett. B* **245** (1990) 271–275.
- [76] **CCFR** Collaboration, S. R. Mishra et al., *Neutrino tridents and $W Z$ interference*, *Phys. Rev. Lett.* **66** (1991) 3117–3120.

- [77] W. Altmannshofer, S. Gori, M. Pospelov, and I. Yavin, *Neutrino Trident Production: A Powerful Probe of New Physics with Neutrino Beams*, *Phys. Rev. Lett.* **113** (2014) 091801, [[arXiv:1406.2332](#)].
- [78] M. González-Alonso and J. Martin Camalich, *Global Effective-Field-Theory analysis of New-Physics effects in (semi)leptonic kaon decays*, *JHEP* **12** (2016) 052, [[arXiv:1605.07114](#)].
- [79] **US Belle II Group, Belle II/SuperKEKB e- Polarization Upgrade Working Group** Collaboration, S. Banerjee and J. M. Roney, *Snowmass 2021 White Paper on Upgrading SuperKEKB with a Polarized Electron Beam: Discovery Potential and Proposed Implementation*, in *2022 Snowmass Summer Study*, 5, 2022. [arXiv:2205.12847](#).
- [80] V. Bernard, M. Oertel, E. Passemar, and J. Stern, *$K(\mu 3)^*L$ decay: A Stringent test of right-handed quark currents*, *Phys. Lett. B* **638** (2006) 480–486, [[hep-ph/0603202](#)].
- [81] V. Cirigliano, J. Jenkins, and M. Gonzalez-Alonso, *Semileptonic decays of light quarks beyond the Standard Model*, *Nucl. Phys. B* **830** (2010) 95–115, [[arXiv:0908.1754](#)].
- [82] R. Alonso, B. Grinstein, and J. Martin Camalich, *Lepton universality violation and lepton flavor conservation in B -meson decays*, *JHEP* **10** (2015) 184, [[arXiv:1505.05164](#)].
- [83] J. C. Hardy and I. S. Towner, *Superaligned $0^+ \rightarrow 0^+$ nuclear β decays: 2014 critical survey, with precise results for V_{ud} and CKM unitarity*, *Phys. Rev. C* **91** (2015), no. 2 025501, [[arXiv:1411.5987](#)].
- [84] M. González-Alonso, J. Martin Camalich, and K. Mimouni, *Renormalization-group evolution of new physics contributions to (semi)leptonic meson decays*, *Phys. Lett. B* **772** (2017) 777–785, [[arXiv:1706.00410](#)].
- [85] A. Celis, J. Fuentes-Martin, A. Vicente, and J. Virto, *DsixTools: The Standard Model Effective Field Theory Toolkit*, *Eur. Phys. J. C* **77** (2017), no. 6 405, [[arXiv:1704.04504](#)].
- [86] J. Aebischer, M. Fael, C. Greub, and J. Virto, *B physics Beyond the Standard Model at One Loop: Complete Renormalization Group Evolution below the Electroweak Scale*, *JHEP* **09** (2017) 158, [[arXiv:1704.06639](#)].
- [87] R. Alonso, E. E. Jenkins, A. V. Manohar, and M. Trott, *Renormalization Group Evolution of the Standard Model Dimension Six Operators III: Gauge*

- Coupling Dependence and Phenomenology*, *JHEP* **04** (2014) 159, [[arXiv:1312.2014](#)].
- [88] J. A. Gracey, *Three loop \overline{MS} -bar tensor current anomalous dimension in QCD*, *Phys. Lett. B* **488** (2000) 175–181, [[hep-ph/0007171](#)].
- [89] K. G. Chetyrkin, B. A. Kniehl, and M. Steinhauser, *Decoupling relations to $O(\alpha_s^3)$ and their connection to low-energy theorems*, *Nucl. Phys. B* **510** (1998) 61–87, [[hep-ph/9708255](#)].
- [90] M. Misiak and M. Steinhauser, *Large- m_c Asymptotic Behaviour of $O(\alpha_s^2)$ Corrections to $B \rightarrow X_s \gamma$* , *Nucl. Phys. B* **840** (2010) 271–283, [[arXiv:1005.1173](#)].
- [91] E. E. Jenkins, A. V. Manohar, and M. Trott, *Renormalization Group Evolution of the Standard Model Dimension Six Operators II: Yukawa Dependence*, *JHEP* **01** (2014) 035, [[arXiv:1310.4838](#)].
- [92] N. Berger et al., *Measuring the weak mixing angle with the P2 experiment at MESA*, *J. Univ. Sci. Tech. China* **46** (2016), no. 6 481–487, [[arXiv:1511.03934](#)].
- [93] **CMS** Collaboration, S. Chatrchyan et al., *Observation of Z Decays to Four Leptons with the CMS Detector at the LHC*, *JHEP* **12** (2012) 034, [[arXiv:1210.3844](#)].
- [94] **ATLAS** Collaboration, G. Aad et al., *Measurements of Four-Lepton Production at the Z Resonance in pp Collisions at $\sqrt{s} = 7$ and 8 TeV with ATLAS*, *Phys. Rev. Lett.* **112** (2014), no. 23 231806, [[arXiv:1403.5657](#)].
- [95] **CMS** Collaboration, A. M. Sirunyan et al., *Measurements of the $pp \rightarrow ZZ$ production cross section and the $Z \rightarrow 4\ell$ branching fraction, and constraints on anomalous triple gauge couplings at $\sqrt{s} = 13$ TeV*, *Eur. Phys. J. C* **78** (2018) 165, [[arXiv:1709.08601](#)]. [Erratum: *Eur.Phys.J.C* 78, 515 (2018)].
- [96] J. M. Gerard, *FERMION MASS SPECTRUM IN $SU(2)$ -L x $U(1)$* , *Z. Phys. C* **18** (1983) 145.
- [97] R. S. Chivukula and H. Georgi, *Composite Technicolor Standard Model*, *Phys. Lett. B* **188** (1987) 99–104.
- [98] G. D’Ambrosio, G. F. Giudice, G. Isidori, and A. Strumia, *Minimal flavor violation: An Effective field theory approach*, *Nucl. Phys. B* **645** (2002) 155–187, [[hep-ph/0207036](#)].
- [99] K. Yumino and D. Jeans, *Measuring the tau polarization at ILC*, in *2022 Snowmass Summer Study*, 3, 2022. [arXiv:2203.07668](#).

- [100] T. Appelquist, B. A. Dobrescu, and A. R. Hopper, *Nonexotic Neutral Gauge Bosons*, *Phys. Rev. D* **68** (2003) 035012, [[hep-ph/0212073](#)].
- [101] R. K. Ellis et al., *Physics Briefing Book: Input for the European Strategy for Particle Physics Update 2020*, [arXiv:1910.11775](#).
- [102] G. F. Giudice, C. Grojean, A. Pomarol, and R. Rattazzi, *The Strongly-Interacting Light Higgs*, *JHEP* **06** (2007) 045, [[hep-ph/0703164](#)].
- [103] V. Gherardi, D. Marzocca, and E. Venturini, *Matching scalar leptoquarks to the SMEFT at one loop*, *JHEP* **07** (2020) 225, [[arXiv:2003.12525](#)]. [Erratum: *JHEP* 01, 006 (2021)].
- [104] J. Aebischer, W. Dekens, E. E. Jenkins, A. V. Manohar, D. Sengupta, and P. Stoffer, *Effective field theory interpretation of lepton magnetic and electric dipole moments*, *JHEP* **07** (2021) 107, [[arXiv:2102.08954](#)].
- [105] V. Cirigliano, W. Dekens, J. de Vries, and E. Mereghetti, *Constraining the top-Higgs sector of the Standard Model Effective Field Theory*, *Phys. Rev. D* **94** (2016), no. 3 034031, [[arXiv:1605.04311](#)].
- [106] K. Hagiwara, R. D. Peccei, D. Zeppenfeld, and K. Hikasa, *Probing the Weak Boson Sector in $e^+ e^- \rightarrow W^+ W^-$* , *Nucl. Phys. B* **282** (1987) 253–307.
- [107] T. Barklow, K. Fujii, S. Jung, M. E. Peskin, and J. Tian, *Model-Independent Determination of the Triple Higgs Coupling at e^+e^- Colliders*, *Phys. Rev. D* **97** (2018), no. 5 053004, [[arXiv:1708.09079](#)].
- [108] **LHC Higgs Cross Section Working Group** Collaboration, D. de Florian et al., *Handbook of LHC Higgs Cross Sections: 4. Deciphering the Nature of the Higgs Sector*, [arXiv:1610.07922](#).
- [109] A. Azatov et al., *Off-shell Higgs Interpretations Task Force: Models and Effective Field Theories Subgroup Report*, [arXiv:2203.02418](#).
- [110] **OPAL** Collaboration, G. Abbiendi et al., *Measurement of W boson polarizations and CP violating triple gauge couplings from W^+W^- production at LEP*, *Eur. Phys. J. C* **19** (2001) 229–240, [[hep-ex/0009021](#)].
- [111] A. V. Gritsan, J. Roskes, U. Sarica, M. Schulze, M. Xiao, and Y. Zhou, *New features in the JHU generator framework: constraining Higgs boson properties from on-shell and off-shell production*, *Phys. Rev. D* **102** (2020), no. 5 056022, [[arXiv:2002.09888](#)].
- [112] J. Davis, A. V. Gritsan, L. S. M. Guerra, S. Kyriacou, J. Roskes, and M. Schulze, *Constraining anomalous Higgs boson couplings to virtual photons*, *Phys. Rev. D* **105** (2022), no. 9 096027, [[arXiv:2109.13363](#)].

- [113] A. V. Gritsan et al., *Snowmass White Paper: Prospects of CP-violation measurements with the Higgs boson at future experiments*, [arXiv:2205.07715](#).
- [114] M. Beneke, D. Boito, and Y.-M. Wang, *Anomalous Higgs couplings in angular asymmetries of $H \rightarrow Z\ell^+\ell^-$ and $e^+e^- \rightarrow HZ$* , *JHEP* **11** (2014) 028, [[arXiv:1406.1361](#)].
- [115] N. Craig, J. Gu, Z. Liu, and K. Wang, *Beyond Higgs Couplings: Probing the Higgs with Angular Observables at Future e^+e^- Colliders*, *JHEP* **03** (2016) 050, [[arXiv:1512.06877](#)].
- [116] T. Ogawa, J. Tian, and K. Fujii, *Sensitivity to anomalous ZZH couplings at the ILC, PoS EPS-HEP2017* (2017) 322, [[arXiv:1712.09772](#)].
- [117] M. Perello Rosello and M. Vos, *Constraints on four-fermion interactions from the $t\bar{t}$ charge asymmetry at hadron colliders*, *Eur. Phys. J.* **C76** (2016), no. 4 200, [[arXiv:1512.07542](#)].
- [118] V. Miralles, M. M. López, M. M. Llácer, A. Peñuelas, M. Perelló, and M. Vos, *The top quark electro-weak couplings after LHC Run 2*, *JHEP* **02** (2022) 032, [[arXiv:2107.13917](#)].
- [119] G. Durieux, A. Irlles, V. Miralles, A. Peñuelas, R. Pöschl, M. Perelló, and M. Vos, *The electro-weak couplings of the top and bottom quarks – global fit and future prospects*, *JHEP* **12** (2019) 098, [[arXiv:1907.10619](#)].
- [120] F. Maltoni, L. Mantani, and K. Mimasu, *Top-quark electroweak interactions at high energy*, *JHEP* **10** (2019) 004, [[arXiv:1904.05637](#)].
- [121] G. Banelli, E. Salvioni, J. Serra, T. Theil, and A. Weiler, *The Present and Future of Four Top Operators*, *JHEP* **02** (2021) 043, [[arXiv:2010.05915](#)].
- [122] N. P. Hartland, F. Maltoni, E. R. Nocera, J. Rojo, E. Slade, E. Vryonidou, and C. Zhang, *A Monte Carlo global analysis of the Standard Model Effective Field Theory: the top quark sector*, *JHEP* **04** (2019) 100, [[arXiv:1901.05965](#)].
- [123] I. Brivio, S. Bruggisser, F. Maltoni, R. Moutafis, T. Plehn, E. Vryonidou, S. Westhoff, and C. Zhang, *O new physics, where art thou? A global search in the top sector*, *JHEP* **02** (2020) 131, [[arXiv:1910.03606](#)].
- [124] A. Buckley, C. Englert, J. Ferrando, D. J. Miller, L. Moore, M. Russell, and C. D. White, *Global fit of top quark effective theory to data*, *Phys. Rev.* **D92** (2015), no. 9 091501, [[arXiv:1506.08845](#)].
- [125] A. Buckley, C. Englert, J. Ferrando, D. J. Miller, L. Moore, M. Russell, and C. D. White, *Constraining top quark effective theory in the LHC Run II era*, *JHEP* **04** (2016) 015, [[arXiv:1512.03360](#)].

- [126] J. J. Ethier, F. Maltoni, L. Mantani, E. R. Nocera, J. Rojo, E. Slade, E. Vryonidou, and C. Zhang, *Combined SMEFT interpretation of Higgs, diboson, and top quark data from the LHC*, [arXiv:2105.00006](#).
- [127] J. Ellis, M. Madigan, K. Mimasu, V. Sanz, and T. You, *Top, Higgs, Diboson and Electroweak Fit to the Standard Model Effective Field Theory*, *JHEP* **04** (2021) 279, [[arXiv:2012.02779](#)].
- [128] G. Durieux, A. G. Camacho, L. Mantani, V. Miralles, M. M. López, M. Llácer Moreno, R. Poncelet, E. Vryonidou, and M. Vos, *Snowmass White Paper: prospects for the measurement of top-quark couplings*, in *2022 Snowmass Summer Study*, 5, 2022. [arXiv:2205.02140](#).
- [129] M. Czakon, P. Fiedler, and A. Mitov, *Total Top-Quark Pair-Production Cross Section at Hadron Colliders Through $O(\alpha_S^4)$* , *Phys. Rev. Lett.* **110** (2013) 252004, [[arXiv:1303.6254](#)].
- [130] **CMS Collaboration**, A. Tumasyan et al., *Measurement of differential $t\bar{t}$ production cross sections in the full kinematic range using lepton+jets events from proton-proton collisions at $\sqrt{s} = 13$ TeV*, *Phys. Rev. D* **104** (2021), no. 9 092013, [[arXiv:2108.02803](#)].
- [131] **ATLAS Collaboration** Collaboration, *Inclusive and differential measurement of the charge asymmetry in $t\bar{t}$ events at 13 TeV with the ATLAS detector*, *ATLAS-CONF-2019-026* (2019).
- [132] LHC Higgs Cross Section Working Group (D. de Florian et al.), *Handbook of LHC Higgs Cross Sections: 4. Deciphering the Nature of the Higgs Sector*, [arXiv:1610.07922](#).
- [133] ATLAS Collaboration, *A combination of measurements of Higgs boson production and decay using up to 139 fb^{-1} of proton-proton collision data at $\sqrt{s} = 13$ TeV collected with the ATLAS experiment*, *ATLAS-CONF-2020-027* (8, 2020).
- [134] A. Broggio, A. Ferroglia, R. Frederix, D. Pagani, B. D. Pecjak, and I. Tsiniikos, *Top-quark pair hadroproduction in association with a heavy boson at NLO+NNLL including EW corrections*, *JHEP* **08** (2019) 039, [[arXiv:1907.04343](#)].
- [135] **ATLAS Collaboration**, G. Aad et al., *Measurements of the inclusive and differential production cross sections of a top-quark-antiquark pair in association with a Z boson at $\sqrt{s} = 13$ TeV with the ATLAS detector*, *Eur. Phys. J. C* **81** (2021) 737, [[arXiv:2103.12603](#)].

- [136] G. Bevilacqua, H. Hartanto, M. Kraus, T. Weber, and M. Worek, *Hard Photons in Hadroproduction of Top Quarks with Realistic Final States*, *JHEP* **10** (2018) 158, [[arXiv:1803.09916](#)].
- [137] G. Bevilacqua, H. Hartanto, M. Kraus, T. Weber, and M. Worek, *Precise predictions for $t\bar{t}\gamma/t\bar{t}$ cross section ratios at the LHC*, *JHEP* **01** (2019) 188, [[arXiv:1809.08562](#)].
- [138] ATLAS Collaboration, *Measurements of inclusive and differential cross-sections of combined $t\bar{t}\gamma$ and $tW\gamma$ production in the $e\mu$ channel at 13 TeV with the ATLAS detector*, *JHEP* **09** (2020) 049, [[arXiv:2007.06946](#)].
- [139] CMS Collaboration, *Measurement of the associated production of a single top quark and a Z boson in pp collisions at $\sqrt{s} = 13$ TeV*, *Phys. Lett.* **B779** (2018) 358–384, [[arXiv:1712.02825](#)].
- [140] CMS Collaboration, *Observation of Single Top Quark Production in Association with a Z Boson in Proton-Proton Collisions at $\sqrt{s} = 13$ TeV*, *Phys. Rev. Lett.* **122** (2019), no. 13 132003, [[arXiv:1812.05900](#)].
- [141] CMS Collaboration, *Evidence for the associated production of a single top quark and a photon in proton-proton collisions at $\sqrt{s} = 13$ TeV*, *Phys. Rev. Lett.* **121** (2018), no. 22 221802, [[arXiv:1808.02913](#)].
- [142] R. Frederix, D. Pagani, and M. Zaro, *Large NLO corrections in $t\bar{t}W^\pm$ and $t\bar{t}t\bar{t}$ hadroproduction from supposedly subleading EW contributions*, *JHEP* **02** (2018) 031, [[arXiv:1711.02116](#)].
- [143] CMS Collaboration, *Measurement of the cross section for top quark pair production in association with a W or Z boson in proton-proton collisions at $\sqrt{s} = 13$ TeV*, *JHEP* **08** (2018) 011, [[arXiv:1711.02547](#)].
- [144] M. Aliev, H. Lacker, U. Langenfeld, S. Moch, P. Uwer, and M. Wiedermann, *HATHOR: HAdronic Top and Heavy quarks crOss section calculator*, *Comput. Phys. Commun.* **182** (2011) 1034–1046, [[arXiv:1007.1327](#)].
- [145] P. Kant, O. Kind, T. Kintscher, T. Lohse, T. Martini, S. Mölbitz, P. Rieck, and P. Uwer, *HatHor for single top-quark production: Updated predictions and uncertainty estimates for single top-quark production in hadronic collisions*, *Comput. Phys. Commun.* **191** (2015) 74–89, [[arXiv:1406.4403](#)].
- [146] ATLAS and CMS Collaborations, *Combinations of single-top-quark production cross-section measurements and $|f_{LV}V_{tb}|$ determinations at $\sqrt{s} = 7$ and 8 TeV with the ATLAS and CMS experiments*, *JHEP* **05** (2019) 088, [[arXiv:1902.07158](#)].

- [147] N. Kidonakis, *Two-loop soft anomalous dimensions for single top quark associated production with a W^- or H^-* , *Phys. Rev. D* **82** (2010) 054018, [[arXiv:1005.4451](#)].
- [148] A. Czarnecki, J. G. Korner, and J. H. Piclum, *Helicity fractions of W bosons from top quark decays at NNLO in QCD*, *Phys. Rev.* **D81** (2010) 111503, [[arXiv:1005.2625](#)].
- [149] ATLAS and CMS Collaborations, *Combination of the W boson polarization measurements in top quark decays using ATLAS and CMS data at $\sqrt{s} = 8$ TeV*, *JHEP* **08** (2020), no. 08 051, [[arXiv:2005.03799](#)].
- [150] N. Kidonakis, *NNLL resummation for s -channel single top quark production*, *Phys. Rev.* **D81** (2010) 054028.
- [151] CDF and D0 Collaborations, *Observation of s -channel production of single top quarks at the Tevatron*, *Phys. Rev. Lett.* **112** (2014) 231803, [[arXiv:1402.5126](#)].
- [152] P. Janot, *Top-quark electroweak couplings at the FCC-ee*, *JHEP* **04** (2015) 182, [[arXiv:1503.01325](#)].
- [153] M. S. Amjad et al., *A precise characterisation of the top quark electro-weak vertices at the ILC*, *Eur. Phys. J.* **C75** (2015), no. 10 512, [[arXiv:1505.06020](#)].
- [154] M. S. Amjad, M. Boronat, T. Frisson, I. Garcia, R. Poschl, E. Ros, F. Richard, J. Rouene, P. R. Femenia, and M. Vos, *A precise determination of top quark electro-weak couplings at the ILC operating at $\sqrt{s} = 500$ GeV*, [[arXiv:1307.8102](#)].
- [155] G. Durieux, M. Perelló, M. Vos, and C. Zhang, *Global and optimal probes for the top-quark effective field theory at future lepton colliders*, *JHEP* **10** (2018) 168, [[arXiv:1807.02121](#)].
- [156] Y. Okugawa, A. Irlles, V. Lohezic, S. Amjad, R. Yonamine, F. Richard, H. Yamamoto, and R. Pöschl, *Production and electroweak couplings of 3rd generation quarks at the ILC*, *PoS LeptonPhoton2019* (2019) 170.
- [157] **CLICdp** Collaboration, H. Abramowicz et al., *Top-Quark Physics at the CLIC Electron-Positron Linear Collider*, *JHEP* **11** (2019) 003, [[arXiv:1807.02441](#)].
- [158] H. Abramowicz et al., *Higgs physics at the CLIC electron-positron linear collider*, *Eur. Phys. J. C* **77** (2017), no. 7 475, [[arXiv:1608.07538](#)].

- [159] T. Price, P. Roloff, J. Strube, and T. Tanabe, *Full simulation study of the top Yukawa coupling at the ILC at $\sqrt{s} = 1$ TeV*, *Eur. Phys. J. C* **75** (2015), no. 7 309, [[arXiv:1409.7157](#)].
- [160] R. Yonamine, K. Ikematsu, T. Tanabe, K. Fujii, Y. Kiyo, Y. Sumino, and H. Yokoya, *Measuring the top Yukawa coupling at the ILC at $\sqrt{s} = 500$ GeV*, *Phys. Rev. D* **84** (2011) 014033, [[arXiv:1104.5132](#)].
- [161] **FCC** Collaboration, A. Abada et al., *FCC-hh: The Hadron Collider: Future Circular Collider Conceptual Design Report Volume 3*, *Eur. Phys. J. ST* **228** (2019), no. 4 755–1107.
- [162] M. L. Mangano et al., *Physics at a 100 TeV pp Collider: Standard Model Processes*, [[arXiv:1607.01831](#)].
- [163] M. L. Mangano, T. Plehn, P. Reimitz, T. Schell, and H.-S. Shao, *Measuring the Top Yukawa Coupling at 100 TeV*, *J. Phys. G* **43** (2016), no. 3 035001, [[arXiv:1507.08169](#)].
- [164] J. A. Aguilar-Saavedra, B. Fuks, and M. L. Mangano, *Pinning down top dipole moments with ultra-boosted tops*, *Phys. Rev. D* **91** (2015) 094021, [[arXiv:1412.6654](#)].
- [165] G. Durieux, F. Maltoni, and C. Zhang, *Global approach to top-quark flavor-changing interactions*, *Phys. Rev. D* **91** (2015), no. 7 074017, [[arXiv:1412.7166](#)].
- [166] M. Chala, J. Santiago, and M. Spannowsky, *Constraining four-fermion operators using rare top decays*, *JHEP* **04** (2019) 014, [[arXiv:1809.09624](#)].
- [167] **CMS** Collaboration, A. M. Sirunyan et al., *Search for new physics in top quark production with additional leptons in proton-proton collisions at $\sqrt{s} = 13$ TeV using effective field theory*, *JHEP* **03** (2021) 095, [[arXiv:2012.04120](#)].